LENS and UNIVERSITÀ DEGLI STUDI DI FIRENZE
DIPARTIMENTO DI FISICA
Facoltà di Scienze Matematiche, Fisiche e Naturali
Settore di appartenenza: FIS/03

PHD THESIS IN
ATOMIC AND MOLECULAR SPECTROSCOPY - XX CYCLE

TUNING OF THE INTERACTIONS IN ULTRACOLD K-RB QUANTUM GASES

PRESENTED BY

MATTEO ZACCANTI

SUPERVISOR..... PROF. GIOVANNI MODUGNO
COORDINATOR ..... PROF. FRANCESCO PAVONE

REFEREES ..... PROF. HANNS CHRISTOPH NÄGERL
PROF. F. JAVIER AOIZ

Firenze, December 2007

Se non si va non si vede

Abstract

During the three years of my PhD I have worked in the laboratory of ultracold atomic K Rb mixtures of Prof. Giovanni Modugno in the group of Prof. Massimo Inguscio at LENS of Florence. In this period two main experiments have been performed by our team: during the years 2005-2006, we investigated a mixture of fermionic potassium (^{40}K) and rubidium (^{87}Rb); more recently, we studied a Bose Einstein condensate of potassium (^{39}K) which we realized for the first time in the year 2007. Both these systems may find applications in a very broad range of research areas. In particular, the Fermi Bose mixture is extremely appealing for studying superfluid, strongly correlated and disordered systems, and it is considered very promising for the creation of ultracold polar molecules. KRb dimers are in general interesting to study because they can be either bosons (^{39}K-^{87}Rb and ^{41}K-^{87}Rb) or fermions (^{40}K-^{87}Rb) and, once in a deeply bound state, they feature a large electric dipole moment. This paves the way to study new kind of ultracold gases with tunable, long-range, anisotropic interactions. Furthermore, when loaded into the sites of an optical lattice, these systems can also be used for implementing new quantum computing schemes.

As for the ^{39}K gas, we instead discovered that it can be employed for the realization of an almost ideal, non-interacting Bose Einstein condensate, and therefore it is one of the most promising candidates for realizing new atom interferometers with trapped condensed gases; moreover, this system can allow the investigation of other physical phenomena for which it is important to reduce the interatomic interaction, that otherwise can mask the underlying physics of interest (a notable example of such phenomena is the so-called Anderson localization).

Both the experiments rely on the possibility of tuning the interatomic interaction

in the gases by means of a so-called *magnetic Feshbach resonance*. In proximity of such kind of features, the s-wave scattering length a -the only parameter needed to describe the interactions in the ultracold regime- shows a dispersive behavior; so it can assume values between $+\infty$ and $-\infty$, just varying the field around the resonance position. This means that a Feshbach resonance offers a unique tool to manipulate the interaction strength within the gas (or mixture of gases), allowing us to range from strongly repulsive/attractive, down to weakly interacting regime, both for hetero- and homo-nuclear samples.

All the physics that I'm going to describe in this work, relies on a detailed knowledge of the scattering properties of the gases we have been studying: this knowledge arises from an exhaustive characterization of both the ^{40}K ^{87}Rb and ^{39}K ^{87}Rb mixtures, and the ^{39}K gas via extensive Feshbach spectroscopy that we have performed during the last three years and that is in itself an interesting result. This allowed us to develop an accurate near threshold quantum collisional model for K-Rb mixtures, and to refine an already existing one for K isotopes. Each of the two models can precisely reproduce the observed spectroscopic patterns, and it can be employed to evaluate the scattering lengths, the dispersion coefficients, the location of other still not observed resonances, and the near threshold molecular states of the system. Furthermore, via mass scaling process, both models have a high prediction power for the collisional properties of still unexplored K Rb and K systems.

In the year 2006 we have for the first time demonstrated the possibility to tune the interaction of the ^{87}Rb-^{40}K mixture in the degenerate regime (BEC + Fermi gas). We have investigated the phenomena that arise in strongly interacting samples: the collapse of the system- when the attractive interaction becomes too strong for the system to have a stable ground state- and the phase separation of the two components of the mixture- when the strong interspecies repulsion causes the expulsion the Rb BEC from the Fermi gas of K. The last phenomenon is peculiar of mixtures and not observable in homonuclear systems.

We have also investigated the possibility to associate molecules performing sweeps in the magnetic field across a Feshbach resonance to associate Rb and K atoms into weakly bound KRb dimers, performing a preliminary characterization of the process.

In the year 2007 the apparatus has been employed for realizing and investigating a Bose Einstein condensate of ^{39}K. This atomic species, despite its unfavorable *zero field* scattering properties ($a \sim$ -33 a_0) that prevented in the past its condensation, is extremely interesting since the presence of very broad Feshbach resonance

allows a fine tuning of its interaction strength. In particular, the accurate control of the scattering length around zero leads to the creation of an almost ideal Bose gas. The realization of the first ^{39}K BEC had not been achievable without the remarkable scattering properties between this atomic species and rubidium, relying on the possibility to tune both inter- and intra-species interactions: the first one offers the possibility to greatly increase the efficiency of sympathetic cooling of potassium atoms with rubidium, and the latter one allows us to stabilize the sample against collapse. We have investigated the possibility to precisely tune the interaction strength of this system within its stability region, limited on one side by three body recombination, due to the vicinity of the FR center, and on the other side by collapse, due to the negative value of the scattering length.

As already mentioned above, an almost ideal BEC is interesting for atom interferometry, since it represents the analog of an optical laser for what concerns monochromaticity and coherence properties. We have recently investigated this by realizing an atom interferometer with a weakly interacting BEC of ^{39}K. The suppression of the atom atom interactions by orders of magnitude that is realized by tuning the external magnetic field greatly enhanced the precision and accuracy of our interferometer, clearly demonstrating a strong suppression of interaction induced decoherence. The possibility to fine tune the scattering length in this system allows us also to control the *size* of the atomic cloud; in particular, the possibility to create samples of ~ 1 micron size (the dimension of an ideal BEC confined in a 100 Hz harmonic trap) makes this system very appealing for precise measurements of weak forces at short distances. Furthermore, one could exploit the tunability of the scattering length of the condensate in order to create number squeezed states and to also open new directions towards Heisenberg-limited interferometry. Concerning this most recent experiment I will here recall just some of the main results.

The thesis is organized as follows: I'll give some details of the experimental procedure used to cool both the mixtures down to temperatures of the order of 1 μK. In fact, as it will be clarified in the following, the Bose-Bose system can be easily achieved starting from an apparatus for Fermi-Bose mixtures and viceversa, by making few changes to the laser lights for potassium, and to the *evaporative cooling* stage. I'll briefly describe also the optical trap and the magnetic coils we employed in all the experiments described in the thesis. The second part is devoted to the construction of quantum collision models able to describe the scattering properties of the atomic gases we investigated, that are based on our characterization of the systems: in order to understand the techniques we used in the experiment, and the successive analysis

of the data, I'll remind some basic theoretical points concerning the scattering theory and the physics related to magnetic Feshbach resonances. Third and fourth parts of this work are devoted to the description of the various experiments we have done with the Fermi-Bose mixture and the ^{39}K gas in the degenerate regime.

Contents

Introduction

The field of ultracold atomic gases is fascinating, since as the temperature of the sample approaches very low values, the quantum behavior of the system becomes visible and an enormous quantity of new phenomena arise. The great success of this recent field of research relies on the experimental ability to cool down to nearly zero temperature the atoms and to store them into magnetic and optical potentials, thus assuring them long lifetimes and nearly perfect isolation from the external environment. Moreover the use of radiofrequency, microwave, optical and magnetic fields allows the manipulation of the atoms in a well controlled way. Therefore, almost pure and well defined quantum systems are achievable, and they can be theoretically treated with extremely high efficacy.

The field of ultracold gases has been further enriched by the achievement of Bose Einstein condensation [1, 2, 3] and of quantum degeneracy in a Fermi gas [4]. These two milestones have paved the way to a large series of investigations, both in experiments and theory: the Bose Einstein condensate, with the macroscopic occupation of the lowest available quantum state, is the matter wave analogue of the optical laser regarding the properties of coherence and monochromaticity. An atomic Fermi gas offers the possibility, especially when trapped into an optical lattice [5], to investigate many solid state physics phenomena, without impurities in the system and in an almost ideal environment.

As well as the achievement of degenerate Bose and Fermi gas, the availability of magnetic Feshbach resonances [6] has given a tremendous impulse to the field of ultracold systems: on one side they offer the possibility to tune the interatomic interaction strength in a well controlled way, from attractive to repulsive and from very small to very large [7, 8]; on the other side they allow formation of weakly bound

molecules. In fact, since their first observation [9], they gave rise to a variety of new experiments and breakthroughs in the last years as, e.g., the preparation of pure molecular quantum gases out of bosonic atoms [10, 11, 12], the formation of bright solitons in a weakly attractive Bose Einstein condensate [13], and the observation of Efimov states [15].

While at the beginning the main aim of this field of research was the investigation of strongly interacting systems, in the last years there has been a growing interest for bosonic systems in which the interatomic interaction can be finely controlled and accurately tuned down to very small values, reaching an almost non interacting Bose gas [16]. Among the reasons that stimulated the research of such kind of systems is that for applications to matter wave interferometry [17] and for investigation of subtle phenomena related to disorder [18], interatomic interaction can be detrimental [19], and mask the real physics of interest [20, 21]. In this context we have investigated the last stable alkali atom brought to Bose Einstein condensation, the ^{39}K, and found it a very interesting candidate to be employed within the field of low interacting condensed gases, as well as ^{7}Li and ^{133}Cs.

In the last years also more complex systems were both experimentally created and theoretically investigated, employing more than a single species, in order to enrich the field of novel quantum phases: both different spin mixtures of the same atom [4] and heteronuclear mixtures [22, 23, 24, 25, 26, 28, 27] opened several interesting new fields of research, especially in combination with the presence of interspecies Feshbach resonances. Notable examples are the recent exploration of BEC-BCS crossover by means of a mixture of two different spin states of a Fermi gas [29, 30, 31] and the achievement of heteronuclear Feshbach molecules [32, 33]. In fact, quantum degenerate atomic mixtures are promising for the study of a variety of novel physical phenomena, such as boson-induced superfluidity of fermions [34], quantum phases of matter in optical lattices [35] or random potentials [36], and production of quantum gases of polar molecules [37]: these compound particles would further enrich the physics of ultracold systems, since they would not only have many more degrees of freedom than atoms to be manipulated, but also they would give rise to new controllable, anisotropic interactions.

In this context, K-Rb mixtures are very promising since both fermion-boson and boson-boson mixtures are easy to bring into the degenerate regime [26, 38, 39, 40], the main isotopic combinations present several accessible Feshbach resonances [41, 42, 43], and their molecular association seems to be very interesting in the field of polar molecules, since the ground state dimer has a large electric dipole moment

[44].

In this thesis I report on experimental studies performed on ultracold gases of potassium and rubidium atoms with tunable interaction. In Chapter 1 I describe the apparatus and the experimental procedures needed to cool the mixture down to temperatures of $\sim 1\mu$K.

The scattering properties of both Fermi-Bose and Bose-Bose systems have been exhaustively investigated and characterized by means of Feshbach spectroscopy; this has allowed us to construct a quantum collision model able to accurately predict resonance positions and molecular levels close to the dissociation threshold for all the K-Rb pairs. Also an ultracold gas of ^{39}K has been investigated for the first time by means of Feshbach spectroscopy: the accurate determination of the magnetic-field resonance locations allowed us to optimize a theoretical model for potassium isotopes able to predict the magnetic-field dependence of scattering lengths and of near-threshold molecular levels. This will be object of Chapter 2.

Chapter 3 describes the experiments performed when a degenerate Fermi-Bose mixture is brought in a magnetic field region close to a broad interspecies Feshbach resonance. A characterization of the regimes of strong attraction and strong repulsion between the system components is described in detail and our first tests of KRb molecule association are discussed.

Chapter 4 describes the realization of the first Bose Einstein condensate of ^{39}K: despite its unfavourable *zero field* collisional properties, the gas is efficiently cooled down to few hundreds nK exploiting forced evaporative cooling of rubidium and sympathetic cooling of potassium into an optical trap. Both interspecies and intraspecies interaction are tuned by means of Feshbach resonances, in order to increase the sympathetic cooling efficiency and to stabilize the ^{39}K against collapse just before reaching the degenerate regime. Due to the presence of broad homonuclear Feshbach resonances the interaction within ^{39}K can be finely tuned over a wide range of values, especially within the weakly interacting regime. First experiments on this new system are described and future ideas are discussed.

Chapter 1

Experimental procedures

The starting point of all the experiments described in my thesis is a spin polarized mixture of an ultracold cloud of ^{87}Rb and ^{40}K or ^{39}K atoms in an optical dipole trap, in presence of a tunable, homogeneous external magnetic field. In this chapter I will give a short overview about the experimental techniques employed to obtain these samples. The individual steps are described in detail in [49] and can be summarized as follows:

- Pre-cooling and trapping of rubidium and potassium atoms in a magneto optical trap (MOT)
- Preparation of the two species into a stable, magnetically trapped mixture
- Evaporative cooling of rubidium and sympathetic cooling of potassium
- Loading of the mixture into an optical dipole trap
- Application of a homogeneous magnetic field and transfer of the two species onto the desired Zeeman sublevels

To obtain a degenerate mixture several technical requirements must be met. We need a special experimental apparatus working at ultrahigh vacuum conditions because at all stages of the experiment the atoms have to be protected from collisions with background gas. This apparatus has been constructed in 2000-2001, using a double chamber scheme. Despite its simplicity and limited optical access, and even though several necessary improvements to the original system performed during the years made it sometimes hardly manageable, the apparatus is robust and extremely

versatile. We need additionally a complex laser and magnetic field system for cooling, trapping and manipulating the atoms. A computer controls at the microsecond level the sequences of the experiment. Only few technical details of the experimental setup will be discussed here, since they have already been described in detail in previous theses in our group [49, 52, 53, 54].

1.1 Preparation of the cold mixtures

1.1.1 The rubidium and potassium atoms

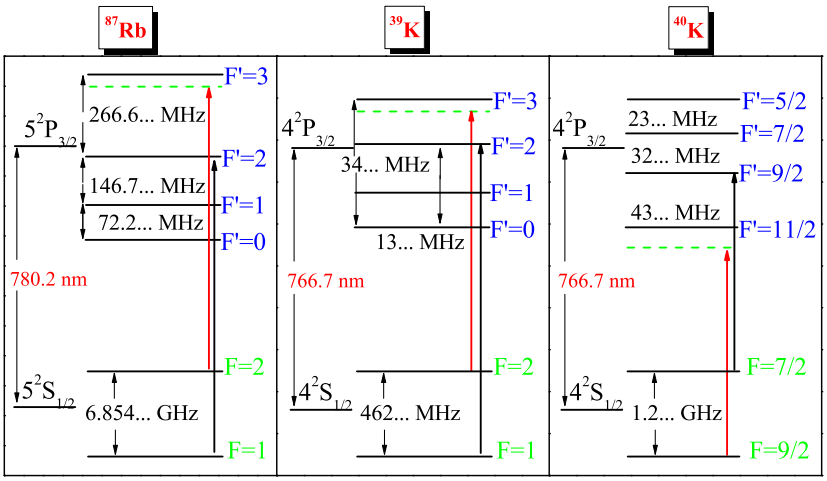

Figure 1.1: Schematic diagram of the levels of the three atoms we employ in our experiments. Black and red arrows indicate the *repumper* and *cooling* transitions for the three atoms. The cooling light is red detuned by some MHz with respect to the atomic transition.

Potassium is an alkali atom and in nature it is present in three different stable isotopes, ^{39}K, ^{41}K and ^{40}K with natural abundance of 93.26%, 6.73% and 0.012% respectively. Two isotopes, the ^{39}K and the ^{41}K are bosons (nuclear spin $I = 3/2$), while the ^{40}K is a fermion (nuclear spin $I = 4$). We have focused our attention to the well known fermionic isotope of potassium [8], and to the most abundant bosonic isotope,

despite its *zero field* scattering properties are unfavourable for achieving a stable Bose Einstein condensate [45]. Also rubidium is an alkali metal and it is present in two stable bosonic isotopes, ^{85}Rb (72.2%), and ^{87}Rb (27.8%). As ^{39}K, ^{85}Rb is characterized by a negative scattering length, that does not allow the formation of a stable condensate, unless its stabilization employing a Feshbach resonance [46, 47]. Conversely, the ^{87}Rb has a positive scattering length [48] and it was the first atom brought to quantum degeneracy in 1995 [1]. Differently from potassium, ^{87}Rb is an easily and efficiently coolable atom and this is the reason why it has been used for the sympathetic cooling of K atoms [25]. The scheme of the hyperfine structure of the three atomic species we employ in the experiments are schematically reported in Fig.1.1. As shown, potassium atoms have a small hyperfine structure, extremely reduced on the excited states in the case of the bosonic isotope, that makes *sub Doppler cooling* schemes unavailable, and the sympathetic cooling with Rb crucial for efficiently reaching the ultracold regime. The atomic gases are generated from a reservoir of rubidium and potassium connected to the vacuum chamber, and heated up to about 40 °C.

1.1.2 Lights for the three species

All the experiments performed with ultracold quantum gases rely on the possibility of laser cooling, and therefore a complex system of lights is required in order to bring the atomic temperature down to few hundreds of μK. The laser sources employed in our apparatus for generating both *cooling* and *repumper* light for the MOT, optical pumping, and imaging lights for rubidium are two standard laser diodes. Potassium laser source is a single Ti:Sa laser, since the small hyperfine structure of this atom allows to achieve all the frequencies just starting from a single laser, and making use of few acousto-optic modulators (AOM). Note that due to the very similar level structure of the two isotopes, their lights preparation is possible using the same laser source, and only small changes in the AOMs scheme are necessary to switch the apparatus from the Fermi-Bose to the Bose-Bose mixture. Furthermore, consider that in the apparatus also a source of ^{41}K enriched to 99% is present, and also this isotope is easily achievable in the MOT by simple changes in the light preparation, see [49].

In order to have large power on the MOT beams the four cooling and repumper lights are injected into two home-made tapered amplifier, and successively combined together by means of optical fibers. These act as filters for the beam quality and make the MOT beams immune from coarse misalignments. Also the four opti-

cal pumping beams and the two imaging beams are combined on optical fibers and brought in the vicinity of the vacuum cell.

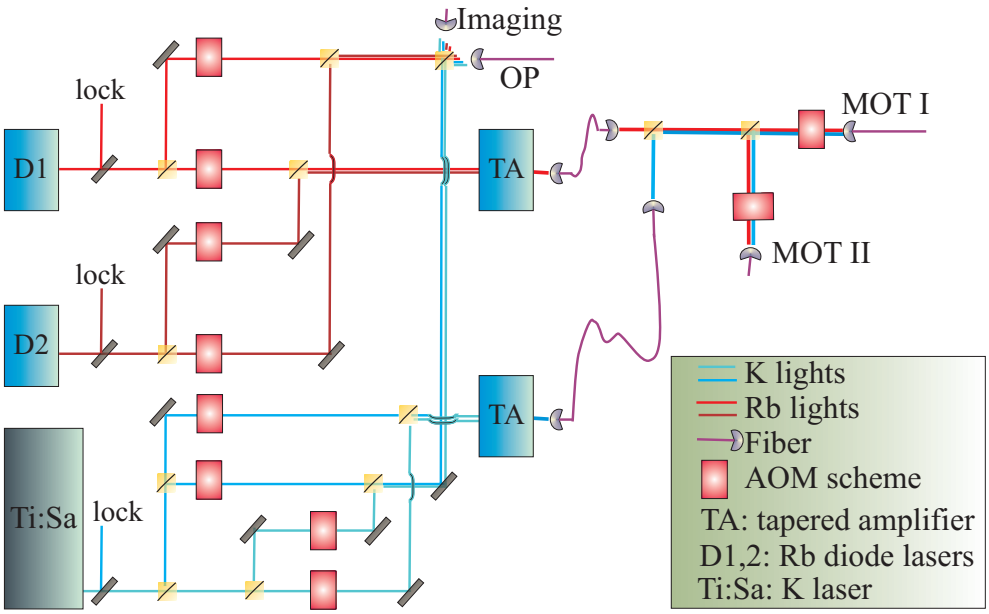

Figure 1.2: Scheme of the laser lights employed in the experiment. The picture doesn't contain all the details of the apparatus and must be regarded just as a qualitative description of the real case.

1.1.3 Scheme of the apparatus

As already mentioned in the introduction of this chapter, our system adopts a standard double MOT chamber scheme. Once the MOT of potassium and rubidium in the first cell is produced (Pressure $\sim 10^{-9}$ Torr), the atoms are pushed into the second cell (Pressure $\sim 10^{-12}$ Torr) by means of a light beam of ~ 1 mW/cm^2 intensity, near resonant with the cooling transition; for potassium the push beam contains also some repumper light. The second MOT is loaded within twenty second of continuous pushing of rubidium and successively eight seconds of pulsed pushing of potassium, after which approximatively 10^9 rubidium atoms at $\sim 100\mu$K and 10^6 (10^7) potassium 40 (39) atoms at $\sim 300\mu$K are stored into the second cell. A C-MOT [50] and molasses cooling phase follow, that lower the temperature of the

mixture down to some tens of μK [1]; then the two species are optically pumped in their stretched Zeeman states by means of a hundred microsecond light pulse. A bias field ($\sim$ 1Gauss) assures the stability of the mixture against *spin-flip* transitions.

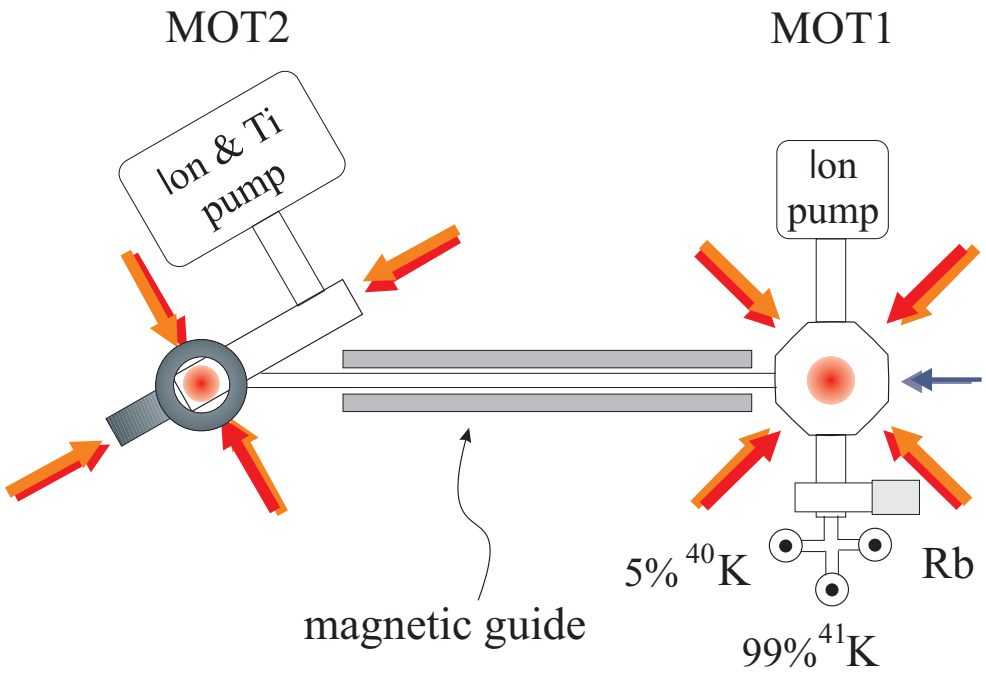

Figure 1.3: Two chamber scheme of our apparatus. Between the two cells differential pressure is maintained. The figure shows also the reservoirs of the atomic species, ^{41}K included.

1.1.4 Magnetic trapping and cooling

Rubidium and bosonic potassium are prepared in the $|f = 2, m = 2\rangle$ state[2], while fermionic potassium is prepared in the $|f = 9/2, m = 9/2\rangle$ state: all these states are *low-field seekers* and therefore magnetically trappable. Both the K-Rb mixtures are then stored in a magnetic potential, created by a QUIC trap (Quadrupole Ioffe-Pritchard Configuration) [51], where evaporative cooling on rubidium and sympathetic cooling of potassium can take place. The axial and radial frequencies of rubid-

[1] For bosonic potassium, whose small hyperfine structure makes inefficient the sub-Doppler cooling, it is crucial the successive thermalization with the rubidium atoms.

[2] I will always use lower case letters for indicating an atomic state, and I'll adopt capital letters for denoting molecular quantum numbers.

ium in the magnetic potential are 16 and 197 Hz respectively; the ones of potassium are $\sqrt{\frac{m_{Rb}}{m_K}}$ times larger. The evaporative cooling of Rb atoms can be performed in two ways: by means of radio frequency resonant with the splitting of the Zeeman levels $|f = 2, m\rangle \mapsto |f = 2, m - 1\rangle$, or by means of a microwave signal resonant with the hyperfine transition $|f = 2, m = 2\rangle \mapsto |f = 1, m = 1\rangle$ at $6.834 GHz$. Both schemes can be efficiently used with fermionic potassium; for the cooling of ^{39}K, instead, only the second one can be employed, since its Zeeman splitting is the same than that of rubidium, and therefore the rf signal would expel it from the trap. In both cases, after $22 - 25$ s of evaporation in the QUIC trap the samples are cold enough to be efficiently transferred in our optical trap. We found the best compromise between low temperatures, atom number and stability against thermal fluctuations of the bottom of the magnetic trap, when we stop the evaporative cooling at temperatures around $800 - 1200$ nK. In this conditions, our samples are typically composed by 10^6 rubidium atoms, mixed with $2 \cdot 10^5$ ($6 \cdot 10^5$) fermionic (bosonic) potassium [3]. Note that further cooling in the magnetic potential is in principle possible, but since both the mixtures must be successively transferred into different Zeeman states, and this unavoidably causes a heating of the sample, it is not convenient to further force the evaporation in the magnetic trap. We therefore adiabatically transfer the sample into an optical potential.

1.2 The optical trap

Our trap is created with two focused laser beams with beam waists of about 100μm and crossing in the horizontal plane, see Fig. 1.4, generated with a 1032 nm Yb:YAG disk laser. The laser frequency is sufficiently far away from the atomic transitions to assure scattering rates lower than 0.1 Hz at the maximum power. The trap depth is initially approximately six times larger than the atom kinetic energy, in order to ensure that no atom losses and no significant heating accompany the transfer from the magnetic to the optical potential.

The raise of the optical potential is performed by means of a 200 ms exponential ramp of the beams power. The two species are then transferred to their absolute ground states via adiabatic rapid passage (see below), and further cooled by

[3] The difference in the potassium populations arises from the different abundance we have of the two gases at the beginning, and not on a major efficiency of sympathetic cooling of the bosonic potassium with respect to the fermionic isotope. The final atom number is actually limited by the flux of atoms present in the first cell: by renewing the reservoirs of the three species we expect to easily increase it by almost an order of magnitude.

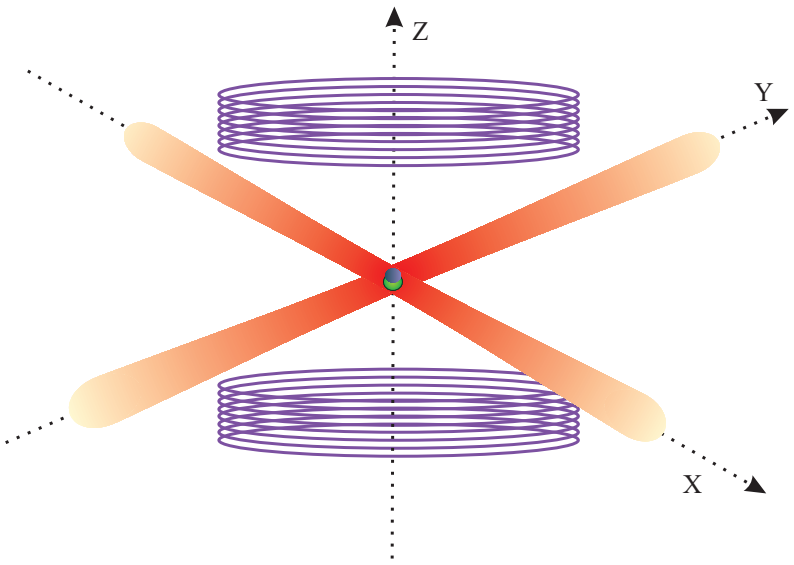

Figure 1.4: Scheme of the optical trap: two focused laser beams (waist $\approx 100\mu$m) crossing in the horizontal plane create a potential that trap both potassium (blue) and rubidium (green). The gravitational sag causes that the two samples overlap only partially along the vertical direction, with the lighter element laying at a larger height than the heavier. The Feshbach coils, placed along the vertical axis, are also shown.

reducing the intensity of the laser beams by means of acousto-optic modulators. The optical trap is designed in such a way to evaporate mainly Rb by exploiting the increased gravitational sag of this heavier element. The optical potential allows us to trap both *low* and *high field seekers* atomic states within an external magnetic field of hundreds of Gauss, and it turns out to be extremely efficient for the storage and the further cooling of the atoms. As it will be explained in chapter 4, by lowering the optical potential we can also reach experimental conditions in which rubidium is completely evaporated, and potassium is still trapped. In general, by modifying the absolute and relative powers of the two directions of the crossed trap, we can easily design potentials of different geometries and depths, reducing or increasing the gravitational sag between the two species, depending on the experiments we want to perform.

1.3 The Feshbach field

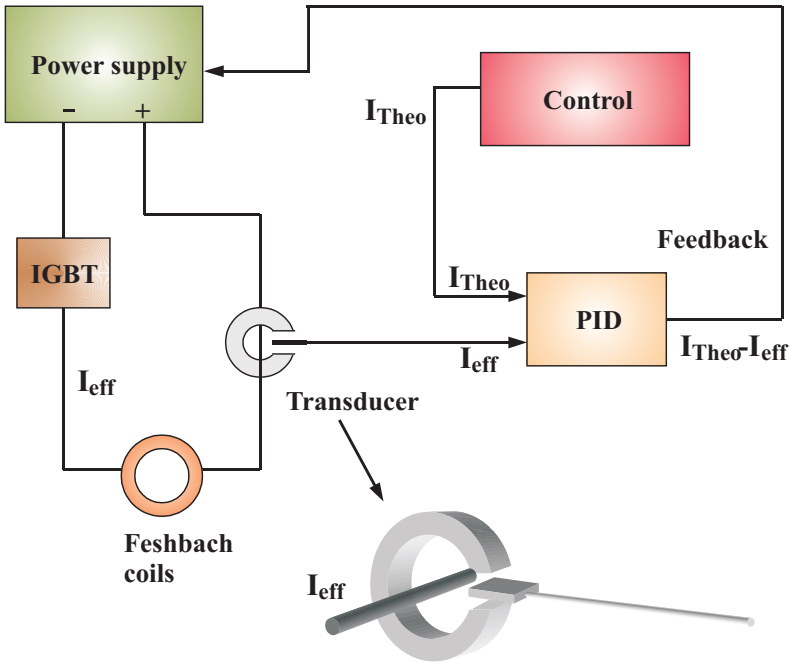

Figure 1.5: Scheme of the stabilization system for the current of the Feshbach coils.

The magnetic field necessary for all the experiments described later is realized by means of a couple of coils in Helmholtz configuration [4], generating a field that points in the vertical direction, and centered on the QUIC position. In principle we could generate it by inverting the current in one of the quadrupole coils of the magnetic trap, but then the axis of the system would be horizontally shifted with respect of the QUIC position of approximately 7 mm. The coils are water cooled, and the field is actively stabilized with a standard PID control (see Fig. 1.5), with a bandwidth of ~ 4 kHz, that ensures for any field value up to 1000 Gauss a short term stability of ~ 30 mGauss , and a long term one (day to day) of better than 100 mGauss. We calibrate the field by means of microwave and radio frequency spectroscopy on the two $|2,2\rangle \longrightarrow |1,1\rangle$, $|2,2\rangle \longrightarrow |2,1\rangle$ transitions of Rb.

[4] Actually, a non perfect symmetry of the coils loops generate an undesired small gradient of $\sim 4{\cdot}10^{-3}{\cdot}$ B(Gauss) Gauss/cm in the direction of the *pinch* axis.

1.4 The mixtures preparation

Feshbach resonances (both homonuclear and heteronuclear) are not possible in stretched states of the system. In order to perform experiments of spectroscopy and control of the interaction is therefore necessary to transfer the atomic species into combinations of states where resonances occur. For both the isotopic pairs, we have studied the ground state manifold: f=1 of ^{39}K and ^{87}Rb system, and f=9/2 of ^{40}K. In order to do this, after the sample is loaded into the optical trap and the magnetic potential is abiabatically switched off, we apply a 10 Gauss homogeneous magnetic field and transfer the atoms into the absolute ground state of the mixture: $|1,1\rangle\oplus|1,1\rangle$ for the pair ^{39}K-^{87}Rb, $|9/2,-9/2\rangle \oplus |1,1\rangle$ for the pair ^{40}K-^{87}Rb [5]. In the case of Bose-Bose mixture this is performed by two consecutive adiabatic rapid passages over the hyperfine transitions around 6857 MHz for ^{87}Rb and 485 MHz for ^{39}K atoms, in a 10 G homogeneous magnetic field. The preparation of the Fermi-Bose mixture employs the same procedure described above for rubidium atoms, and a 3.5 MHz rf sweep resonant with the Zeeman spacing of the ground state manifold for the fermionic potassium. In fact, at such a low field the Zeeman effect is linear, both in the case of potassium and rubidium, and Landau-Zener tunneling between the different sublevels of the hyperfine states can efficiently take place. The transfer efficiency is typically better than 90 % and the non transferred atoms are removed by means of a few microsecond blast of resonant light. Note that in the procedure the sequence of the two transfers is important in order to have a mixture always stable against *spin exchange collisions*. Such processes conserve the projection of the hyperfine angular momentum in the direction of the magnetic field, $M_F = m_{fa} + m_{fb}$. If states with internal energy lower than the initial one and with the same value of m_f exist, the system will in general undergo rapid spin-exchange decay: the internal energy released in the collision will be converted into kinetic energy, that usually exceeds the trap depth, allowing the atoms to escape from the confining potential. As an example, I report in Fig. 1.6 the energies of different combinations of Zeeman states in the Bose-Bose mixture. They are identified by the value of m_f, and the stability region of every mixture is marked with solid lines.

Most of the measurements described in the following chapters concern the absolute ground state of both mixtures. Nevertheless, in the Feshbach spectroscopy experiment we have investigated also different combinations of states. In order to do

[5] We adopt here the notation $|f_a, m_{fa}\rangle \oplus |f_b, m_{fb}\rangle$, where the first state refers to potassium and the second one to rubidium.

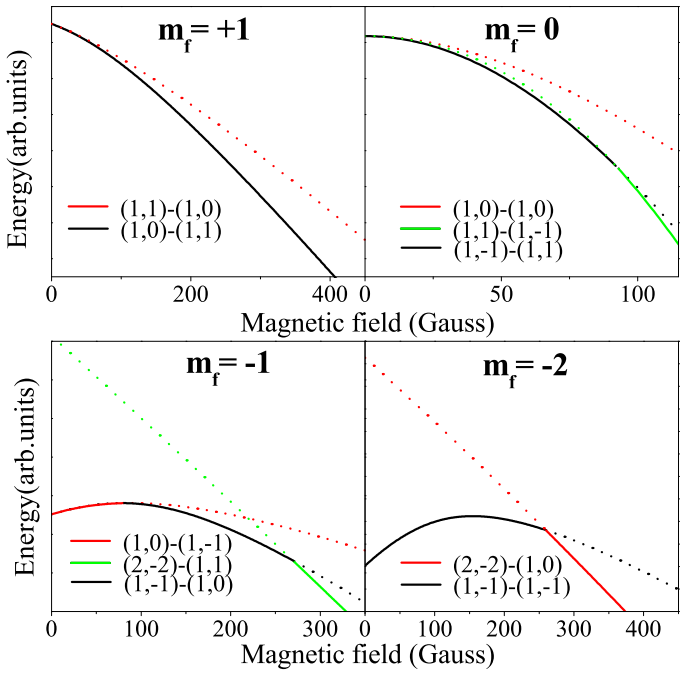

Figure 1.6: Level scheme of different spin mixtures of ^{39}K and ^{87}Rb with $m_f = +1, 0, -1, -2$. For each spin combination, the solid (dotted) line indicates the region where the mixture is stable (unstable) against spin-exchange collisions.

this, we always started from the absolute ground state mixture and performed one or more successive transitions in the linear or anomalous Zeeman regimes of magnetic field. In the latter case the spacing between the consecutive Zeeman sublevels is not constant and the rf sweep allows to populate one particular level. Moreover in the case of a mixture the two species levels under investigation must differ enough to allow the selective transfer of one species without inducing the transition in the other.

Two examples can clarify the experimental procedure: suppose that we want to investigate the Bose-Bose mixture to the $|1,-1\rangle \oplus |1,-1\rangle$ state. For low fields, the Zeeman splitting is the same for potassium and rubidium; therefore we apply a

radio frequency sweep about 7.6 MHz at the 10 G field and induce on both the atoms the transition from $|1,1\rangle$ to $|1,-1\rangle$. Suppose now we want to investigate the mixture $|1,0\rangle \oplus |1,1\rangle$: for the transfer of the potassium atoms from $|1,1\rangle$ to $|1,0\rangle$ state we ramp the magnetic field up to 38.5 G, where the Zeeman splitting of potassium and rubidium already differ by some MHz, and apply a radio frequency sweep around 28.5 MHz. In this way we do not have any Rb atom in the $|1,0\rangle$ state or any K atoms in the $|1,-1\rangle$ state.

Chapter 2

Feshbach spectroscopy

This chapter is devoted to describe the experimental work we have performed to characterize the K-Rb and ^{39}K systems by means of Feshbach spectroscopy. The experimental effort in determining the location of more than 30 resonances within the Bose-Bose and Fermi-Bose mixtures was of fundamental importance for the devising of a quantum collision model able to describe the scattering properties and the behavior of the near threshold potentials of K-Rb isotopic pairs. Only two previous works existed in this context. A first theoretical work predicted the position of Feshbach resonances within the 0-500 Gauss region in various hyperfine states [62]. Four resonances in the ground state were then discovered in an experiment at JILA, and a tentative model able to reproduce to some extend the observed pattern was proposed [63, 64]. We successively found that such model was not able to reproduce most of the Feshbach resonances we observed, indicating a need for an alternative model. The development of the model has been done by Dr. Andrea Simoni from University of Rennes, with which we have been working in very strict collaboration. The scattering properties, the resonances locations and the molecular levels close to dissociation threshold can be accurately determined for all the isotopic pairs, and this is intriguing for two reasons: the first one is that we can predict with high precision the behavior of many still unexplored mixtures; the second one is that by means of such a model, combined with information about the short range part of the interaction potential that come from photo-association studies and standard molecular spectroscopy [55, 56], one can develop schemes for efficient transfer of Feshbach molecules down to the ground state.

The homonuclear Feshbach spectroscopy we performed on ^{39}K was necessary for

having an exhaustive knowledge of the system. The investigation performed on this species allowed us to refine an already existing model, that is based on photoassociation spectra of ^{39}K, see [57, 58], data relative to shape [59] and Feshbach resonances [8, 60] in ^{40}K, and two-photon spectroscopy of ^{39}K near-dissociation molecular levels [61]. In this context, the Feshbach spectroscopy we have performed allowed enhancing the precision of the determination of the scattering parameters, and the prediction power of the model.

In order to understand the phenomena related to the physics of cold collisions, the problems concerning the development of a quantum collision model and the experimental methods we employed in our system for detecting the resonance locations, I will first dedicate few pages to recall some theoretical aspects of the problem.

2.1 Elements of theory

Although all the physics described in this thesis occur in dilute gases, atomic interactions play a major role in them: for example, they determine the shape and stability of Bose Einstein condensates, assure thermalization in the traps and therefore the efficiency of evaporative and sympathetic cooling, and they set constraints to the experimental possibilities. Since we are in the low density regime, basically *binary collisions dominate*, and then the theoretical treatment is facilitated by the simplicity of the system. Interactions between ultracold samples have become the subject of intensive study, not only because of their importance in all the areas of cold-atom physics, but also because cold-atom interaction have proved to be a powerful tool for measuring atomic and molecular parameters. Moreover, in the recent past ultracold collisions became object of a growing number of theoretical and experimental studies, since in some atomic species they can be easily manipulated employing static magnetic fields [6, 65], giving rise to new interesting phenomena.

The basic two body problem is introduced in its general aspects; the notion of cross section and scattering length, collision channels, near threshold molecular levels, and Feshbach resonance are briefly discussed. Even if in the Chapters 3 and 4 the discussion will be done within the standard *mean field* treatment and therefore the real shape of the two body hamiltonian will be somehow washed out, also there concepts like scattering length and interatomic interaction will play a crucial role, and can be derived from the microscopic treatment of the problem that follows. I will try here to give just the essential notions needed to understand the experimental and theoretical work that has been done in the context of this thesis. For

further information and exhaustive description of the general problems described in the following, standard books of quantum mechanics and molecular physics can be consulted [66, 67].

2.1.1 Two-body hamiltonian and scattering theory

The starting point for describing two colliding particles of masses M_1 and M_2 is the following hamiltonian:

$$H' = \frac{p_1^2}{2M_1} + \frac{p_2^2}{2M_2} + V(\mathbf{r_1} - \mathbf{r_2}) \tag{2.1}$$

This can be easily decomposed within two parts related to the center of mass motion and the relative motion:

$$H' = \frac{P^2}{2M} + (\frac{p^2}{2\mu} + V(\mathbf{r})) \tag{2.2}$$

where μ is the reduced mass of the system and $\mathbf{r} \equiv \mathbf{r_1} - \mathbf{r_2}$. Therefore the binary collision can be described as a *single particle* quantum mechanical problem. All the information about the properties of the colliding pair are carried by the interaction potential $V(\mathbf{r})$. One has therefore to treat the time independent Schrödinger equation

$$H\psi(\mathbf{r}) = E\psi(\mathbf{r}) \tag{2.3}$$

H being the second term in eq. (2.2), and extract the eigenvalues of the system: the bound and the continuum states of the system fully characterize the properties of the colliding pair.

Since general issues can be derived even without any information on the interaction potential, and since several important notions will be deeply used in the following, let's briefly reconstruct some of the most important results of the *scattering theory*. We look for stationary states $\psi_{\mathbf{k}}(\mathbf{r})$ that solve eq. (2.3) that have the asymptotic form

$$\psi_{\mathbf{k}}(\mathbf{r}) \sim e^{i\mathbf{k}\cdot\mathbf{r}} + f(k, \mathbf{n}, \mathbf{n}')\frac{e^{ikr}}{r} \tag{2.4}$$

relative to eigenvalues $E_k = \hbar^2 k^2/2\mu$. Here $\mathbf{n} \equiv \mathbf{k}/k$ and $\mathbf{n}' \equiv \mathbf{r}/r$. This kind of solutions have an intuitive meaning: the first part of (2.4) represents an incident plane wave propagating with wave-vector $\mathbf{k}$, while the second one is the diffuse wave. The amplitude of the diffuse wave, $f(k, \mathbf{n}, \mathbf{n}')$ is called *the scattering amplitude* and assumes the general implicit form [67]:

$$f(k, \mathbf{n}, \mathbf{n}') = -\frac{\mu}{2\pi\hbar^2}\int \exp(-i\mathbf{k}'\cdot\mathbf{r}')V(\mathbf{r}')\psi_{\mathbf{k}}(\mathbf{r}')d^3r' \tag{2.5}$$

where $\mathbf{k}' \equiv k\mathbf{n}'$. This is related in a very simple way to the *differential* and *total scattering cross-section*:

$$\frac{d\sigma}{d\Omega} = |f(k, \mathbf{n}, \mathbf{n}')|^2; \quad \sigma(k, \mathbf{n}) = \int |f(k, \mathbf{n}, \mathbf{n}')|^2 d^2n' \tag{2.6}$$

The solution of such a 3D problem is in general non trivial. Fortunately, in many real cases one works with potentials that have a central symmetry:

$$V(\mathbf{r}) = V(r) \tag{2.7}$$

In this case the hamiltonian H commutes with the angular momentum l and the 3D original problem reduces to a 1D problem for the radial wavefunction. In fact, since

$$[H, l] = 0 \tag{2.8}$$

a simultaneous set of eigenvectors of H and l exists. In this case we can separate the generic function in a radial and an angular part and therefore write it in the following form:

$$\psi_{\mathbf{k}}(\mathbf{r}) = \sum_{l=0}^{\infty} \sum_{m=-l}^{m=l} Y_{l,m}(\theta, \phi) \frac{u_{k,l,m}(r)}{r} \tag{2.9}$$

where ϕ is the azimuthal angle and $Y_{l,m}(\theta, \phi)$ are the spherical harmonic functions (i.e. the eigenfunctions of the angular momentum l). Therefore the problem (2.3) reduces to solve for every k, l, m Eq.

$$u''_{k,l,m}(r) + (k^2 - \frac{l(l+1)}{r^2} - \frac{2\mu V(r)}{\hbar^2}) u_{k,l,m}(r) = 0 \tag{2.10}$$

At the beginning we said that we were interested to find states with asymptotic behavior (2.4): we can rewrite this condition now decomposing the function in terms of eigenstates of the angular momentum. We can assume the incoming plane wave directed along the z axis without losing generality, and this is eigenvector of the l_z operator with eigenvalue $m = 0$. Its expansion in terms of spherical harmonic functions (that reduce to Legendre polynomials in the case $l_z = 0$, not depending on the azimuthal angle φ) is well known:

$$e^{ikz} \simeq \frac{1}{2ikr} \sum_{l=0}^{\infty} (2l+1) P_l(\cos\theta)((-1)^{l+1} e^{-ikr} + e^{ikr}) \tag{2.11}$$

As a consequence of the conservation of l_z for every r, also the function in the expansion (2.9) will not depend on the azimuthal quantum number; and based on

the behavior (2.11) of the plane wave, $\psi_{\mathbf{k}}(\mathbf{r})$ will have the form:

$$\psi_{\mathbf{k}}(\mathbf{r}) \simeq \frac{1}{2ikr}\sum_{l=0}^{\infty}(2l+1)P_l(\cos\theta)((-1)^{l+1}e^{-ikr}+\alpha_l e^{ikr}) \tag{2.12}$$

Since the conservation of the flux must be satisfied for every partial wave in the case of spherical symmetry, necessarily $|\alpha_l| = 1$ for every l, i.e.

$$\psi_{\mathbf{k}}(\mathbf{r}) \simeq \frac{1}{2ikr}\sum_{l=0}^{\infty}(2l+1)P_l(\cos\theta)((-1)^{l+1}e^{-ikr}+e^{i2\delta_l}e^{ikr}) \tag{2.13}$$

For every l contribution, the knowledge of δ_l solves the scattering problem. Let's compare the expression (2.13) with the asymptotic behavior (2.4), considering that (2.11) is valid: in terms of the phases δ_l we then obtain

the asymptotic behavior of the radial wavefunction:

$$u_{k,l,m}(r) \propto (-1)^{l+1}e^{-ikr}+e^{2i\delta_l}e^{ikr} \tag{2.14}$$

the scattering amplitude:

$$f(k,\theta) \;=\; \frac{1}{2ik}\sum_{l}(2l+1)(e^{2i\delta_l}-1)P_l(\cos\theta) \tag{2.15}$$

the scattering cross-section $\sigma(k)$:

$$\sigma(k) \;=\; \sum_{l=0}^{\infty}\sigma_l(k) \tag{2.16}$$

having defined the partial wave contributions as

$$\sigma_l(k) \;=\; \frac{4\pi}{k^2}(2l+1)\sin^2\delta_l(k) \tag{2.17}$$

In the case of two identical colliding particles, all the expressions derived above in terms of partial wave expansion must be modified, taking into account the symmetry (antisymmetry) properties of the pair of bosons (fermions) under the particle exchange. Remember that the Legendre polynomials have $(-1)^l$ parity: it is then clear that the expansion for identical bosons (fermions) will contain only even (odd) waves. Moreover a factor of 2 appears in the formulas for the cross section, arising from the (anti)-symmetrization of the wavefunction; therefore for identical particles we have that:

$$\sigma(k) = \frac{8\pi}{k^2}\sum_{even,odd}(2l+1)\sin^2\delta_l \tag{2.18}$$

Some important results can be derived from this expressions. It is possible to demonstrate that in the limit of vanishing k the phases δ_l have the following behavior

$$\delta_l(k) \approx k^{2l+1} \quad for\, k \to 0 \tag{2.19}$$

Note In fact, for a spherical potential that vanishes as $r^{-\alpha}$ for $r \to \infty$, the behavior indicated above is valid only if $\alpha > 2l + 3$. Otherwise the behavior is different and one can find that $\delta_l(k) \approx k^{\alpha-2}$. Note that in the case of potentials decreasing with $\alpha \leq 3$ this behavior causes that **all partial waves contribute at low energy!** I will come back on this point in subsection (2.2.2), where I'll show how this fact can have important consequences on the scattering properties of the system.

In all the other cases, from eq. (2.19) it follows that for low energies the nonzero contribution to the total scattering cross section will be given just from few partial waves, and in the limit of *zero energy* only s-wave scattering will take place. This causes two consequences: the scattering process in the limit of *zero energy* is isotropic[1], and collisions result fully suppressed in the case of two identical fermions. Within this regime, the corresponding cross section for distinct particles (bosons) can be written in terms of the *s-wave scattering length* as:

$$\sigma_{l=0}(k) = (2\times)4\pi a^2 \quad for\, k \to 0 \tag{2.20}$$

being the *s-wave scattering length*

$$a = -\lim_{k\to 0} \frac{\tan \delta_0(k)}{k} \tag{2.21}$$

Note that the concept of *s-wave scattering length* is crucial in general in the field of cold gases: provided that the gas is in the dilute regime (i.e. $n|a|^3 \ll 1$, where n is the spatial density of the gas) and that it is cold enough to be in the region of validity of (2.20), it can be shown that the many body description of the system depends *only* on the scattering length and *not* on the details of the interaction potential. This means that if two distinct interatomic potentials generate the same scattering length, they lead to the same properties for the atomic system, even if they have a completely different microscopic shape (e.g. one being attractive and the other being repulsive)!

[1] This could also be deduced from the general form of the scattering amplitude (2.5); the only contributions to the integral are from $\mathbf{r}'$ inside the sphere of action of the potential delimited by the range b of the potential, i.e. $|\mathbf{k}' \cdot \mathbf{r}'| \leq kb$. As $k \to 0$ we have that $kb \ll 1$, and therefore one can replace $\exp(-i\mathbf{k}' \cdot \mathbf{r}')$ by 1, i.e. the integral in (2.5) is independent of the scattering direction $\mathbf{n}'$. Since the problem is time reversal symmetric, i.e. $f(k, \mathbf{n}, \mathbf{n}') = f(k, -\mathbf{n}', -\mathbf{n})$, one derives that $f(k, \mathbf{n}, \mathbf{n}')$ is independent also of the incident direction, and therefore the scattered wave is spherical.

2.1.2 A simple model case: the square potential well

Let's apply now the results described in the subsection 2.1.1 to the simple case of a square potential well. The results related to such a toy model are easy to be derived but at the same time extremely general: therefore, even if the problem is very well known and can be found in several standard books of quantum mechanics (see e.g. [67, 68]), I'll spend some pages about it in this section.

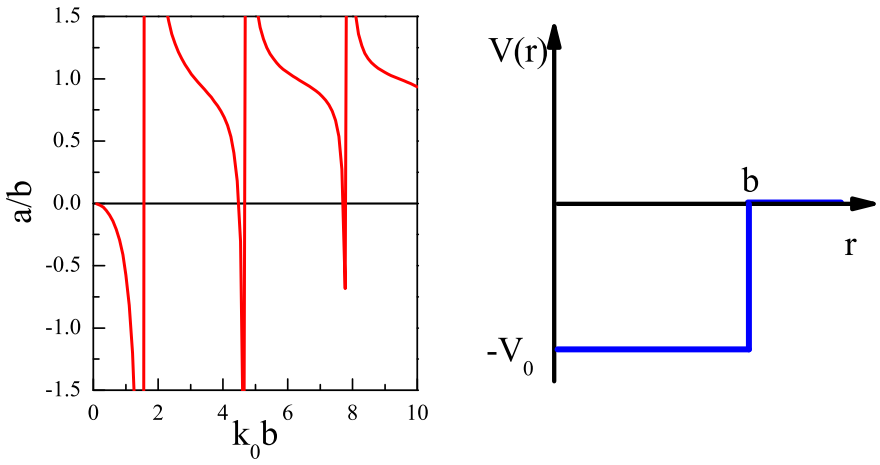

Figure 2.1: (a) Scattering length as a function of the parameter $k_0 b$. The scattering length can be either positive or negative: it diverges for values of k_0 corresponding to the appearance of a bound state. (b) Square potential well.

Consider a potential of the form

$$V(r) = \begin{cases} -V_0 & \text{if } r < b \\ 0 & \text{otherwise} \end{cases}$$

and look for the solution with zero energy of the 1D Schrödinger equation for s-wave scattering (2.10):

$$u''(r) - \frac{2\mu V(r)}{\hbar^2} u(r) = 0 \tag{2.22}$$

with asymptotic behavior deduced from (2.14):

$$u(r) \sim r - a \quad \text{for large r} \tag{2.23}$$

The result is immediately derived:

$$u(r) = \begin{cases} C_1(r-a) & \text{if } r < b \\ C_2 \sin(k_0 r) & \text{otherwise} \end{cases}$$

$k_0 \equiv \sqrt{2\mu V_0}/\hbar$. The continuity of the wavefunction and of its first derivative at the boundary b requires that:

$$a = b - \frac{\tan(k_0 b)}{k_0} \tag{2.24}$$

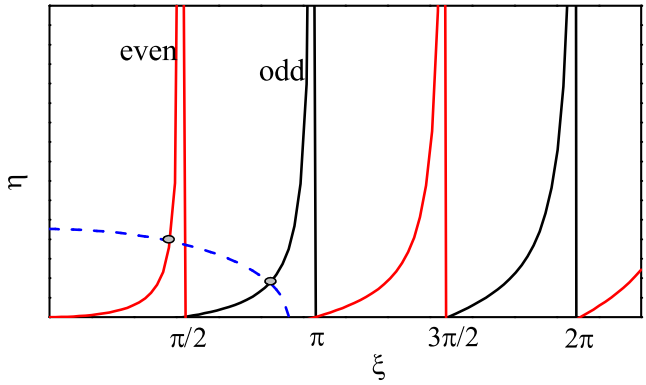

Figure 2.2: Graphic solution of the determination of bound states of the 1D well potential. The red (black) line refers to the boundary conditions for the even (odd) eigenvectors. The blue line is the graph of eq. (2.2): every intersection of the blue line with the red (black) one indicates the presence of an even (odd) bound state. In the case of a spherical potential well only the odd functions must be taken into account, therefore only potentials deep enough can support at least a bound state.

From this toy model some basic and general ideas can be derived. Note the following points:

- If the well is small, $k_0 b < \pi/2$ and the scattering length is negative. This condition is equivalent to have a scattering potential too low for supporting a bound state.

  This fact can be derived with the standard treatment of the quantum mechanics, reaching the solutions of the eq. (2.22) at negative energy values $-E$,

$E \in (0, V_0)$. In the case of the purely 1D well for $-b < x < b$ one can separate the eigenfunctions of the system into odd and even. The result is the following:

$$\psi_{odd}(x) = \begin{cases} B\exp(-k|x|) & \text{if } |x| > b \\ A\text{sin}(k'r) & \text{otherwise} \end{cases}$$

$$\psi_{even}(x) = \begin{cases} B\exp(-k|x|) & \text{if } |x| > b \\ A\text{cos}(k'x) & \text{otherwise} \end{cases}$$

being $k \equiv \sqrt{2\mu(V_0 - E)}/\hbar$ and $k' \equiv \sqrt{2\mu E}/\hbar$. The conditions of continuity of ψ and ψ' at $|x| = b$ require that:

$$k'/\tan(k'b) = -k \quad \text{for odd functions}$$

$$k'/\tan(k'b) = k \quad \text{for even functions}$$

The problem can be solved with a graphic method, introducing the variables

$$\eta \equiv k'b, \quad \xi \equiv kb$$

in terms of which, the two boundary conditions above are given by

$$\eta = -\xi\tan\xi\,(odd)\ \ \eta = \xi\tan\xi\,(even)$$

From the definitions of k and k' one has also

$$\xi^2 + \eta^2 = \frac{2\mu V_0 b^2}{\hbar^2} \tag{2.25}$$

The result is plotted in Fig. (2.2). The abscissa corresponding to the intersection between the two curves and the circumference (2.25) give us the values of k' that satisfy the boundary conditions. The number of bound states is always finite and in the purely 1D problem the potential always supports one (even) bound state; the first odd bound state appears as $\sqrt{2\mu V_0}/\hbar = \pi/2$. This is exactly the condition found above for the 3D problem: in this case, in fact, the even reduced wavefunctions must be excluded, since a total even wavefunction would exhibit a singularity in $r = 0$.

- Increasing the depth of the potential one reaches the condition for which the first bound state appears at threshold: this is accompanied by a divergence of the scattering length. And this happens every time that $k_0 b = (2n+1)\pi/2$: the appearance of a bound state in the potential well is related to a divergence of the scattering length, see (2.24). This relation is general and is known as *Levinson's Theorem*.

- When V_0 is slightly lower than the value required for the appearance of a new bound state at threshold, the scattering length a is large and negative; if, instead, it is slightly above this threshold the scattering length is large and positive (see Fig. 2.1). This result is also absolutely general.

Both these properties will be recovered in the real situations.

2.1.3 The real case

In real systems the problem we treated in the last subsections become definitively more complex for two main reasons. The first is that one has to consider the colliding particles not as simple point-like masses M_1 and M_2, but as atoms, composed of electrons and nuclei. The treatment is performed then within the Born Oppenheimer approximation: at first, one has to solve the electronic problem and extract the eigenvalues parameterized in terms of the positions of the nuclei; and after one inserts these eigenvalues in the hamiltonian of the relative motion of the two nuclei as an effective potential. The second one is that this potential is not known and therefore, before starting to solve the eq. (2.2) for the nuclei, one has to *construct* it. The complexity of the problem makes fully *ab initio* calculations of the scattering properties of a real system impossible, unless in the simplest case of Hydrogen collisions. The standard procedure that is used in order to treat these kind of problems is the following:

- Theoreticians construct a microscopic potential to insert in the hamiltonian from *ab initio* calculations.
- Experimentalists measure the spectra of the system by means of optical and Feshbach spectroscopy.
- Based on the spectroscopic measurements theoreticians refine the potential shape, adjusting the system parameters in order to reproduce as closely as possible the experimental data.

Let's see here more in detail the interactions that take place when the colliding particles come close one to each other.

First of all, when we treat the process of collision of a pair of cold alkali atoms, we have to consider that in general the kinetic energy of the pair can be orders of magnitude less than the hyperfine and Zeeman energy splitting $E_{kin} \ll E_{hf}, \Delta E_Z(B)$, and therefore the scattering properties of the system will depend both on the hyperfine

and Zeeman states of the two colliding particles. As convention we adopt here the notation $|f, m_f\rangle$ for describing the internal state of an atom immersed in a magnetic field, indicating both the Zeeman level and also the hyperfine level at which it adiabatically correlates as $B \to 0$. Moreover, in the reduced mass system, the particles will have in general an orbital momentum l, and projection m_l, characterizing the scattering process. We will indicate the generic *scattering channel* with the notation

$$\alpha \equiv \{f_1, m_1, f_2, m_2, l, m_l\} \tag{2.26}$$

specifying the quantum numbers that describe the two atoms system when the particles are initially separated. Note that as already mentioned in sec. 2.1.1 identical bosons (fermions) can have only symmetric (antisymmetric) wave functions with respect to a pair permutation: this is indicated by the braces. 2.26 is usually indicated as *separated atom spin basis* description of the scattering channel. The energy associated to the generic α-channel is $E_\alpha = E_{f_1 m_1} + E_{f_2 m_2}$: a channel is called *closed* (*open*), if its energy is larger (smaller) than the energy E of the entrance channel. If $E < E_\alpha$ for all α, then all the channels are closed and E can refer just to molecular discrete levels. If instead it exists one α for which $E > E_\alpha$, then at least one channel is open and E is associated to a stationary state of the continuum.

The great complexity of the two body problem in the case of alkali atoms arises from the fact that at short distances the different channels couple one to each other by means of the interaction potential, and therefore the hamiltonian is no more diagonal in the separated atom spin basis: this means that the various channels are intrinsically coupled.

In order to solve the problem one has to consider many coupled Schrödinger equations for the different channels; defining the radial wavefunction of the α channel as $\psi_\alpha(r, E) = u_\alpha(r, E)/r$ following the partial wave expansion (2.9) one has:

$$\frac{\partial^2 u_\alpha(r, E)}{\partial r^2} + \frac{2\mu}{\hbar^2} \sum_\beta [E\delta_{\alpha\beta} - V_{\alpha\beta}] u_\beta(r, E) = 0 \tag{2.27}$$

where $V_{\alpha\beta}$ has the following form:

$$V_{\alpha\beta}(r) = [E_{f_1 m_1} + E_{f_2 m_2} + \frac{\hbar^2}{2\mu r^2} l(l+1)]\delta_{\alpha\beta} + V^{int}_{\alpha\beta}(r) \tag{2.28}$$

The complex part of the scattering is inside the interaction matrix $V^{int}(r)$, that contains the Born Oppenheimer potentials and electron spin dependent interactions. This matrix can be divided into other parts:

$$V^{int}(r) = V_{el}(r) + V_{ss}(r) \tag{2.29}$$

The first one describes the interactions between the electronic clouds of the atoms, and it gives the main effect. At short distances strong coupling between electronic spin occur, giving rise to singlet (${}^1\Sigma^+_{(g)}$) and triplet (${}^3\Sigma^+_{(u)}$) states, with a (g, u) symmetry that is present only in the homonuclear case. Therefore V_{el} can be conveniently written in the form:

$$V_{el}(r) = V_0(r)P_0 + V_1(r)P_1 \tag{2.30}$$

where $P_{0,1}$ are the projectors onto the subspaces with total electronic spin $S = 0, 1$ and

$$V_S(r) = -(\frac{C_6}{r^6} + \frac{C_8}{r^8} + \frac{C_{10}}{r^{10}} + ...) - (-1)^S V_{exch} \tag{2.31}$$

the two potentials differing of twice an exchange potential that has an asymptotic behavior [69]:

$$V_{exch}(r) \sim Jr^{\frac{7}{2\alpha}-1} \exp^{-2\alpha r} \tag{2.32}$$

The above contributions to the potential maintain some symmetry properties:

- the system is invariant under independent rotation of the spin system and of the orbital system around the quantization axis, and therefore m_l, m_F are good quantum numbers.
- Since both $V_0(r)$ and $V_1(r)$ are central, the orbital angular momentum $\mathbf{l}$, is conserved.

As a consequence, this first part is a block diagonal matrix, each block having a well defined l value.

The second part of the potential describes the (weak) interaction between the electronic spins via their magnetic moments, and contributions deriving from second order spin orbit interactions [2]. Both the contributions have a functional form:

$$V_{ss}(r) = f(r)[\mathbf{s_1} \cdot \mathbf{s_2} - \mathbf{3}(\mathbf{s_1} \cdot \hat{\mathbf{r}})(\mathbf{s_2} \cdot \hat{\mathbf{r}})] \tag{2.33}$$

where asymptotically

$$f(r) \sim \begin{cases} 1/r^3 & \text{for dipole dipole interaction} \\ \exp(-\beta(r - r_S) & \text{for second order spin orbit interaction} \end{cases}$$

The V_{SS} contribution is weak but not negligible, and must be taken into account. It is not diagonal both in f_1, m_1, f_2, m_2 and in l, m_l. Since it is a tensor of rank 2, it can

[2] In the case of ground state alkali atoms the first order spin orbit contribution $V_{SO} \sim \sum_i \mathbf{l_i} \cdot \mathbf{s_i}$ is zero, since $l_i = 0$.

couple blocks corresponding to $l' = l$ and $l' = l \pm 2$ for Wigner-Eckart theorem [70]. Therefore it couples many states.

The resulting matrix is a three-diagonal block matrix of the form shown in Fig. 2.3.

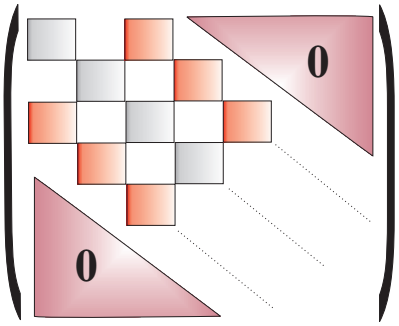

Figure 2.3: Schematic form of the interaction potential developed in the separated atom spin basis. Every gray block corresponds to a well defined value of the orbital momentum; the red blocks correspond to coupling between l and $l \pm 2$ due to the V_{SS} potential.

Since the interaction potential couples different scattering channels as the internuclear distance become small, it is sometimes useful to indicate the state we are referring to in terms of other short range basis. We can couple $\mathbf{s_1}$ and $\mathbf{s_2}$ to form a total spin $\mathbf{S} = \mathbf{s_1} \oplus \mathbf{s_2}$; the same can be done for the nuclear spins, that generate a total nuclear spin $\mathbf{I} = \mathbf{i_1} \oplus \mathbf{i_2}$. Then $\mathbf{S}$ and $\mathbf{I}$ can couple each other and create $\mathbf{F}$, that further couples to the orbital momentum $\mathbf{l}$ to give the total angular momentum of the dimer $\mathbf{F_{TOT}}$. Therefore we can treat the problem also in terms of the molecular basis $(S, I)F, l, F_{TOT}, M_{TOT}$, taking advantage that at short range the electronic part of the potential is diagonal in S.

2.1.4 The Feshbach resonance

In subsection 2.1.2 we have seen how the vicinity of a bound state at threshold can cause a strong modification in the scattering length value: the phenomenon is well known and indicated as zero energy scattering resonance. In general the situation of a bound state E_b nearly resonant with the entrance channel E_α might appear quite difficult to be experimentally observed: instead, at least in some real cases, and in particular for all alkali atoms, this situation can be easily achieved, by ac-

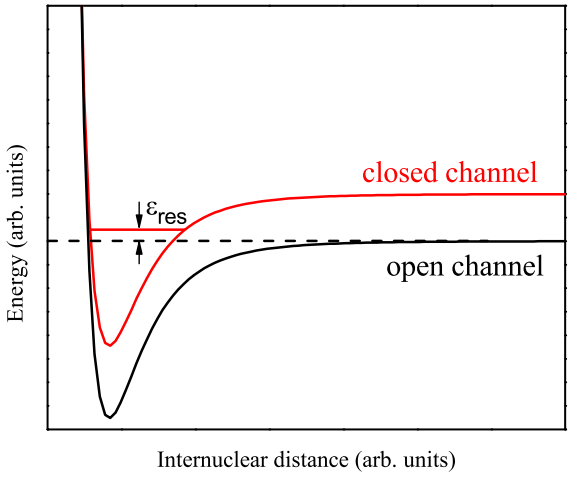

Figure 2.4: The scheme of how a Feshbach resonance arises. The energy detuning between a bound molecular level and the threshold of the two colliding atoms can be tuned by means of the external magnetic field.

tively tuning the entrance channel energy with respect to the bound state level. In fact, since the atoms have a Zeeman splitting when a magnetic field is applied, and the energies of different channels usually vary in different ways as functions of the field, i.e. $\partial E_\alpha/\partial B \neq \partial E_\beta/\partial B$, it might happen that a bound state supported by a closed channel becomes resonant with the entrance channel threshold. This situation is what is called a magnetic Feshbach resonance and that is schematically indicated in Fig. 2.4. In general we will refer to $\partial E_\alpha/\partial B$ as the *magnetic moment* of the channel α, and it is usually indicated as μ_α. The magnetic field dependence of the scattering length in the vicinity of a magnetic resonance can be described by the well known approximate formula [72]:

$$a(B) = a_{bg}(1 - \frac{\Delta}{B - B_0}) \tag{2.34}$$

a_{bg} being the scattering length far from the resonance, B_0 the center of the resonance, $\Delta \equiv B_{ZC} - B_0$ the width of the resonance, and B_{ZC} the point at which the scattering length vanishes, called *zero crossing*.

The experimental ability to bring two colliding particles resonant with a molecular bound state allows three main kind of phenomena to occur, as I already mentioned in the Introduction: it opens the way to the association of ultracold molecules, if one is able to adiabatically transfer the unbound pair across the resonance onto the molecular level [10, 11, 12]; it offers the possibility to control the interaction, since the real case does not differ very much from the toy model case of Fig. 2.1: one can in principle scan values of the scattering length from very negative to very positive, just tuning the molecular level above or behind the threshold shifting it via Zeeman effect. Finally - and this is what I'm going to report herein- the knowledge of the location of Feshbach resonances allows to refine quantum collision models, and offers the possibility to have very precise information about the scattering properties of a system.

2.1.5 Three body losses

Up to now, in the discussion about cold collisions between two atoms I spoke about scattering events that are *elastic*. Actually, if we consider the realistic potentials of subsection 2.1.3, both elastic and inelastic scattering processes can be supported (see e.g. [71]). In general, three kind of inelastic processes can take place in a real atom trap:

- Collisions of the trapped atom with the background gas: they induce an exponential decay of the number of trapped particles, $\dot{N} = -N/\tau$.
- Two body spin relaxation: atoms trapped into a magnetic potential have their magnetic moment antiparallel to the field (low field seekers), and therefore the atom-field interaction is given by: $-\mu \cdot \mathbf{B} = \mu B$. The dipolar interaction between two magnetic moments, see (2.33), can induce a spin flip of one of the two colliding atoms. It can be derived that this process release an amount of energy of the order of μB, see e.g. [73]: consequently, since this energy can greatly exceed the trap depth, the process induces losses of atoms.
- Three body recombination: when three atoms are closed enough, two of them can form a molecule, and the third one carries away the released momentum and energy. They induce a decay of the form:

$$\dot{n} = -K_3 n^3 \tag{2.35}$$

  This process usually causes losses from the trap, since the energy of the resulting particles exceeds the trap depth. At the same time it can cause a heating of

the remnant sample, since the recombination takes place preferentially into the more dense (and cold) part of the gas, and losses concern mostly the coolest particles. This can be seen if one considers the mean potential energy associated to a thermal atom (at temperature T) trapped in a harmonic potential and undergoing a three body process:

$$\langle U \rangle = \frac{\int U n^3 dV}{\int n^3 dV} = \frac{1}{2} k_B T \tag{2.36}$$

This energy is less than the mean potential energy in the gas $\frac{3}{2}k_B T$; therefore every atom lost by means a three body process releases in the system an excess energy $k_B T$. Consequently, the temperature associated to the remnant gas is higher than the starting one. I will come again to speak more in detail about three body processes in Chapter 3 and Chapter 4, showing two cases where the three body recombination doesn't produce any heating, or even it can have a cooling effect on the sample. In general, at very large scattering lengths values, one has to consider that an extra heating occurs due to the vicinity of a molecular level of energy ε to the dissociation threshold. In this case, not only the process takes place preferentially within the more dense part of the cloud, but the molecule and the third atom produced after collision have kinetic energies $\varepsilon/3$ and $2\varepsilon/3$ respectively, that can be smaller than the trap depth. Consequently, the products of the collision can remain in the trap: the molecule collides rapidly with a fourth atom and decays on a deeply bound state, releasing a large energy and escaping from the trap, while the atom involved in the first collision remains in the sample with the extra energy $2\varepsilon/3$ [74].

In particular, V_{el} is responsible for elastic scattering and inelastic spin-exchange collisions, and gives rise to the broadest resonances; V_{ss}, instead, is responsible for inelastic spin dipolar relaxation and originates narrow resonances.

Both broad and narrow resonances are accompanied by an increment of the three body losses, as one approaches the center of the resonance: in fact it has been shown both theoretically [75] and experimentally [74] that the three body coefficient scales as $K_3 \sim a^4$; therefore, the divergence of the scattering length at resonance causes a raise in the number of three body processes. This seriously limits the possibilities to exploit the resonance for tuning the scattering length in regions of very strong interactions; nevertheless, losses and heating can be exploited as an indication of the presence of a Feshbach resonance, and this is what is usually done in Feshbach spectroscopy.

2.2 Interisotope Feshbach spectroscopy on K Rb mixtures

2.2.1 Detection of the resonances: three body losses and molecule association

We have performed extensive Feshbach spectroscopy in the K-Rb mixtures we have in our apparatus, following the idea described at the end of last section. The starting point of the experiment is the following: a mixture of spin polarized potassium and rubidium atoms held in an optical trap, with a temperature around $800 - 1000$ nK, immersed in a magnetic field. Once the desired mixture is prepared, we change the external magnetic field in few tens of ms and actively stabilize it to any value between 0 and 1000 G. Heteronuclear Feshbach resonances are detected as an enhancement of three-body losses. We look at the mixture populations after some time spent in the trap[3] as a function of the magnetic field, and locate the resonances as absorbtion-like peaks in the atom numbers. A typical feature indicating the presence of a Feshbach resonance is shown in Fig. 2.5: this corresponds to an s-wave resonance between $|9/2, -7/2\rangle$ and $|1, 1\rangle$ states of the Fermi Bose mixture located around 598 Gauss. Despite the change of sign of the scattering length on the two sides of the resonance, the behavior is more or less symmetric and we fit it with a Gaussian function. Note that the width associated with three body losses is not connected to the width Δ, at least not in a trivial way. Nevertheless this is an important parameter that we employed in the fitting procedure for developing our model (see below). In general, in the Fermi-Bose mixture, fermion-fermion-boson ($F + F + B$) collisions are suppressed by effects related to the statistics [81]: in fact, since the possibility of having these processes depends on the probability to have the three particles sufficiently close one to the others, the $B + B + F$ processes are more probable than the $B + F + F$ ones. One has therefore to expect twice the losses for rubidium than for potassium. In the Bose-Bose mixture this does not take place, and the losses are "symmetric" in the two species.

At the typical temperatures of the mixture thermal broadening [76] is already negligible: nevertheless, for an accurate detection of also weak features, such as the resonances near 248 G in the $|1, 1\rangle$-$|1, 1\rangle$ Bose-Bose mixture or the one located at 674 G in $|1, 0\rangle$-$|1, 1\rangle$ collisions, see Tab. 2.2, we have performed studies also at lower tem-

[3] The time we wait can vary from one resonance to another, depending on their *strength* and on the conditions of temperature and densities they are investigated. Typically it varies between 1 second for weak resonances/ very dilute samples, to few tens of ms, in the case of strong features/nearly degenerate samples.

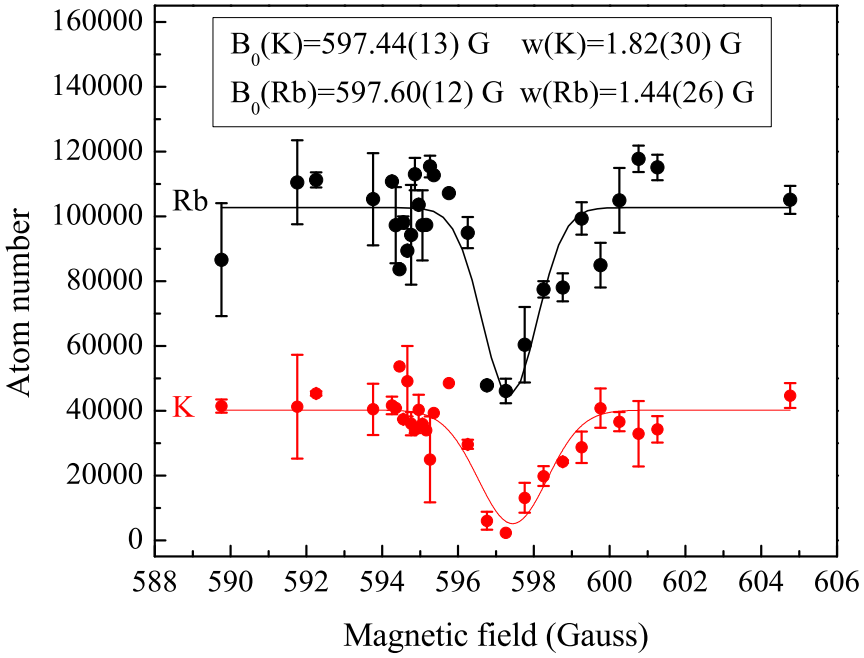

Figure 2.5: Standard detection of a Feshbach resonance, by looking at three body losses. Both samples, after some time spent in the trap immersed in the external magnetic field, have lost atoms when the interspecies scattering length is increased towards very large values.

peratures (250-350 nK) and higher densities. These experimental conditions allow to reduce the waiting time necessary to get a good spectroscopic signal, and are crucial for resolving p-wave resonances, as it will be discussed in the next subsection. The mixture is cooled by reducing the trap depth in 2.4 seconds with an exponential ramp in the power of the two laser beams. As already mentioned, the optical potential is designed in such a way to force evaporation of rubidium along the vertical direction, while potassium is sympathetically cooled without significant atom losses.

An alternative way to detect the location of Feshbach resonances with high precision is to associate molecules by an adiabatic sweep across the feature [77]: the

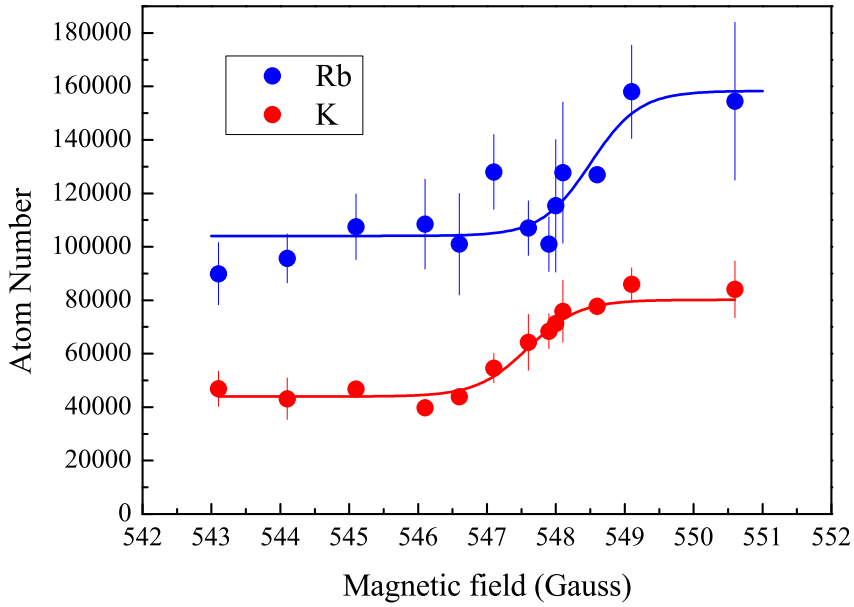

Figure 2.6: Detection of the s-wave Feshbach resonance in the Fermi-Bose mixture between $|9/2, -9/2\rangle$ and $|1, 1\rangle$ located around 546 Gauss by looking at molecule association. We perform a sweep in the magnetic field, from the region of negative scattering length to positive scattering length, adiabatically transferring the atom pairs in the entrance channel into weakly bound dimers. The dimers that are created cannot be detected by the imaging light and they appear as losses in the atom populations.

application of this method leads to measurements like the one shown in Fig. 2.6. In this case, we perform linear sweeps in the magnetic field, slow enough to be sure of the adiabaticity of the process, but fast enough to avoid three body processes to affect the populations of the mixture. The final value of the field is varied and suddenly after the end of the sweep we take an absorption image of the atoms. Since the sweep transfers the unbound pairs onto the molecular state, the imaging light - resonant with the atomic transition - is not able to detect the dimers, already for small magnetic field detunings; moreover, the dimers are lost within few hundreds

microseconds by via atom molecule collisions (see Chapter 3). The resulting behavior is fitted with a Boltzmann growth function, from which we deduce the resonance center. Note that this detection method in principle is not accompanied by heating, unless the sweep rate is too slow, or you wait for too long before acquiring the image, letting three body processes take place. All Feshbach resonances experimentally detected both in the Fermi-Bose and Bose-Bose mixtures are summarized in first column of tables 2.1 and 2.2.

2.2.2 Detection of p-wave resonances

I have previously pointed out that at ultralow temperatures all $l \neq 0$ partial waves do not contribute to the total scattering cross section, unless the interaction potential has an asymptotic behavior $r^{-\alpha}$, $\alpha \leq 3$, see the note in subsection 2.1.1: in this case, all partial waves contribute to the total cross section even for $T \to 0$. This happens in the case of p-wave resonances, in contrast to s-wave features: in fact, they experience a non vanishing contribution of dipole dipole interaction in lowest order, that has a r^{-3} dependence and that is contained in V_{SS}, see section 2.1.3, that makes p-wave scattering possible even at very low temperatures.

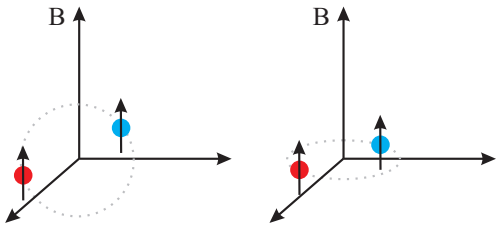

Figure 2.7: Schematic representation of classical dipoles interacting in different circular orbits. In the first picture is shown the case of an orbit with $m_l = 0$, which is in a plane containing the magnetic field. Here the dipoles sometimes attract and sometimes repel each other. In the second picture is shown an orbit with $|m_l| = 1$, in a plane perpendicular to the magnetic field. Here the dipoles predominately repel one another.

$l = 1$ Feshbach resonances exhibit two main behaviors that differentiate them from the s-wave case:

- The presence of a centrifugal barrier (the interaction potential (2.28) has the repulsive contribution $\hbar^2/2\mu r^2$) through which the wavefunction must tunnel to access the resonant state makes the scattering process extremely sensitive

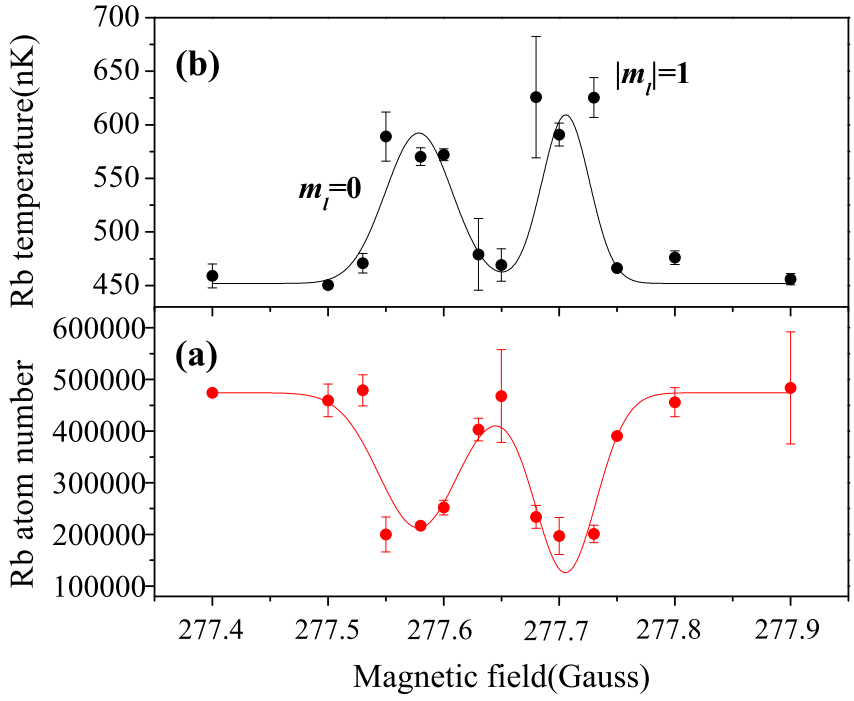

Figure 2.8: (a): Experimental Rb loss features due to a ^{39}K-^{87}Rb heteronuclear $|1,1\rangle + |1,1\rangle$ p-wave resonance. The doublet structure is peculiar of the p-wave character of the resonance. Losses are accompanied by heating of the sample, as shown in panel (b). A similar behavior has been observed on the potassium cloud.

on temperature and on magnetic field: only within a narrow region of these parameters the continuum wavefunction can be influenced significantly by the bound state.

In ref. [76] the peculiarities of higher order partial wave resonances in a Fermi gas of ^{40}K have been investigated. In particular, the authors remark a non trivial behavior of these features with respect to the temperature of the sample, showing a sudden raise of the cross section as temperature is lowered, and a high dependence of the tails of the resonance to thermal broadening, which grows dramatically as the temperature increases. The raise of the scattering

cross section takes place from the sudden appearance of a narrow resonance at positive collision energies as the magnetic field is tuned, and it is not temperature dependent. By contrast, the high-field tail of the resonance is sensitive to temperature and thermal broadening is particular important in that region.

- p-wave features have a complex structure that arises mainly from the magnetic dipole dipole interaction included in V_{SS}. In fact, its anisotropic character makes that different coupling occurs for distinct values $|m_l|$ of the projections of the orbital angular momentum of the pair. In particular, the $m_l = 1$ case takes place at higher energies with respect to $m_l = 0$: this can be easily understood in a classical picture of dipolar interaction, see Fig. 2.7. $m_l = 0$ corresponds to the case of two (classical) dipoles that rotate one with respect to the other in a plane that contains the magnetic field direction. In this case they alternate repulsive interaction (side by side) to attractive interaction (head to tail); viceversa, $m_l = 1$ corresponds to two dipoles that rotate in a plane perpendicular to the field, therefore they are always feeling repulsive interaction. Since the dipole-dipole interaction for $m_l = 1$ has only a repulsive influence, it forms a resonant state with higher energy.

  In general when higher order partial waves resonances are considered, their complex structure will exhibit $l + 1$ peaks corresponding to distinct $|m_l|$.

The complex structure associated to p-wave resonances can be experimentally resolved if temperature is low enough to avoid that thermal broadening masks it. This has already been observed in a Fermi gas [76], and more recently in the ^{40}K-^{87}Rb fermion boson mixture [78]. Also we have observed this multi-peak feature for two resonances located at 277.5 Gauss (see Fig. 2.8) and 495.5 Gauss respectively, in the Bose-Bose mixture. As already remarked in [76], the doublet splitting represents a direct evidence of the p-wave character of such resonances. As I will discuss in next subsection 2.2.4, the splitting between the peaks experimentally measured for these two features has been crucial for refining our quantum collision model parameters.

2.2.3 Detection of the zero crossings

In our investigation, we have looked also at some *zero crossings* associated to broad Feshbach resonances: this is not easy in general in the case of homonuclear systems, and would require tedious studies of cross thermalization. In the case of a K-Rb mixture, instead, the detection of a zero crossing is extremely easy, since its

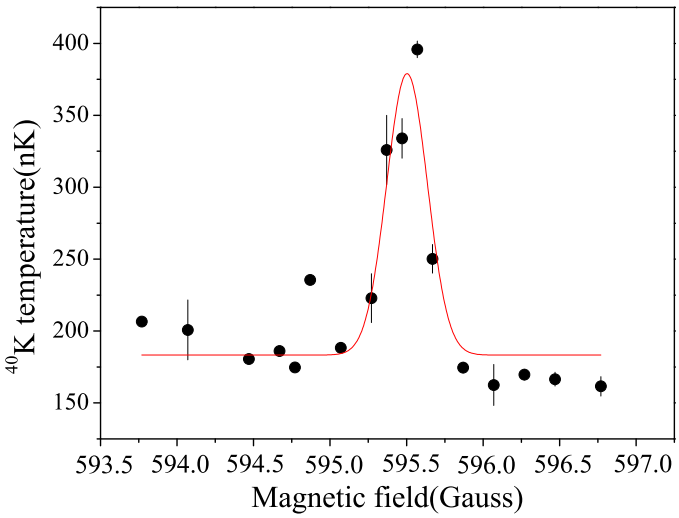

Figure 2.9: Experimental observation of the zero crossing near the 598.4 G Fermi Bose resonance. As the magnetic field assumes values close to the zero crossing point, the heterouclear elastic cross section vanishes and the efficiency of sympathetic cooling during further evaporation in the optical trap decreases. A similar behavior has been observed in the Bose Bose mixture for the zero crossing associated to the resonance located at 318 G, see Tab. 2.2.

position is revealed by the cooling of potassium. The location of the zero crossing has been determined both in the Fermi Bose and Bose Bose mixtures by recording the efficiency of sympathetic cooling of potassium as a function of the magnetic field applied during the evaporation in the optical potential, see [79]. In fact, we have shown how in the ultracold regime the total elastic cross section vanishes with the s-wave scattering length: and this results in a strongly reduced sympathetic cooling rate. For this kind of investigation we lowered the beam intensities of the optical trap and after 2.4 s of forced evaporation measured the temperature of the potassium cloud as a function of the external magnetic field. As shown in Fig. 2.9, the position of the zero crossing appears then as a sharp peak in the K temperature.

In Tab. 2.1 and Tab. 2.2 we report zero crossing positions for few broad resonances, as well as the doublet splitting of p-wave resonances for the boson-boson

mixture.

m_{fa}, m_{fb}	$B_{\rm exp}$(G)	$B^a_{\rm th}$(G)	$B^b_{\rm th}$(G)	$\Delta_{\rm th}$(G)	$a_{\rm bg}$ (a_0)	$-\mu(\mu_B)$	ℓ
1, 1	247.9(2)	248.05(3)	247.97(12)	0.28	34	2.8	0
	277.57(5)	277.53(3)	277.44(11)				1
	277.70(5)	277.70(3)	277.6(2)				1
	317.9(5)	318.30(3)	318.23(14)	7.6	34	2.0	0
	325.4(5)*	325.92(3)*	325.84(14)*				0
	495.19(6)	495.19(3)	495.15(7)				1
	495.62(6)	495.65(3)	495.61(8)				1
	531.2(3)	530.72(3)	530.68(16)	2.5	35	2.0	0
	616.06(10)	615.85(4)	615.80(16)	9.5[-2]	35	1.9	0
0, 1	623.47(6)	623.48(5)	623.41(18)	6[-3]			0
	673.62(8)	673.76(4)	673.7(2)	0.25			0
$-1, -1$	117.6(4)	117.59(3)	117.59(8)	-1.3			0

Table 2.1: Experimental magnetic-field positions $B_{\rm exp}$ and theoretically calculated positions $B_{\rm th}$ for collisions of ^{39}K and ^{87}Rb in the $f_a = 1$, $f_b = 1$ manifold. Zeeman states of the atomic fragments correlate in zero field with $|f_a = 1, m_{fa}\rangle$ and $|f_b = 1, m_{fb}\rangle$, respectively (first column). Theoretical model [a] is based on both isotopes, model [b] on the fermion-boson pair only, assuming the correct singlet potential. Calculations use parameters of Eq. (2.38) and (2.40), respectively. Errors shown in parenthesis represent one standard deviation for both experimental and the theoretical values. In addition, the magnetic widths Δ are provided for the observed s-wave features. In view of future experiments on molecule formation the background scattering length $a_{\rm bg}$ and magnetic moment μ are also given for resonances in the lowest Zeeman sublevel.

2.2.4 The near threshold model

Let's see now how the spectroscopic signal experimentally observed in our experiment allowed us in collaboration with Andrea Simoni to construct an accurate near threshold model for K-Rb mixtures. The starting point are *ab initio* or spectroscopic singlet $X^1\Sigma^+$ and triplet $a^3\Sigma^+$ potentials that can be found in literature: several of them are available, slight differences distinguishing one from another. If one is interested in creating a model able to accurately describe a single specific system (e.g. only the ^{39}K-^{87}Rb mixture), one can adopt indifferently one or another potential curve. They are parameterized in terms of the a_s and a_t scattering lengths, respectively: then a comparison of the experimental data to maxima in the two-body elastic cross section computed for different $a_{s,t}$ is performed, until a good agreement

$\lvert f_a m_{fa}\rangle + \lvert f_b m_{fb}\rangle$	$B_{\rm exp}$(G)	$B^a_{\rm th}$(G)	$B^b_{\rm th}$(G)	ℓ
$\lvert 9/2,-9/2\rangle + \lvert 1,1\rangle$	456.1(2)	456.31(7)	456.32(12)	1
	495.6(5)	495.31(12)	495.3(2)	0
	515.7(5)	515.35(7)	515.38(11)	1
	543.3(5)*	543.66(8)*	543.70(12)*	0
	546.6(2)	546.75(6)	546.78(9)	0
	658.9(6)	659.02(13)	658.99(16)	0
	663.7(2)	663.80(10)	663.78(16)	2
$\lvert 9/2,-7/2\rangle + \lvert 1,1\rangle$	469.2(4)	469.03(13)	469.09(18)	0
	584.0(10)	584.01(11)	583.99(14)	0
	591.0(3)	590.85(7)	590.8(2)	2
	595.5(5)*	595.60(7)*	595.63(10)*	0
	598.4(2)	598.17(6)	598.20(8)	0
	697.3(3)	697.37(9)	697.41(14)	0
	705.0(14)	704.33(13)	704.31(16)	0
$\lvert 9/2,-9/2\rangle + \lvert 1,0\rangle$	542.5(5)*	542.79(5)*	542.81(7)*	0
	545.9(2)	545.95(7)	545.97(10)	0
	957.6(5)*	957.70(13)*	957.70(18)*	0
	962.1(2)	962.04(13)	962.03(17)	0
$\lvert 9/2,7/2\rangle + \lvert 1,1\rangle$	299.1(3)	298.51(5)	298.53(7)	0
	852.4(8)	851.93(14)	851.9(2)	0

Table 2.2: Same as Tab. 2.1 but for collisions of ^{40}K and ^{87}Rb. As already mentioned in Tab. 2.2, few experimental zero crossing positions have been used for theoretical modeling and are also here identified by an asterisk.

is found. A global least square fit is done, leading to the best fit parameters. Also dispersion coefficients C_i are left to vary in the fit procedure: depending on the richness of the experimental data, one can let them completely free to vary and to extract independent values, or in the case of few available features one can adopt their values known from literature (see e.g. [82, 83]) and let them vary within their estimated uncertainty. Differences between two similar spectroscopic potentials will be immaterial, and the model will work well in both cases.

When instead one wants to generate a model able not only to reconstruct the resonance observed pattern but also to infer the resonance location and the near threshold behavior of other isotopes (or isotopic pairs), then also small deviations between two similar potentials can become important, and can lead to significant differences in the model: in particular an uncorrect potential shape can lead to the same accuracy for the single species, but it can generate predictions for the other isotopes (or

isotopic pairs) affected by systematic errors. Usually these details concern the shape of the interaction potentials at short internuclear distances, therefore they regard the deeply bound molecular physics of the system. In particular, the number of bound states supported by these potentials is crucial in order to construct a model with high prediction power.

Usually, the correct details of the potentials are inferred by optical spectroscopy, that investigates the short range interactions, while cannot be deduced by Feshbach spectroscopy, that can detect only long range behavior of the system. In the case of potassium-rubidium mixtures the uncertainty by few units [41, 56, 84] on the number of bound states supported by the singlet and triplet interaction potentials limited the prediction power of the model with regard to different isotopic pairs. In fact, a first characterization of the single Bose-Fermi mixture [41] lead to the construction of a model that accurately fitted the experimental resonance pattern and made predictions also for other isotopic pairs; this was based on the two *ab initio* potentials $^1\Sigma^+$ and $^3\Sigma^+$, developed by Rousseau [85]: in particular they support a number of vibrational levels equal to $N_S^b = 98$ and $N_T^b = 32$, respectively. Once we started to characterize the other mixture, we found the resonances locations in good agreement with the positions predicted in [41]. This circumstance is by itself sufficient to conclude that the $N_T^b = 32$ is correct, as variations of ± 1 in N_T^b gives rise to shifts of ^{39}K^{87}Rb Feshbach resonances as large as 10 G, for fixed values of $a_{S,T}(40-87)$. Shifts are in general less dramatic upon variation of the dissociation energy of the deeper $^1\Sigma^+$ potential. In addition, the Bose Bose resonances observed here have mostly triplet character, and therefore predictions from the model based on the only fermion-boson system are most of the time accurate, even if an uncorrect number of bound states of the singlet potential is used. Fortunately, the specific feature at ~ 616 G shown in Fig. 2.10 has sufficient singlet mixing for its position to shift of about ± 3 G per bound state added or subtracted from the $^1\Sigma^+$ potential. This has been sufficient to conclude that the number of bound states $N_S^b = 98$ of the Rousseau singlet potential was uncorrect: the location of this resonance fixes conclusively $N_S^b = 100$. This fact is important, since this is the first time that a typical *short range* information concerning the details of the interaction potential can be accurately fixed by means of Feshbach spectroscopy, that instead usually refers to *long range* properties of the system. This has been possible since the spectroscopy regarded *two* different isotopic pairs: it had not been possible even with hundreds of resonances of just a *single* mixture. The validity of this result has been confirmed by recent accurate spectroscopic studies [56].

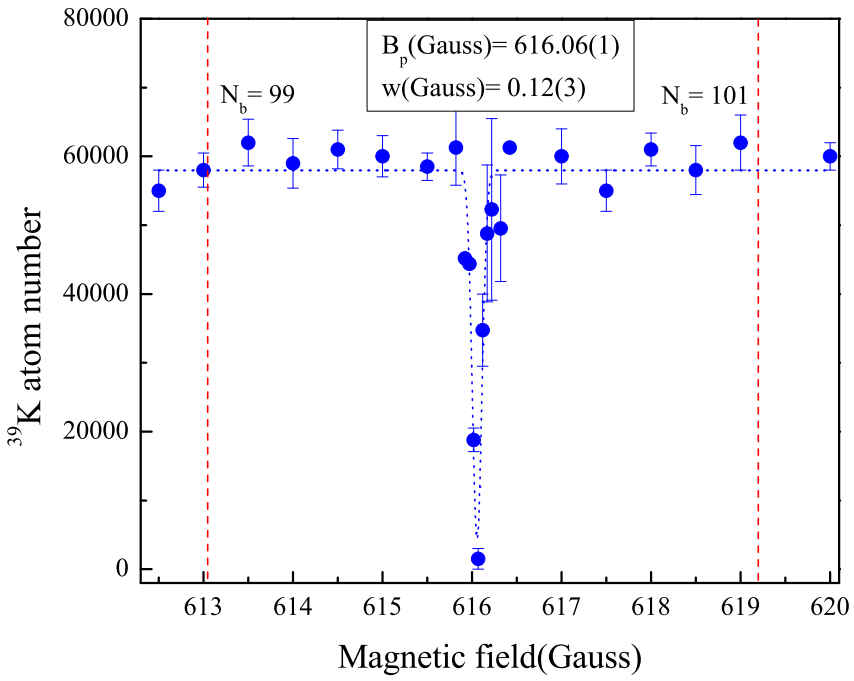

Figure 2.10: Experimental determination of the *singlet character* interspecies Feshbach resonance located around 616 Gauss by looking at three body losses on potassium: this feature allowed us to univocally fix the number of bound states supported by singlet and triplet potentials. The uncertainty of the measurement is of ~ 100 mGauss, while a variation of ± 1 singlet bound state would cause a shift of the maximum of the losses of 3 Gauss, indicated in the figure by red lines.

We therefore adopted the spectroscopic singlet $^1\Sigma^+$ potential of Amiot [86] obtained at regular internuclear distances using the near-dissociation coefficients given by Amiot [86] and the RKR1 code [87], that supports the correct number $N_S^b(40\text{-}87) = 100$ vibrational levels. Since the experimental data here available are many more than in our first work, it is possible to determine independently of *ab-initio* calculations both leading long-range coefficients C_6 and C_8. As already mentioned, the model is also parameterized in terms of s-wave singlet-triplet scattering lengths $a_{S,T}$ of the Fermi Bose mixed system, and includes relativistic spin-spin and second-order spin order corrections [88]. After the preliminary characterization of the interaction

potentials, that allows us to check the correct interaction potentials to adopt, we proceed to fine-tune the potential shape in order to reproduce the present experimental spectra. The presence of narrow resonances in our data is crucial to improve the parameters precision, as their position can be determined experimentally with high precision [45]. The experimental width of the losses peak is exploited as a weight of the corresponding resonance in the fitting procedure: the narrower is the width of the feature, the more significative is the experimental datum.

It has been recently remarked in Ref. [56] that the splitting observed in the ^{40}K-^{87}Rb mixture [78] between $\ell = 1$ resonances with different projections $m = 0$ and $|m| = 1$ of ℓ along the magnetic field, cannot be accounted for by electron spin-spin interactions only. Comparison of two $\ell = 1$ doublet features of the boson boson system (see Tab. 2.1) with theoretical calculations confirms this observation. In particular, the spin-spin induced splitting of the doublet at ~ 495 G is found theoretically to be of 900 mG, versus an observed value of ∼500 mG. With the present resolution (50 mG) this discrepancy might be sufficient to bias our analysis. Hence, a preliminary χ^2 minimization including only s-wave resonances is performed: in fact, they are virtually unaffected by spin interactions. Next, we introduce a phenomenological second order spin-orbit operator of the form [88]

$$V_{so}(R) = \frac{C\alpha^2}{2} e^{-\beta(R-R_S)} \left(3S_z^2 - S^2\right) \tag{2.37}$$

where α is the fine-structure constant, S is the total electrons spin and z is taken along the internuclear axis. The parameters β and R_S are assigned the arbitrary yet reasonable values $0.085 a_0^{-1}$ and $10 a_0$ and the strength is fixed to $C = 1.910^{-3} E_\mathrm{h}$ in order to reproduce the observed doublet separations. We perform a final optimization including all $\ell > 0$ features for both isotopes. Result of the fit is :

$$\begin{aligned} a_S &= -110.6(4)\, a_0 \\ a_T &= -214.0(4)\, a_0 \\ C_6 &= 4290(2)\, a_0^6 E_\mathrm{h} \\ C_8 &= 4.79(4)10^5\, a_0^8 E_\mathrm{h}. \end{aligned} \tag{2.38}$$

The reduced chi-square (i.e. the χ^2 per degree of freedom) is $\tilde{\chi}^2 = 0.84$ and the maximum discrepancy with the experimental data is less than two standard deviations. The $a_{S,T}$ fully agree with our determination in Ref. [41]. The C_6 is consistent to about one standard deviation with the value 4274(13) given by Derevianko *et al* [82] while our C_8 deviates by two standard uncertainties from the result $4.93(6) a_0^8 E_\mathrm{h}$ of Ref.[83].

Note that potential parameters are statistically correlated: for instance, if C_6 and C_8 were kept constant the position of a given experimental feature could be approximately obtained by increasing a_S (i.e. by making the $^1\Sigma$ *more* binding) and concurrently decreasing a_T (i.e. by making the $^3\Sigma$ *less* binding). As all parameters are left to vary correlations become more complex and can be summarized in the symmetric covariance matrix:

$$\mathcal{C}(\text{a.u.}) = \begin{pmatrix} 0.14 & 2.4[-2] & -0.47 & -9.2[2] \\ & 0.18 & -0.10 & 8.3[2] \\ & & 2.1 & 4.5[3] \\ & & ..... & 1.6[7] \end{pmatrix} \tag{2.39}$$

The $\mathcal{C}$ matrix has been used to compute error bars on the theoretical resonance positions (second column in Tabs. 2.1, 2.2) using standard error propagation, whereas neglect of correlations might lead to grossly overestimated uncertainties.

Our improved model can be used to determine the evolution of molecular levels near dissociation, taking advantage of the profound relation between near-threshold bound states and scattering properties. Molecular levels for the Fermi Bose system have been recently presented in Ref. [43]. Here we discuss the nature of boson boson molecules focusing on the experimentally relevant case of $\ell = 0$ molecules that can be magnetically associated starting from atoms in the lowest Zeeman sublevel $|11\rangle + |11\rangle$.

With reference to Fig. 2.11, the bound level at -0.2 Ghz running parallel to the energy of the separated atoms is associated to background scattering. That is, its position would correspond to single channel scattering with the same background scattering length and long-range coefficients. It is characterized by Hund's case (e) quantum numbers $(f_a, f_b, f) = (1, 1, 2)$, where $\mathbf{f} = \mathbf{f_1} + \mathbf{f_b}$. The triplet near -1 Ghz is formed by $S = 1$ molecules with different total nuclear spins I, split by hyperfine interactions. They are described by Hund's case (b) quantum numbers (S, I, f) equal to $(1, 3, 4)$, $(1, 2, 3)$, and $(1, 1, 2)$, respectively. Next two levels at -1.5 Ghz are singlet-triplet mixed levels: the degree of mixing can be quantified by the average value of the electron spin operator $\langle S^2 \rangle \approx 1.2 - 1.3$. These levels are still exactly characterized by $f = 2, 3$. Moreover the strong hyperfine interaction forces coupling of Rb electron and nuclear spin to form $f_b = 1$. The other quantum numbers are otherwise undefined.

In the procedure we followed for the analysis described above, we have used the mass scaled interatomic potential for the two isotopes, thus assuming validity

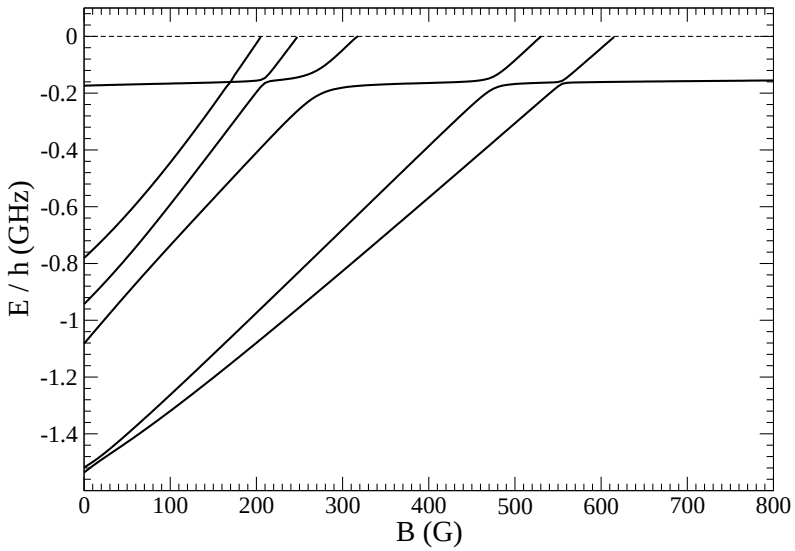

Figure 2.11: Near threshold ^{39}K^{87}Rb $\ell = 0$ molecular levels magnetically coupled to atoms in the lowest Zeeman sublevel. The energy of the separated atoms is taken as zero (dashed line). Collision parameters are from Eq. (2.38).

of the Born Oppenheimer approximation [89]. We can quantify the accuracy of this hypothesis first optimizing the potential on a single isotopic pair, and then deriving the location of the resonances of the other mixture via mass scaling procedure. We make this test by creating the single species model with the Fermi Bose system, which is found to provide tighter error bars when taken into account *alone*. The best fit parameters in this case are found to be the following:

$$\begin{aligned} a_S &= -110.7(7)\, a_0 \\ a_T &= -214.1(11)\, a_0 \\ C_6 &= 4290(9)\, a_0^6 E_\mathrm{h} \\ C_8 &= 4.8(3)10^5\, a_0^8 E_\mathrm{h}. \end{aligned} \tag{2.40}$$

As expected, the quality of the fit is good (see second column in Tab. 2.2) with $\tilde{\chi}^2 = 0.6$ the same value obtained (for ^{40}K-^{87}Rb) from the model optimized on both isotopes.

Next, we recalculate the resonance pattern for ^{39}K-^{87}Rb, see third column in Tab. 2.2. The average discrepancy between theory and experiment, weighted with

K-Rb pair	$a_S(a_0)$	$a_T(a_0)$
39-85	33.78(6)	63.27(2)
39-87	1.98(4) 10^3	35.61(3)
40-85	65.39(5)	-28.63(6)
41-85	103.25(6)	349.0(4)
41-87	7.13(9)	163.82(6)

Table 2.3: Calculated singlet and triplet s-wave scattering lengths for collisions between K and Rb isotopic pairs employing all our spectroscopic data both of the Fermi Bose and of the Bose Bose mixture.

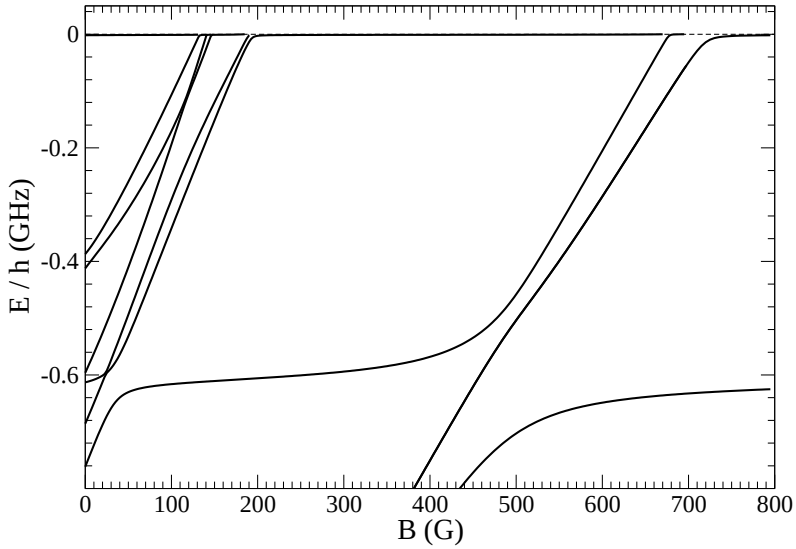

Figure 2.12: Same as Fig. 2.11 but for $^{41}K^{85}Rb$. With reference to table 2.3, note how the presence of a bound state very close to threshold causes a large and positive background value of the interspecies scattering length, see subsection 2.1.2.

the in-quadrature combination of experimental end theoretical errors is of 0.2: this has to be compared with the value 0.3 obtained from the two-isotope parameters of Eq. (2.38). We remark that theoretical resonance positions do not show any preferential, positive or negative shift with respect to the experimental ones. We also note that optimization of the Bose Bose model alone does not lead to any significant improvement. We can conclude that even at the present level of precision no evidence

is found for breakdown of the Born Oppenheimer approximation. Mass-scaling can then be used for predicting properties of other isotopes. In particular, the $a_{S,T}$ along with the long-range coefficients determined in this work are sufficient in order to predict all relevant threshold properties of any K-Rb pair.

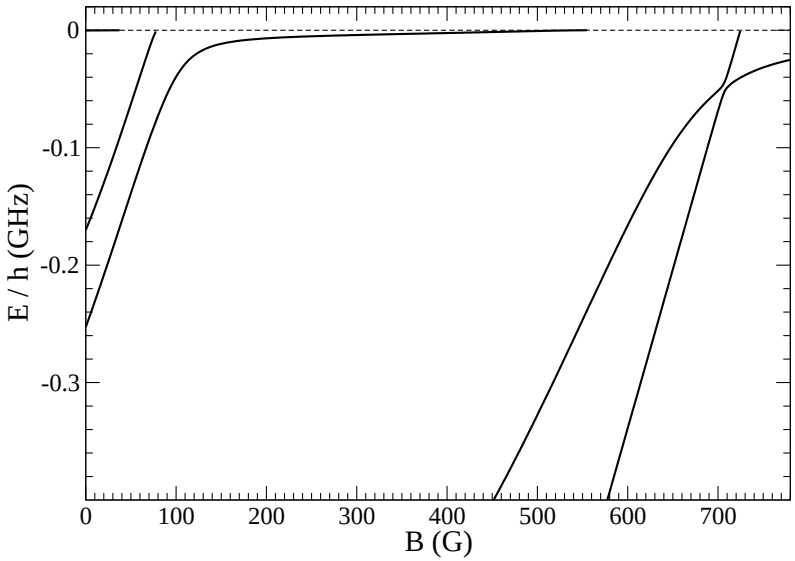

Figure 2.13: Same as Fig. 2.11 but for ^{41}K^{87}Rb.

The s-wave singlet-triplet scattering lengths are shown in Tab. 2.3 for all isotopic combinations. We can also predict with high precision the value of the s-wave scattering length for the absolute ground state, see Tab. 2.4. Two isotopic pairs already discussed in our previous work [41] are especially interesting: ^{41}K-^{85}Rb, and ^{41}K-^{87}Rb. In the first case one could use a sample of ^{41}K to optimize the evaporation of ^{85}Rb atoms which is typically very inefficient in a pure homonuclear sample due to occurrence of the first zero in the ^{85}Rb cross-section already at temperatures on the order of 100 μK [24]. In fact, we have checked that the large magnitude of the zero energy interspecies cross section persists even up to the mK regime. The availability of several Feshbach resonances at relatively low field could also prove to be useful for the production of binary Bose-Einstein condensates where both the self- and the interspecies interaction are tunable. In the case of the ^{41}K-^{87}Rb pair, a system for which the production of a stable binary condensate has already been reported [26, 40], availability of very broad resonances allow the mutual interaction to be

K-Rb	a (a_0)	$B_{\rm th}$ (G)	$\Delta_{\rm th}$ (G)	$a_{\rm bg}$ (a_0)	$-\mu$ (μ_B)
39-85	58.01(2)				
40-85	−21.06(6)				
39-87	28.29(3)				
40-87	−184.4(3)				
41-85	283.1(3)	132.39(7)	0.19	242	2.33
		140.98(5)	$2.0\ 10^{-4}$	242	3.42
		146.4(3)	0.025	242	2.88
		185.2(9)	3.5	327	2.14
		191.72(7)	0.48	327	2.14
		672.19(15)	5.7	343	1.89
		695.90(12)	14	343	1.70
41-87	640(3)	39.4(2)	37	284	1.65
		78.92(9)	1.2	284	1.59
		558.0(4)	81	173	0.012
		724.8(3)	0.07	90	1.93

Table 2.4: Predicted zero-field s-wave scattering lengths for the absolute ground state of K-Rb isotopes. Resonance positions and widths, background scattering length and magnetic moments associated to the Feshbach state are also provided for two isotopic pairs of experimental interest.

precisely tuned, and make this system also interesting for ultracold molecule formation. For both isotopomers the scattering parameters and molecular levels have been calculated: note that the resonance positions are slightly shifted with respect to the ones of our previous predictions in Ref. [41] because of the different number of bound states in the singlet potential.

Finally, we present in Figs. 2.12 and 2.13 near threshold-molecular potentials for the two pairs. These data should represent a key piece of information for implementing efficient transfer scheme to low vibrational levels using Feshbach molecules as a bridge, and for the calculation of Franck-Condon overlap matrix with excited states.

2.3 Feshbach spectroscopy on ^{39}K

As mentioned in the Introduction of this thesis, we have performed also extensive Feshbach spectroscopy on the bosonic potassium isotope we employ in our apparatus. Potassium systems have been characterized in the last years, both by means of photoassociation studies [90, 91, 92] on ^{39}K and Feshbach spectroscopy on the

fermionic potassium [8]: in particular, the intensive study of two specific resonances in ^{40}K was motivated by possible applications to fermionic superfluidity. Even if magnetic Feshbach resonances had not yet been investigated in the bosonic potassium isotopes, some indication about the presence of broad features at relatively low fields in the ^{39}K system already existed before our study was performed [90, 93]: this, combined with a small (negative) background scattering length, motivated us to investigate this still not well known system, since it seemed to be finely tunable in the weakly interacting regime. If sympathetic cooling of this atom with rubidium had already been demonstrated to be efficient [40] by our colleagues at LENS, and therefore it was clear that the system was easily available within the ultracold regime, nevertheless the achievement of a Bose Einstein condensate of ^{39}K was not so straightforward: in particular, due to the negative sign of the zero field scattering length of this system, it was evident that its condensation could take place just by stabilizing the sample in the vicinity of a Feshbach resonance. For this purpose, that will be described in chapter 4 we have performed a characterization of this atomic species, by means of which we could locate eight resonances with high precision, and derive an accurate model able to describe the scattering properties of the system.

I report here the results of Feshbach spectroscopy in three different hyperfine states of ^{39}K performed by observing on-resonance enhancement of inelastic three-body losses and molecule formation, following the same techniques described for the mixtures. The observed resonance locations are used to construct an accurate theoretical quantum model which explains both present and pre-existing observations [8]. The model allows us to compute both scattering properties (evaluating background scattering lengths and resonance widths), and hyperfine-coupled molecular levels near the dissociation limit. As I already mentioned in the case of potassium rubidium mixtures, all this study relies on the close collaboration between our group and Andrea Simoni.

2.3.1 Experimental detection of the ^{39}K Feshbach resonances

We have studied Feshbach resonances in all the states immune from spin-exchange collisions, the three Zeeman sublevels of the $F = 1$ manifold. The starting point of the experiment is the absolute ground state ($|1,1\rangle \oplus |1,1\rangle$) of the potassium rubidium mixture optically trapped at a temperature of $\sim 1\mu K$. We further lower the temperature of the mixture down to $200 - 500$ nK by decreasing the laser beams power with a 2.4 s exponential ramp. During this phase we also increase the efficiency

of sympathetic cooling between the mixture components, fixing the magnetic field value close to the interspecies Feshbach resonance located at 316 Gauss, see subsection 2.2.4. Once the final temperature is achieved, rubidium atoms are completely evaporated from the optical potential, and a pure sample of ultracold potassium is available. The transfer in the $|1,0\rangle$ ($|1,-1\rangle$) state is performed by lowering the field at 38.5 (10) Gauss, and applying a radio-frequency sweep about 28.5 (7.6) MHz. After the atomic sample is prepared, the field is ramped up again and actively stabilized to any desired value below 1000 Gauss.

^{39}K presents both very narrow ($B < 0.5$ Gauss) and very broad resonances ($B \sim 50$ Gauss). Examples of two such resonances in the $|1,1\rangle$ state are shown in Fig. 2.14. The narrow resonance around 26 Gauss gives rise to a rather sharp, symmetric loss

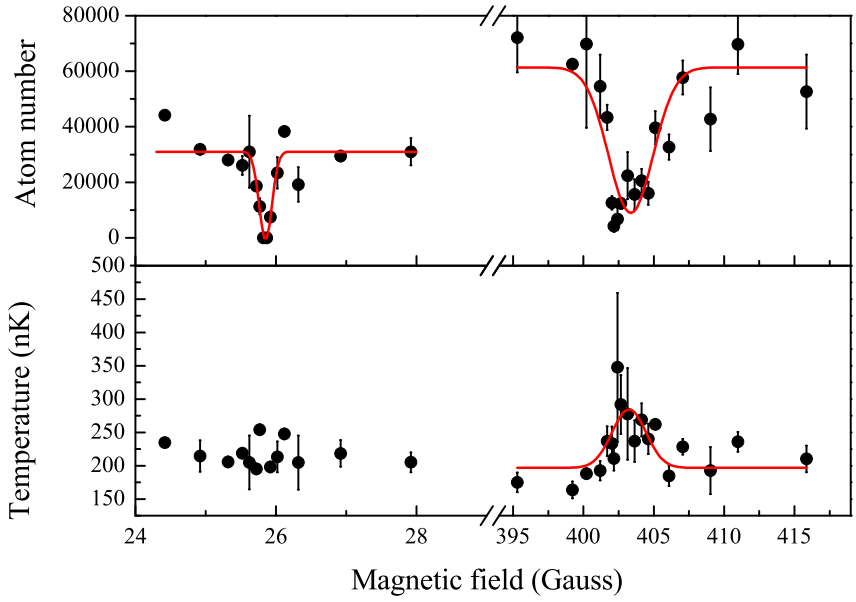

Figure 2.14: Experimental determination of Feshbach resonances in the $|1,1\rangle$ state of 39K: (a) remaining atom number; (b) sample temperature. The hold time for the low field (high field) resonance was 480 ms (36 ms). The curves are phenomenological fits with Gaussian distributions.

features centered at B_0. On the converse, the broad resonance around 400 Gauss

originates a broader, highly asymmetric loss and heating feature. A possible source of asymmetry will be discussed later. The different strength of the two resonances is indicated by the different hold time required to have about 90% peak losses; this amounts to 480 ms for the narrow resonance and 36 ms for the broad one.

The same procedure was repeated for the two other hyperfine states. In total we have studied eight Feshbach resonances, whose centers are listed in first column of table 2.5. For most broad resonances, we have found the asymmetry in loss and heating profiles similar to the one shown in Fig. 2.14. In the absence of a precise model of our system, we have fitted the experimental profiles with a single Gaussian to determine the resonance centers B_{exp}. The error we give on B_{exp} is the quadratic sum of our magnetic-field accuracy and of the error deriving from the fit, which is usually dominating for broad loss profiles.

$\|m_{fa}\rangle + \|m_{fb}\rangle$	$B_{\rm exp}$(G)	$B_{\rm th}$(G)	$-\Delta_{\rm th}$(G)	$-\mu(\mu_B)$	$a_{\rm bg}$ (a_0)	(SIf) $\{SIM_S\}$
$\|1\rangle + \|1\rangle$	25.85(10)	25.9	0.47	1.5	-33	(133)
	403.4(7)	402.4	52.0	1.5	-29	
		745.1	0.4	3.9	-35	{113}
	752.3(1)	752.4	0.4	3.9	-35	{111}
$\|0\rangle + \|0\rangle$	59.3(6)	58.8	9.6	0.83	-18	(133)
	66.0(9)	65.6	7.9	0.78	-18	(111)
		471.0	72.0	3.9	-35	
		490.0	5.0	1.70	-28	
		825.0	0.032	3.92	-36	{113}
		832.0	0.52	3.90	-36	{111}
$\|-1\rangle + \|-1\rangle$	32.6(1.5)	33.6	-55.0	-1.9	-19	(112)
	162.8(9)	162.3	37.0	1.2	-19	(133)
	562.2(1.5)	560.7	56.0	1.4	-29	

Table 2.5: Experimental magnetic-field positions B_{exp} and theoretically calculated positions B_{th}, widths Δ, magnetic moments μ, background scattering length a_{bg}, and approximate quantum numbers (see text) of ^{39}K l = 0 Feshbach resonances.

2.3.2 Near threshold model for ^{39}K

As mentioned at the beginning of this section, early information about K collision properties was obtained from the analysis of photoassociation (PA) spectra of the bosonic isotope ^{39}K, see [90, 91]. The collision model has then been refined by

theoretically analyzing observed shape [59] and Feshbach resonances [8] in fermionic ^{40}K. Subsequently, the Nist/Connecticut groups have inferred potential parameters from two-photon spectroscopy of ^{39}K near-dissociation molecular levels [92]. Finally, cold collision (CC) measurements have been performed on ^{39}K from our colleagues at LENS [40]. These different determinations are summarized in table 2.6 (scattering quantities are defined in the following). As in the case of potassium ru-

Reference	$a_S(a_0)$	$a_T(a_0)$	C_6(a.u.)
This work [45]	138.90(15)	-33.3(3)	3921(8)
CC [40]		-51(7)	
CC [8, 60]	139.4(7)	-37(6)	3927(50)
PA [92]		-33(5)	3897(15)
CC [59]		$> -80, < -28$	3813 [95]
PA [91]	$> 90, < 230$	$> -60, < -15$	3813 [95]
PA [57],[90]	140^{+6}_{-9}	$-21 - 0.045\delta C_6 \pm 20$	

Table 2.6: Comparison of collisional parameters for ^{39}K determined from CC measurements and PA spectroscopy of ultracold atoms. Some analysis did not determine the value of C_6, which was taken from theory (value and reference are then reported in the third column of the table). The δC_6 is the shift in C_6 from the value C_6 = 3897 a.u. of [82].

bidium mixtures, the present collision model developed for potassium isotopes comprises adiabatic Born Oppenheimer singlet $X^1\Sigma_g^+$ and triplet $a^3\Sigma_u^+$ interaction potentials determined from spectroscopic data [86, 94]. The adiabatic potentials asymptotically correlate with the dispersion plus exchange analytical form of eq. (2.31), and a short-range correction is finally added to the adiabatic potentials to model the data [90]. Also in the homonuclear case, experimental resonance locations are used in a weighted least square procedure to determine the correction size. The resulting optimized potentials are parameterized in terms of s-wave singlet a_S and triplet a_T scattering lengths and of the long-range parameters C_n, n = 6, 8, 10. Resonance positions are mainly sensitive to the leading van der Waals coefficient C_6, which along with the $a_{S,T}$ is a parameter in the fitting procedure. In order to obtain maximum constraint we also include in the empirical data the positions of two already known ^{40}K resonances [8, 60], and a p-wave resonance we have recently discovered at ~ 436 Gauss in collisions of ^{40}K $|9/2, 7/2\rangle$ atoms. We use the same potential for the two isotopes assuming thereby the validity of the Born Oppenheimer approximation. Result

of the fit is:

$$a_S = (138.90 \pm 0.15)a_0$$
$$a_T = (-33.3 \pm 0.3)a_0$$
$$C_6 = (3921 \pm 8)\text{a.u.}$$

The final reduced value is χ^2= 0.52 only. The singlet-triplet scattering lengths herein derived agree well with previous determinations (see Tab. 2.6) and our result represents an improvement of more than one order of magnitude in a_T. The C_6 agrees to one standard deviation with the accurate value of Derevianko et al. [82], $C_6 = 3897 \pm 15a.u.$ If we calculate the singlet-triplet scattering lengths of ^{40}K with the present model, they result 104.56 ± 0.10 and 169.7 ± 0.4 respectively, in very good agreement with [8].

I have already remarked that a magnetic Feshbach resonance arises at a value B_0 of the magnetic field when the energy of the separated atom pair becomes degenerate with the energy of a molecular bound level. Scattering near a magnetic resonance is fully characterized [71] by assigning B_0, Δ, the background scattering length a_{bg}, the C_6 coefficient, the magnetic moment μ of the molecule associated to the resonance with respect to free atoms

$$\mu = \frac{\partial(E_{at} - E_{mol})}{\partial B} \tag{2.41}$$

where E_{at} and E_{mol} represent the energy of the separated atoms and of the molecule, respectively, and the derivative is taken away from resonance. The parameters values for observed and theoretically predicted resonances are listed in Tab. 2.6. Also Feshbach resonances due to molecular states with $l \neq 0$ are in principle present in this system, even if we haven't investigated them. In cases where resonances are overlapping (i.e. when the magnetic width is comparable to their magnetic field separation) we will parameterize the effective scattering length with one background parameter a_{bg}, two widths Δ_i and two positions $B_{0,i}$ (i=1, 2) as

$$a(B) = a_{bg}(1 - \frac{\Delta_1}{B - B_{01}} - \frac{\Delta_2}{B - B_{02}}) \tag{2.42}$$

This expression clearly reduces to Eq. (2.34) when the resonances are isolated, $|B_{0,2} - B_{0,1}| \ll \Delta_1, \Delta_2$. A comparison of experimental and theoretical resonance locations in Tab. 2.6 indicates that all measured resonances with large Δ feature an asymmetric profile. In all these cases, the center of the gaussian fit to the loss profiles is indeed shifted towards the region of negative scattering lengths, as in

the case reported in Fig. 2.14. A possible explanation for such asymmetry is the onset of mean field effects for large positive and negative scattering lengths close to the resonance center. In fact, for $B > B_0$ ($B < B_0$) the density is expected to increase (decrease) with respect to the noninteracting value. This would accordingly vary the loss rates through their density dependencies and promote losses on region with $B > B_0$. In absence of a detailed model of our finite temperature system, we made an independent experiment to determine the center of the broad ground-state resonance in Fig. 2.14, by studying molecule association, using the scheme already described for the heteronuclear case.

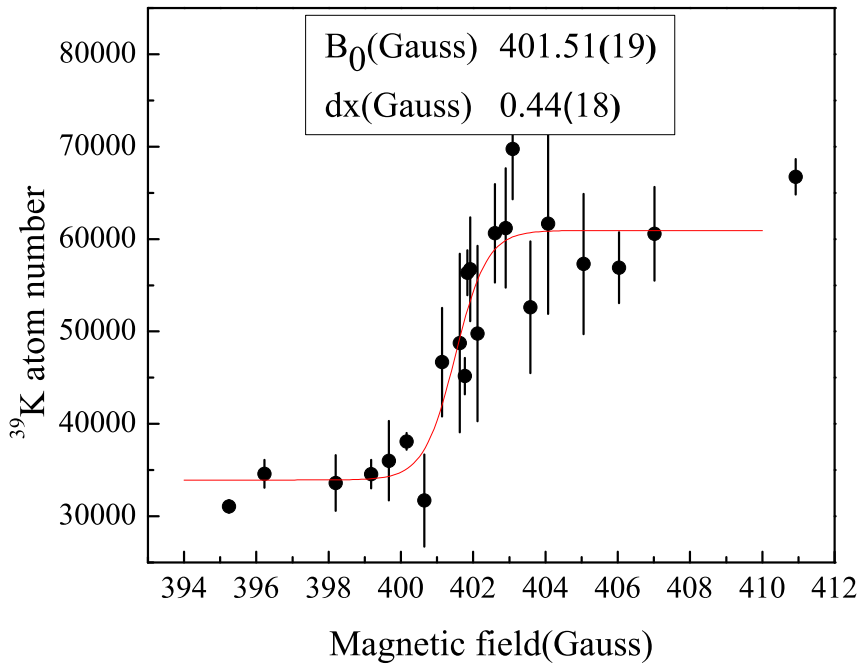

Figure 2.15: Molecule formation at the broadest Feshbach resonance in the $|1,1\rangle$ state of ^{39}K. The magnetic field is linearly swept from 410 Gauss to a final field B in 2 ms. The resonance center $B_0 = 401.5(5)$ Gauss is determined by fitting the atom number with a Boltzmann growth function.

In general, molecule formation can be studied in ^{39}K, as well as in other bosonic

systems, employing a cold but thermal sample, or a three-dimensional optical lattice that prevents collapse of the condensate on the atomic side of the resonances and shields inelastic decay of molecules [96]. We have used the standard technique of adiabatic magnetic-field sweeps over the resonance from the atomic to the molecular side [77]. We start with a cold thermal gas of ^{39}K at a temperature of 220 nK, initially prepared at a magnetic field well above the resonance center, $B_i = 410$ Gauss. The field is then swept to a lower value B in 2 ms, allowed to stabilize for 0.1 ms, and suddenly after switched off. As shown in Fig. 2.15, as B crosses the resonance the atom number drops to about 50% of the initial value, in the absence of any heating of the system. This indicates that a fraction of the atoms are converted into weakly-bound molecules. The dimers are then very rapidly lost from the trap via inelastic collisions. A fit using a Boltzmann growth function gives a resonance center of $B_0 = 401.5(5)$ Gauss. This is almost 2 Gauss lower than the center of the broad loss profile, and is consistent with both $B_{th} = 402.4(2)$ Gauss and the value at which the maximum atom loss and heating is seemingly taking place in the data shown in Fig. 2.14, $B = 402.2(2)$ Gauss. This agreement confirms that the global fit we make is able to accurately fix the position of all resonances, although the broad resonances centers are individually determined with poorer accuracy by loss measurements.

As I already showed for K-Rb mixtures, the development of the quantum collision model enables us to have a detailed knowledge of the molecular levels close to dissociation threshold for the potassium systems: even if heteronuclear molecules appear to be extremely more interesting than homonuclear dimers, let's briefly see the characterization of the potassium isotopes from the molecular point of view. In particular, we can assign the correct quantum numbers that must be used to label the Feshbach molecules. Neglecting weak dipolar interactions and for vanishing magnetic field the internal angular momentum of the dimer $\mathbf{F} = \mathbf{S} + \mathbf{I}$ is conserved. Moreover, because of the small hyperfine splitting of ^{39}K with respect to the splitting between neighboring singlet-triplet levels, S and I separately are approximately good quantum numbers, at least for low B. Because of the spherical symmetry of the problem, the orbital angular momentum l of the atoms is also a conserved quantity. All of the observed resonances have $l = 0$. Zero-energy quantum numbers are shown in Figs. 2.16, 2.17, 2.18 for the closest to dissociation levels in the $|1,1\rangle$, $|1,0\rangle$, $|1,-1\rangle$ states of ^{39}K.

As the field increases, these quantum numbers are not any longer good. In fact, for intense magnetic fields the Zeeman energy becomes larger than both the hyperfine and the singlet/triplet vibrational splitting. In this regime **S** and **I** uncouple, and

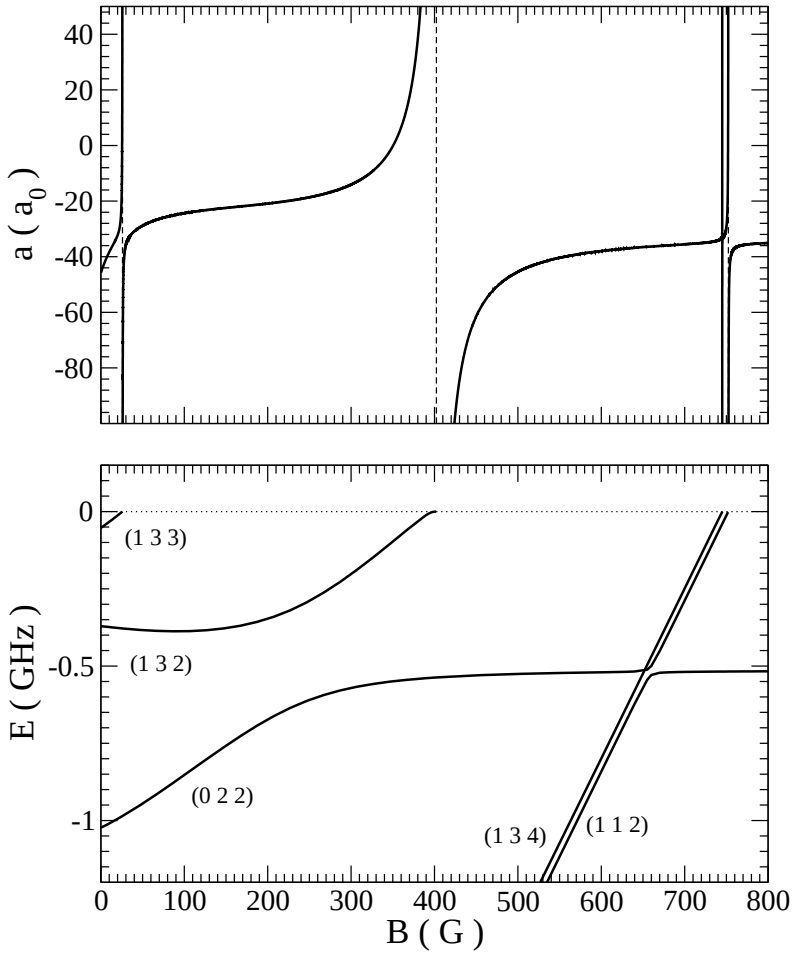

Figure 2.16: Upper panel: magnetic field dependence of the effective scattering length for $|1,1\rangle$ ^{39}K collisions. Dashed lines indicate the resonance positions. Lower panel: near-threshold molecular levels for $M_F = 2$. Zero energy is taken at the separated atoms limit. The quantum numbers shown in brackets (SIF) are good in general only for weak magnetic fields, see text.

precede independently about the magnetic field. The molecular quantum state can then be identified by S, I and by the spin projections M_S and M_I on the quantization axis. In the intermediate regime neither coupling scheme is accurate as singlet and triplet levels are sufficiently close to be strongly mixed by off-diagonal hyperfine

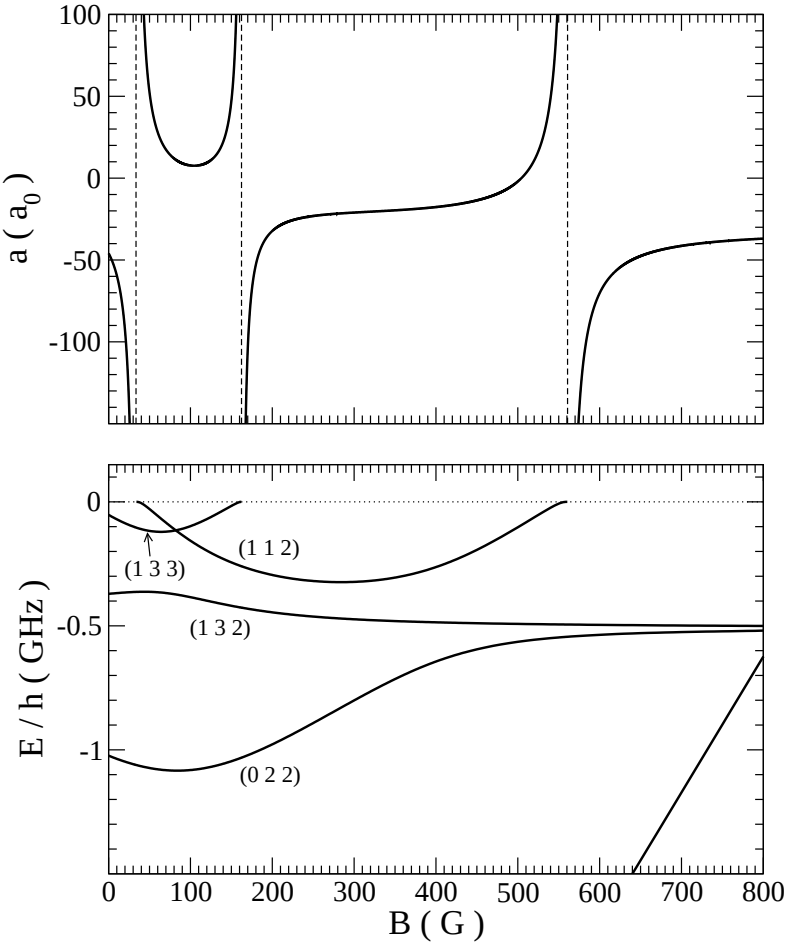

Figure 2.17: Same as Fig. 2.16 but for $|1,0\rangle$ atoms and $M_F = 0$.

interactions. However, since the axial symmetry of the problem is always maintained, the magnetic quantum number M_F (i.e. the axial projection of F) is always a good quantum number. Examples of resonances arising from such mixed levels are the 402 Gauss (Fig. 2.16), the 561 Gauss (Fig.2.17), and the 471 and 490 Gauss (Fig. 2.18) features. One can note from the figures broad avoided crossings caused by spin-exchange interaction between levels of different S and same F. An approximate assignment constructed for low and high field by averaging the appropriate spin operators on the molecular wavefunctions is presented in Tab. 2.5. Resonances

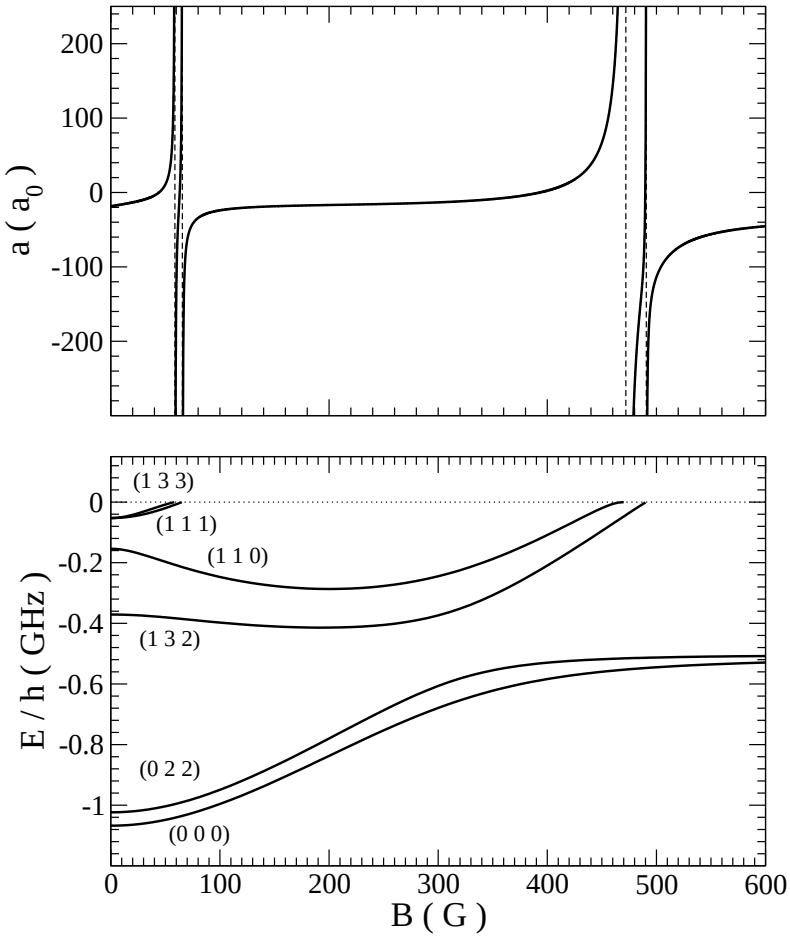

Figure 2.18: Same as Fig. 2.16 but for $|1,-1\rangle$ atoms and $M_F = -2$.

arising from mixed levels are left unassigned. Their zero-field correlation can be easily inferred from the figures.

- **Note** The quantum numbers discussed above are in principle only valid away from resonance. Actually, there is always a range of magnetic fields near resonance where the amplitude of the molecular state is almost entirely transferred to the open background channel [97], which is not represented by the same quantum numbers as the molecule. This magnetic field region can be estimated

as

$$\frac{B - B_0}{\Delta} \ll \frac{M a_{bg}^2 \mu \Delta}{\hbar^2}$$

M being the atomic mass, and the other parameters being already defined before. As convention, the resonances for which the right hand side term of the above expression is rhs $\gg 1$ ($\ll 1$) are called *open* (*closed*) *channel dominated*. When the above condition is fulfilled, the energy of the molecule takes the *universal* form

$$E_{mol}(B) - E_{at}(B) = -\frac{\hbar^2}{M(a(B) - l_{vdW})^2}$$

having defined

$$l_{vdW} = \frac{1}{2}(\frac{MC_6}{\hbar})^{\frac{1}{4}}$$

and scattering can be described in terms of a single effective channel. The present resonances range from closed channel dominated to an intermediate situation (rhs$\simeq$1): the universal behavior is only attained in a region of few Gauss even near the broadest resonances with $\Delta \simeq 50$ Gauss. Outside this region, at least a two-channel model based on the parameters reported in Tab. 2.6 is needed [97].

In conclusion of this section, I firstly remark that the ^{39}K system has at least one broad resonance ($\Delta \simeq 50$ Gauss) available in each level of the lowest hyperfine manifold. By virtue of their large width such resonances can be used to precisely tune the interactions in ultracold samples: the small background scattering length makes this system particularly appropriate for the exploration of regimes of weak interactions, as well as Cesium and Lithium: for example, at the zero-crossing location (350.4 ± 0.4) Gauss for $|1,1\rangle$ collisions, the model predicts a small magnetic-field sensitivity $\partial a/\partial B = 0.55 a_0/G$. This implies a control of a to zero within 0.05 a_0 for a field stability of 0.1 Gauss. I will discuss in detail the possibilities of such a fine tuning of the interaction in a ^{39}K gas in Chapter 4. In general, the system might allow one to study a broad range of phenomena: from atom interferometry with weakly interacting condensates and strongly-correlated systems in optical lattices, to molecular quantum gases and Efimov physics [14, 15, 98].

Concerning the magnetic field dependence of the scattering properties of the $|1,0\rangle$ atoms shown 2.17 note how the magnetic-field region around 80 Gauss in

which the scattering length of this state is small and positive ($a \simeq 11a_0$) coincides with the maximum in energy of the state: within this region an ultracold ^{39}K sample presents at the same time a relatively weak interatomic interaction strength and a nearly vanishing magnetic moment. This peculiar combination is clearly interesting for interferometric applications, and it could be object of further investigation.

Finally, we can also use the model to calculate the magnetic-field dependent scattering length of the other bosonic isotope, ^{41}K. Bose-Einstein condensation of this species can be achieved without the need of Feshbach resonances, because of the naturally positive scattering length [26]. Our analysis shows that even if some resonances exist for magnetic fields in the range 0-1000 Gauss, they are much narrower than in ^{39}K, making ^{41}K less interesting for applications where a precise tuning of the interactions is needed.

Chapter 3

Bose Fermi mixture with tunable interaction

In this chapter I will discuss the experiments I performed on a degenerate Fermi-Bose mixture. The starting point of all the measurements described herein is a Fermi gas of potassium atoms and a Bose Einstein condensate of rubidium atoms trapped in a harmonic potential, close to an interspecies Feshbach resonance that allows us to tune the strength of the interspecies interaction. In section 3.1 I will recall some elements of theory, that will be useful to describe the observed phenomena presented in the next of the chapter. I will briefly describe the achievement of the degenerate mixture in section 3.2.1; section 3.2.2 is instead devoted to describe the experimental results concerning the tuning of the interaction within the degenerate mixture. Finally, in section 3.3 I describe the first tests of molecule association we performed within our dipole trap by means of magnetic field sweeps across resonance.

3.1 Elements of theory of quantum gases

The *quantum lengthscale* of a classical object is determined by the De Broglie thermal wavelength $\lambda_{DB} = h/(2\pi M k_B T)^{1/2}$, h being the Plank's constant, k_B the Boltzmann's constant, T and M the temperature and the mass of the particles of the gas. If the mean inter particle distance $n^{-1/3}$ is sufficiently low (n being the mean density of the gas) and the temperature of the sample sufficiently high such that $\lambda_{DB}/n^{-1/3} \ll 1$, the system can be very well described by classical thermodynamics, that allow us to derive the spatial and momentum distribution of the particles,

and the thermodynamical quantities of interest. On the contrary, as the temperature of a gas approaches zero, the quantum nature of the composing particles becomes apparent (see the schematic picture in Fig. 3.1), and this can modify macroscopically the shape and the dynamic of the sample, significantly moving away from classical behavior. A different description is then needed, involving the quantum-mechanical features of the gas.

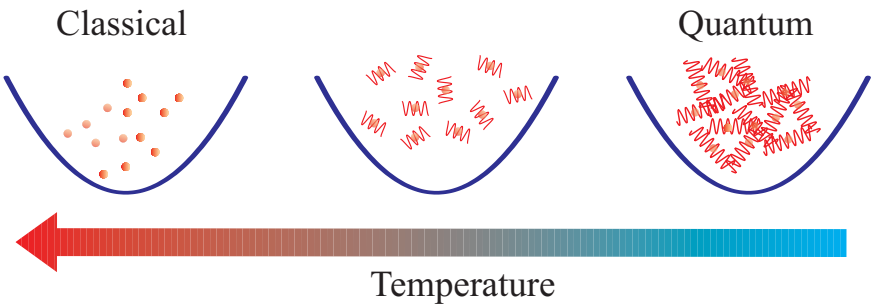

Figure 3.1: Crossover from classical to quantum behavior of an atomic gas as a function of the temperature and for fixed density: at high temperatures the atoms are distinguishable and the thermal De Broglie wavelength λ_{DB} is small compared to the interparticle distance. Decreasing the temperature, λ_{DB} becomes comparable and then larger than the interparticle distance: the atoms lose their individual identity, interference between matter wave packets occur and quantum description is needed.

In nature two different kind of particles are present: fermions and bosons. For the first ones, Pauli principle states that *the only possible states of a system of two fermions are those that can be represented by vectors that are antisymmetric under the exchange of the two particles. For a system composed of more than two fermions the only possible states are those represented by vectors that are antisymmetric with respect to the exchange of any pair of particles*. The states of a bosonic system, on the contrary, are represented by vectors that are *symmetric* under the exchange of two particles.

As the sample is cooled down this different symmetry of the many body wavefunction generates a completely dissimilar behavior: the bosons undergo a phase transition, known as Bose Einstein condensation, that favors the macroscopic occupation of the ground state of the system. The fermions, instead, do not show any transition and tend to occupy the lowest energy levels of the system one by one following the Pauli exclusion principle.

Let's briefly review the main properties of a thermal sample, a Bose gas and a Fermi gas, and of a mixture of such kind of systems, respectively, when trapped in a harmonic potential. The following description is not exhaustive and complete, and just wants to summarize some aspects of the physics of these systems that will be useful in the next of the chapter in order to discuss the experimental results.

3.1.1 Thermal gas

In the case of $\lambda_{DB} n^{-1/3} \ll 1$, N classical particles trapped in a harmonic potential characterized by the frequencies $(\omega_x, \omega_y, \omega_z)$ arrange themselves following the Maxwell Boltzmann distribution:

$$f_c(E) = A \exp^{-\frac{E}{\beta}} \tag{3.1}$$

being $\beta \equiv K_B T$, A a normalization constant, such that

$$\int_0^\infty f_c(E) dE = N$$

and

$$E = \frac{p^2}{2M} + \frac{1}{2} M(\omega_x^2 x^2 + \omega_y^2 y^2 + \omega_z^2 z^2) \tag{3.2}$$

This means that the gas has a gaussian distribution, both in coordinate and in momentum space, whose dimensions are set by the temperature and by the trap geometry. The distribution of the particles in coordinate space has the form:

$$f_c(\mathbf{r}) = \frac{N}{(2\pi)^{3/2} \overline{\sigma}^3} \exp\{-(\frac{x^2}{2\sigma_x^2} + \frac{y^2}{2\sigma_y^2} + \frac{z^2}{2\sigma_z^2})\} \tag{3.3}$$

where the width of the gaussian along the direction i is given by

$$\sigma_i = \sqrt{\frac{K_B T}{M \omega_i^2}} \tag{3.4}$$

and $\overline{\sigma} \equiv (\sigma_x \sigma_y \sigma_z)^{1/3}$ is the mean width of the sample. Note that in the limit of zero temperature the dimensions of a classical gas vanish with $\sqrt{T}$ dependence.

The momentum distribution is instead isotropic despite the asymmetry of the trap, and is given by:

$$f_c(\mathbf{k}) = \frac{N}{(2\pi)^{3/2} \sigma_k^{3/2}} \exp(-\frac{k_x^2 + k_y^2 + k_z^2}{2\sigma_k^2}) \tag{3.5}$$

indicating $\mathbf{p} = \hbar \mathbf{k}$ and having defined $\sigma_k = \sqrt{\frac{M K_B T}{\hbar^2}}$.

In general, in the experiments, all information about the system- like the spatial and velocity distribution, the presence of excitations in the gas etc.-, are obtained by taking an absorption image of the atoms. One can reveal the particles in two ways: by means of *in situ* imaging, that gives the spatial atom distribution within the harmonic potential, or after a certain expansion time, once the trapping potential is switched off: the expansion of the thermal gas is ballistic and the imaged spatial distribution of the expanding cloud can be directly related to the initial momentum distribution as $t_{exp} \to \infty$. The time evolution of the widths of a thermal sample is the following (i=x, y, z):

$$< r_i^2 > (t) = \sigma_i^2(0)(1 + \omega_i^2 t^2) \tag{3.6}$$

Therefore, observing the shape of the system in a plane perpendicular to one of the trap axes (e.g. y axis) as a function of the time of flight, one will see the gas changing its *aspect ratio* from

$$AR(0) = \frac{\sigma_z}{\sigma_x}(0) = \frac{\omega_x}{\omega_z}$$

in the case of in situ image, to the asymptotic value

$$AR(t \to \infty) = 1$$

that reflects the isotropy of the momentum distribution described above.

3.1.2 Fermi gas

I consider here a gas composed by N identical fermionic atoms trapped in a harmonic potential: the single particle hamiltonian will be then of the form:

$$H = \frac{p^2}{2M} + \frac{1}{2}M(\omega_x^2 x^2 + \omega_y^2 y^2 + \omega_z^2 z^2) \tag{3.7}$$

I suppose here in the following to work in the zero temperature limit[1]: the problem must be treated quantum-mechanically, and the spectrum of the three dimensional harmonic oscillator (3.7) is well known :

$$E(n_x, n_y, n_z) = \hbar\omega_x(\frac{1}{2} + n_x) + \hbar\omega_y(\frac{1}{2} + n_y) + \hbar\omega_z(\frac{1}{2} + n_z)$$

Remember also that the ground state of the harmonic oscillator is a gaussian of the form:

$$\psi_0(\mathbf{r}) = (\frac{M\overline{\omega}}{\pi\hbar})^{3/4} \exp[-\frac{M}{2\hbar}(\omega_x x^2 + \omega_y y^2 + \omega_z z^2)] \tag{3.8}$$

[1] A more exhaustive description of the Fermi gas at finite temperature can be found, for example, in [99].

where $\overline{\omega} = (\omega_x\omega_y\omega_z)^{1/3}$ is the geometrical average of the frequencies of the trap. The width of the ground state along the i-direction is given by $a_{ho,i} = (\hbar/M\omega_i)^{1/2}$, that is the size $\sqrt{\langle x_i^2\rangle}$ of the ground state of (3.7).

Since the Pauli exclusion principle forbids the multiple occupation of a single energetic level, in the lowest energy configuration the fermions will occupy one by one all the energy levels of the system until the last is filled. In general, the energy of the highest level is called the Fermi energy E_F, and it corresponds to the Fermi temperature T_F=E_F/k_B. In general the ratio between the temperature T and T_F, T/T_F, defines the degree of degeneration of the system. Indeed, if $T/T_F \gg 1$, the probability that a single quantum state is occupied is low and the system is classical, while if $T/T_F \leq 1$ the system enters in the degenerate regime.

For describing the fermionic atoms in the low temperature limit, the Maxwell Boltzmann distribution must be replaced by the Fermi-Dirac distribution that is given by:

$$f_F(E) = \frac{1}{e^{\frac{(E-\mu)}{\beta}} + 1} \tag{3.9}$$

where μ is the chemical potential and β has been defined above. In the case of $T = 0$, the chemical potential is just the Fermi energy, $\mu = E_F$, and the Fermi distribution reduces to the simple form:

$$f_F(E) = \begin{cases} 1 & \text{for } E \leq E_F \\ 0 & \text{otherwise} \end{cases}$$

Note that the expression above is anyway a good approximation even for finite temperatures, provided that $T \ll T_F$, see [100]. In the momentum space, this corresponds to define a sphere of radius $k_F \equiv (2ME_F/\hbar^2)^{1/2}$: i.e. at $T = 0$, all the particles of the system must have momentum $k \leq k_F$ and all momentum states with $k \leq k_F$ are occupied.

In general, if $\hbar\omega_i \ll k_B T$ for $i = x, y, z$, it is possible to neglect the discreteness structure of the harmonic oscillator levels, and then to write the density of states as follows:

$$g(E) = \frac{E^2}{2(\hbar\overline{\omega})^3} \tag{3.10}$$

At the mean time, if also the condition $T \ll T_F$ is fulfilled, one can employ the density of states (3.10) and approximate the Fermi distribution with the simple step function (3.1.2), and therefore one can easily evaluate the expression for the Fermi energy:

$$N = \int_0^{E_F} dE g(E) \tag{3.11}$$

from which it follows the explicit expression for the Fermi energy:

$$E_F = \hbar\overline{\omega}[6N]^{1/3} \tag{3.12}$$

The first important information it is possible to get from (3.12) is the size of the Fermi gas, given by:

$$R_{Fi} = [2E_F/M\omega_i^2]^{1/2} \tag{3.13}$$

$i = x, y, z$. In terms of the harmonic oscillator length, the Fermi radius is given by:

$$R_{F,i} = a_{ho,i}\sqrt{\frac{\overline{\omega}}{\omega_i}}(48N)^{1/6} \tag{3.14}$$

Note that the mean dimensions $R_F = (R_{F,x}R_{F,y}R_{F,z})^{1/3}$ of the trapped Fermi cloud will be in general much greater than the ground state size of the trap $a_{ho,i}$, as a consequence of the Pauli exclusion principle, that induces an effective "repulsion" between fermions in the trap (Fermi pressure) and forbids to the fermions to occupy the ground state of the system even at very low temperature.

In order to find out the spatial and momentum distribution of the Fermi gas trapped at $T = 0$ in the harmonic confinement (3.7), let's define a "local" Fermi wavenumber $k_F(\mathbf{r})$ by:

$$\frac{\hbar^2 k_F^2}{2M} + V(\mathbf{r}) = E_F \tag{3.15}$$

The spatial density $n(\mathbf{r})$ is given by the volume of the Fermi sea in momentum space times the density of state $1/(2\pi)^3$, i.e.

$$n(\mathbf{r}, T = 0) = \frac{k_F^3(\mathbf{r})}{6\pi^2} \tag{3.16}$$

with the assumption that $n(\mathbf{r}) \neq 0$ only if $|\mathbf{r}| < R_F$. If we substitute (3.15) inside (3.16), we obtain:

$$n(\mathbf{r}, T = 0) = \frac{2ME_F^{3/2}}{6\hbar^2\pi^2}[1 - (\frac{M\omega_x^2}{2E_F}x^2 + \frac{M\omega_y^2}{2E_F}y^2 + \frac{M\omega_z^2}{2E_F}z^2)]^{3/2} \tag{3.17}$$

The cloud is an ellipsoid with diameters $R_{F,i}$ in the x, y, z directions respectively, and the aspect ratios taken along any imaging direction are the same as that of a classical gas in the same potential. The momentum distribution for a Fermi gas can be obtained similarly to (3.17) and it results to be:

$$n(\mathbf{k}, T = 0) = \frac{N}{k_F^3}\frac{8}{\pi^2}[1 - \frac{|\mathbf{k}|^2}{k_F^2}]^{3/2} \tag{3.18}$$

where the maximum wavenumber populated is $k_F = (48N/R_F^3)^{1/3}$. As for classical gases, the momentum distribution of a Fermi gas is isotropic despite the anisotropy of the trap due to dependence of (3.18) only from the magnitude of $\mathbf{k}$.

In the case of Fermi gas, the evolution of the expanding cloud after release from the trap is similar to the one described above for thermal samples: from equation (3.18), we see that even in this case, we expect to have a complete isotropic expansion of the cloud. Indeed, solving the Boltzmann transport equation [101] for this case, and then extracting the temporal evolution of the radii of the Fermi gas, we get:

$$< r_i^2 > (t) = \frac{1}{4} R_{F,i}^2 (1 + \omega_i^2 t^2) \tag{3.19}$$

$$\tag{3.20}$$

that, except for the initial dimensions and shape, is analog to the classical gas case. Consequently, the evolution of the aspect ratio of the Fermi gas will be of the same kind of that of a thermal sample trapped into the same potential.

3.1.3 Bose gas

The fact that the many body wavefunction of a system of N bosons must be symmetric under the exchange of any couple of particles causes that, as the quantum effects become visible ($\lambda_{DB}^3 n \sim 1$), the gas is no longer well described by the Maxwell Boltzmann distribution function (3.1), that must be replaced by the Bose Einstein distribution function [100]:

$$f_B(E) = \frac{1}{e^{\frac{E-\mu}{\beta}} - 1} \tag{3.21}$$

where μ is the chemical potential. Note that, as in the case of the Fermi distribution function, at hight temperatures the (3.21) is approximately:

$$f_B(E) \simeq f_c(E) = e^{-\frac{\epsilon-\mu}{\beta}} \tag{3.22}$$

i.e. the classical case (3.1). Defining the fugacity as $\Lambda = \exp(\frac{\mu}{\beta})$, the relation (3.21) can be written as:

$$f_B(E) = \frac{\Lambda}{e^{\frac{E}{\beta}} - \Lambda} \tag{3.23}$$

It is evident that $0 < \Lambda < 1$: assuming that $E = 0$ is the energy of the ground state, (3.23) becomes:

$$f_B(E=0) = \frac{\Lambda}{1-\Lambda} \tag{3.24}$$

that is the occupation number $f_B(E=0)$ of the lowest energy level of the system, that can be extremely large if the fugacity Λ goes to 1. It is possible to show that the mean occupation number of all the other energy states with energy bigger than zero cannot exceed a certain value fixed the temperature T [102]. This means that all the other atoms that are added to the system must occupy the lowest possible energy level, the ground state, whose population becomes then macroscopically large. It can be shown that the onset of the degenerate regime is reached for a critical value for the quantity $n\lambda_{DB}^3$, precisely [103]

$$n\lambda_{DB}^3 = 2.6 \tag{3.25}$$

Eq. (3.25) simply says that when the mean interparticle distance $d \propto (n)^{-1/3}$ is larger than the DeBroglie wavelength λ_{DB} then we lose completely the possibility of distinguish the particles between themselves, because the wave-packets associated to each atom start to interfere. The system must be described by quantum mechanics laws, and in particular, in the case of N identical bosons by a single wavefunction, namely the *order parameter*: at this point the system is said to be a Bose Einstein condensate (BEC).

It is possible also to show ([103]) that in the case of a cylindrical potential ($\omega_a = \lambda\omega_r$),

$$N - N_0 = \frac{\zeta(3)}{\lambda}\left(\frac{k_B T}{\hbar\varpi}\right)^3 \tag{3.26}$$

where N_0 is the condensate fraction and $\zeta(x)$ is the Riemann function. If we set $N_0 = 0$, then we can obtain the expression for the critical temperature T_C:

$$T_C = \frac{\hbar\omega_r}{k_B}\left(\frac{N\lambda}{\zeta(3)}\right)^{1/3} = 0.94\frac{\hbar}{k_B}\omega_r(N\lambda)^{1/3} \tag{3.27}$$

Combining Eq. (3.26) and Eq. (3.27) we get the T-dependence of the condensate fraction:

$$\frac{N_0}{N} = \left(1 - \frac{T}{T_C}\right)^3 \tag{3.28}$$

In the case of an ideal gas of bosons at zero temperature trapped in a harmonic potential (3.7) the description of the system is trivial: every atom is described by

means of the wavefunction given by the expression (3.8), and the density distribution of the trapped condensate is given by $\sim N|\psi_0^2(\mathbf{r})|$, normalized to the total atom number N. This has a gaussian shape, as in the thermal gas case, but now the width of the envelope (along the direction i), instead of being $\sigma_i = \sqrt{\frac{K_B T}{M\omega_i^2}}$, it is given by $a_{ho,i}/\sqrt{2} = \sqrt{\frac{\hbar}{2M\omega_i}}$. The peak density is proportional to the condensed atom number, while the extension of the system is "number independent".

The expansion of the ideal BEC is described by the relations:

$$< r_i^2 > (t) = \frac{1}{2} a_{ho,i}^2 (1 + \omega_i^2 t^2) \tag{3.29}$$

$$\tag{3.30}$$

and in this case the aspect ratio evolves from

$$AR(0) = \frac{a_{ho,z}}{a_{ho,x}}(0) = \sqrt{\frac{\omega_x}{\omega_z}}$$

in the case of in situ image, to the asymptotic value

$$AR(t \to \infty) = \sqrt{\frac{\omega_z}{\omega_x}}$$

that differs both from the thermal gas and the Fermi gas expansion.

However, in real situations bosonic condensed atoms strongly differ from the ideal case, and the effects of atom atom interaction deeply affect the behavior of the condensate: if we "turn on" the interaction between particles spatial shape, momentum distribution, evolution of the cloud after release from the trap, are influenced by such interaction, and the scenario changes completely.

The dilute nature of these system (the mean interparticle distance is almost ten times the range of the interatomic force), allows to describe the interaction between atoms by a single parameter, the s-wave scattering length, a, see (2.1.1), and the complex effective atom atom interaction can be described by means of a mean field potential, given by

$$U = \frac{4\pi\hbar^2 a}{M} n(\mathbf{r}) \equiv g n(\mathbf{r}) \tag{3.31}$$

having defined the coupling constant $g = 4\pi\hbar^2 a/M$. Remember that the sign of the scattering length sets the nature of the interaction: in case of positive (negative) sign of a, the interaction between atoms create a repulsive (attractive) contact potential. Within the mean-field approximation, the ground state of the system is obtained by solving the the Gross-Pitaevskii equation (GPE):

$$\frac{\partial}{\partial t}\Phi(\mathbf{r},t) = \left(-\frac{\hbar^2\nabla^2}{2M} + V_{ext}(\mathbf{r}) + g n(\mathbf{r},t)\right)\Phi(\mathbf{r},t) \tag{3.32}$$

with $n(\mathbf{r}) = |\Phi(\vec{r},t)|^2$. In this approximation it is possible to write the wavefunction as $\Phi(\mathbf{r},t) = \phi(\mathbf{r})exp(-i\mu/\hbar)$ and the (3.32) as:

$$(-\frac{\hbar^2\nabla^2}{2M} + V_{ext}(\mathbf{r}) + g\phi^2(\mathbf{r}))\phi(\mathbf{r}) = \mu\phi(\mathbf{r}) \tag{3.33}$$

where μ is the chemical potential and must be normalized to the total number of atoms.

Note that the ground state of (3.33) not always exists: in the case of attractive interaction, the solution exists only if the number of condensed atoms doesn't exceed a critical value ([103]):

$$\frac{N_{crit}|a|}{a_{ho}} = 0.575 \tag{3.34}$$

a_{ho} being the mean oscillator length $\sqrt{\frac{\hbar}{M\overline{\omega}}}$ and $\overline{\omega} \equiv (\omega_x\omega_y\omega_z)^{1/3}$. If the atom number exceeds this critical value, within few time, set by the trap frequencies, the system *collapses*: essentially due to the mean field potential the system minimizes its energy if the density at the center of the BEC increases; this causes a dramatic increase of the three body losses rate, that causes the destruction of the condensate [104].

The solution of (3.33) is particulary simple if the mean field energy is positive and larger than the kinetic energy (Thomas-Fermi regime):

$$n(\mathbf{r}) = \phi^2(\mathbf{r}) = g^{-1}[\mu - V_{ext}(\mathbf{r})] \tag{3.35}$$

Since the trapping potential is quadratic, the shape of the density profile is an inverted parabola. The Thomas-Fermi (TF) approximation is valid only if $Na/a_{ho} \gg 1$, thus for large number of atoms and/or large interaction strength. From the normalization on the number of atoms, it is possible to obtain the expression for the chemical potential μ:

$$\mu = \frac{\hbar\overline{\omega}}{2}(\frac{15Na}{a_{ho}})^{2/5} \tag{3.36}$$

It is also possible to write down the expression for the radius of the condensate in the TF regime,

$$R_i = (\frac{2\mu}{M\omega_i^2})^{1/2} = \frac{\overline{\omega}}{\omega_i}a_{ho}(\frac{Na}{a_{ho}})^{1/5} \tag{3.37}$$

defined as the position along every trap axis i at which the density (3.35) vanishes. The mean square radius for every direction i in the three dimensional case is given by

$$\sqrt{\langle x_i^2\rangle} = R_i/\sqrt{7} \tag{3.38}$$

The effect of the interaction is then to increase the size of the condensate with respect to the noninteracting case and to give a dependence of the radius from the number of atoms. Furthermore, the value of the density in the center of the trap is $n(0) = \mu/g$ and if we compare it with the one found in the noninteracting regime, we get:

$$\frac{n(0)}{n_{ho}} \propto (\frac{Na}{a_{ho}})^{-3/5} \tag{3.39}$$

i.e. $n(0)$ decreases if N increase: this is another effect due to the repulsive interaction between the atoms in the BEC.

The mean field interaction causes not only the modification of the shape of the in trap distribution with respect to the ideal case, but also of the ballistic expansion of the BEC [103]: after release from the trap, the mean-field energy is transformed in kinetic energy. Within the Thomas Fermi approximation and for a cigar shaped potential (frequencies ω_r and $\omega_a \equiv \lambda\omega_r \ll \omega_r$) one finds the following analytic expansion laws [105] for the axial and radial dimensions of the BEC respectively:

$$\begin{aligned} R_r(t) &= R_r(0)\sqrt{1+\tau^2} \\ R_a(t) &= R_a(0)(1+\lambda^2[\tau \text{arctan}\tau - ln\sqrt{1+\tau^2}]) \end{aligned} \tag{3.40}$$

where $\tau \equiv \omega_r t$. The velocity of the expansion is determined from the initial confinement of the cloud: the most confined directions expands faster. To understand this, consider that the interaction is density dependent ($U = gn$) and in particular, if we take the gradient of the mean-field potential, ($\nabla U \approx g\nabla n$), one can see that the mean field force acting on the atoms when the trapping potential is switched off is larger in the more confined direction. Note that this causes an evolution of the aspect ratio from

$$AR(0) = \frac{R_r(0)}{R_a(0)} = \frac{\omega_a}{\omega_r} = \lambda$$

to the asymptotic value

$$AR(t \to \infty) = \frac{\pi}{\lambda}$$

differing from the one relative to thermal, Fermi or ideal Bose gases.

3.1.4 Thermal Bose-Fermi mixtures.

In this subsection I want to point out few characteristics that distinguish a thermal mixture of bosons and fermions from a single component thermal gas: in particular, I'll focus on the description of the effects induced by three body processes that

take place within the mixture, since a different behavior with respect to homonuclear systems (see section 2.1.5) is expected, and because this may help to better understand the comparison between a thermal and a degenerate tunable mixture. In particular, I suppose here that the two atomic species have the same temperature, but different masses and different trapping frequencies that, if we assume a harmonic confinement, are related by the relation:

$$\omega_{i,F} = \sqrt{\frac{M_B}{M_F}}\omega_{i,B} \tag{3.41}$$

Recalling the relation (3.4) derived for the thermal single species gas, one can see that once the temperature of the components is the same, also their widths will be the same:

$$\sigma_i = \sqrt{\frac{K_B T}{M_B \omega_{i,B}^2}} = \sqrt{\frac{K_B T}{M_F \omega_{i,F}^2}} \tag{3.42}$$

Along the vertical direction, due to their different masses, the two species have different equilibrium positions within the harmonic trap (different gravitational sags): the centers of mass of the two atomic clouds are shifted by

$$z_0 = g\left(\frac{1}{\omega_{z,B}^2} - \frac{1}{\omega_{z,F}^2}\right) \tag{3.43}$$

In the case of potassium and rubidium, the relative sag is $\sim 13\mu m$ for $\omega_{z,B} = 100$ Hz, being potassium cloud placed at a larger height than rubidium. Therefore, generally the overlap between the two clouds will be only partial, and the lower is the temperature of the system, the smaller will be the overlap region. As an example, in Fig. 3.2 is plotted the density distribution along the vertical direction of two clouds of potassium and rubidium, whose population are in a ratio 1:2, at temperatures of 1000, 500 and 300 nK respectively, with a trapping frequency for rubidium equal to 30 Hz along the vertical direction: the overlap region is only partial, and it is reduced as the temperature of the samples is lowered.

This causes a peculiar behavior of three body losses: in the homonuclear case, we have said (see section 2.1.5) that three body recombination always causes a heating of the sample, since the collisions preferentially take place within the denser part of the thermal cloud. In the heteronuclear mixtures in general this is not necessarily true: in fact, due to the presence of a sag, under certain conditions of trapping frequencies and temperature the three body processes can cause losses of atoms that have an energy larger than the mean thermal energy; in fact, as the temperature is reduced,

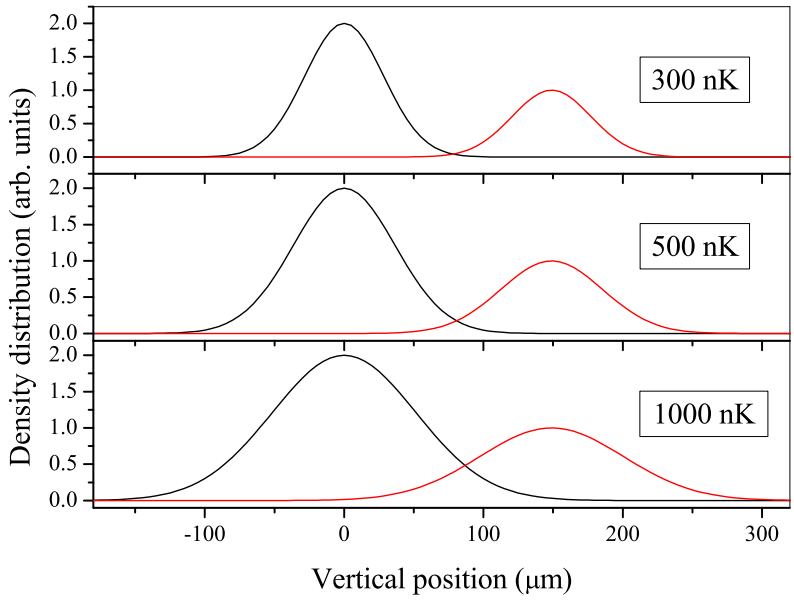

Figure 3.2: Density distribution along the vertical direction for a thermal sample of rubidium and potassium atoms confined in a trapping potential of 30 Hz for Rb for three different values of the common temperature. The populations of Rb (black line) and K (red line) are in a ratio 2:1, and the relative gravitational sag is approximatively 150 μm. As the temperature is lowered, the overlap region decreases.

the three body processes take place preferentially in the periphery of the two clouds, i.e. in the warmer parts. This can be seen in the Fermi Bose mixture by evaluating the mean energy of an atom undergoing a three body collision. As I already discussed in chapter 2, such processes at low temperatures mainly involve for statistical reasons two bosons and one fermion ($B + B + F \rightarrow BF + B$): therefore the rate equations for the mixture are given by:

$$\dot{n_B} = -K_3 n_B^2 n_F \tag{3.44}$$

$$\dot{n_F} = \dot{n_B}/2 \tag{3.45}$$

Let's evaluate the mean potential energy U of a bosonic atom with the weighting function $n_B^2 n_F$, being both n_B and n_F gaussian distributions always with the same

temperature and displaced along the vertical direction by z_0 given by (3.43). The result is:

$$\langle U \rangle = \frac{\int U n_B^2 n_F dV}{\int n_B^2 n_F dV} = \frac{1}{2} k_B T + \frac{1}{18} \omega_{B,z}^2 z_0^2 \equiv \frac{1}{2} k_B T + k_B T_S \tag{3.46}$$

having defined an effective temperature T_S that is present because of the different sags of the two atomic species: note that this extra temperature is $T_S \propto \omega_{B,z}^{-2}$. The same mean energy is associated to the fermionic atoms involved in three body processes. Therefore, one can see that in the case of Fermi Bose heteronuclear mixture the energy released from atoms undergoing three body collisions to the remnant sample is given by

$$E_{rel} = K_B (T - T_S) \tag{3.47}$$

considering that the mean potential energy of an atom in the gas is given by $3/2 k_B T$. This quantity is usually positive, but as $T \leq T_S$ it can become zero or even negative: therefore, in this case three body losses do not affect, or even can lower, the sample temperature. This is a peculiar feature of heteronuclear mixtures that in principle can be observed in experiments. A simple model can be built up for the evolution of the atom number and temperature of the mixture: I follow the ideas developed in [74], assuming an immediate thermalization of the two components, in such a way that at every time the temperature of the two gases is the same. Integrating the rate equations (3.44), and considering (3.47), one can obtain the following system of coupled equations for the atom number and the temperature of the Bose Fermi mixture:

$$\frac{dN_B}{dt} = -\gamma \frac{N_B^2 N_F}{T^3} \exp(-\frac{6T_S}{T}) \tag{3.48}$$

$$\frac{dN_F}{dt} = \frac{1}{2} \frac{dN_B}{dt} \tag{3.49}$$

$$\frac{dT}{dt} = \frac{\gamma}{2} \frac{T - T_S + T_h}{T^3} \frac{N_B^2 N_F}{N_B + N_F} \exp(-\frac{6T_S}{T}) \tag{3.50}$$

where T_S has been defined above, T_h is a parameter that takes into account the extra heating due to the presence of a weakly bound state in the vicinity of a Feshbach resonance (see section 2.1.5 and [74]) and where $\gamma \equiv K_3 (M_B \overline{\omega}^2 / 2\pi k_B)^3 / \sqrt{27}$. The three coupled equation can be solved numerically, and in Fig. 3.3 I plot the evolution of temperature of a sample of $5 \cdot 10^6$ Rb and $3 \cdot 10^5$ K atoms loaded at different T_{LOAD} in a trap that for Rb has frequencies $(100, 100, 30)$ Hz along (x, y, z): for these trap parameters $T_S \sim 460$ nK[2]; I assume here $T_h = 0$, that is reasonable for the bo-

[2]Consider that, since $T_S \propto \omega_{B,z}^{-2}$, in real experiments one can hope to observe this effect only working

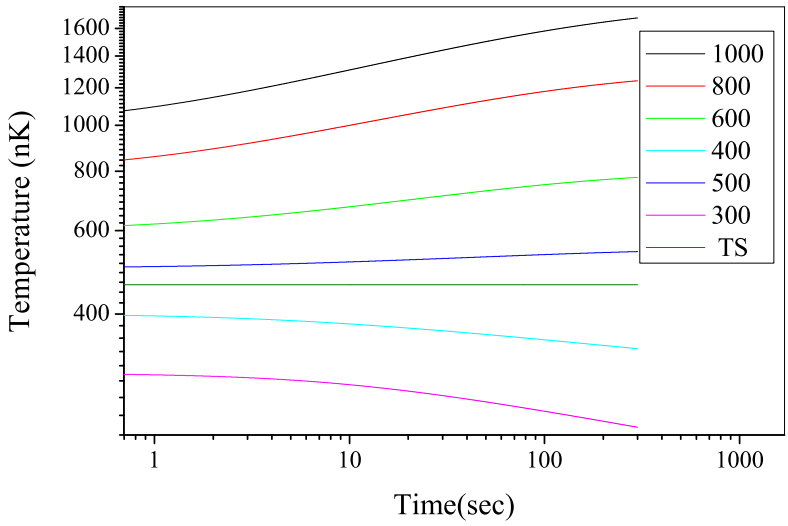

Figure 3.3: Evolution of temperature of a sample of $5 \cdot 10^6$ Rb and $3 \cdot 10^5$ K atoms loaded at different T_{LOAD} in a trap that for Rb has frequencies $(100, 100, 30)$ Hz along (x, y, z): for these trap parameters $T_S \sim 460$ nK. As the loading temperature is decreased, the heating due to three body collisions decreases, until $T_{LOAD} = T_S$, for which the sample does'nt heat up; for even lower initial temperatures the three body processes cool down the sample, showing a behavior that is not present in the homonuclear case.

son fermion mixture we are working with, since the molecular binding energy of the ^{40}K ^{87}Rb Feshbach molecules greatly exceeds the trap depth, even at few hundred mGauss far from the center of the broadest resonances. One can see that as the loading temperature is decreased, the heating due to three body collisions decreases, until $T_{LOAD} = T_S$ for which the sample doesn't heat up; for even lower initial temperatures the three body processes cool down the sample. The same effect can be seen considering the main energy released in the system from an atom lost for a three body process (3.47) normalized to the mean energy $3/2k_BT$:

$$E_{rel} = \frac{2}{3}(1 - \frac{T_S}{T}) \tag{3.51}$$

with shallow vertical confinement; for example, for a trapping frequency of 100 Hz $T_S \sim 40$ nK, that is usually well below the onset of the degenerate regime for both the mixture components.

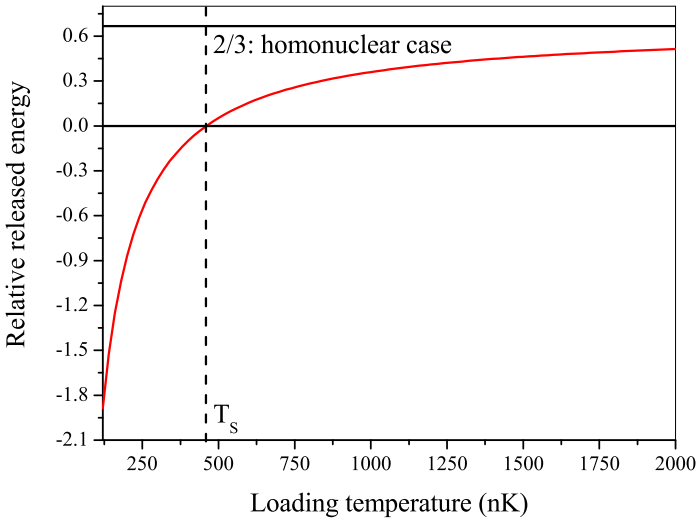

Figure 3.4: Behavior of Eq. (3.51) versus the loading temperature assuming $\omega_{B,z} = 30$ Hz: for low temperatures the released energy is negative, i.e. three body processes cool down the sample. As the temperature exceeds the value T_S (that in this case is 460 nK) the three body collisions cause a heating of the sample, that saturates at $T/T_S \gg 1$ to the value $2/3$, of the homonuclear case.

as a function of the loading temperature. In Fig. 3.4 is plotted the relation (3.51) for a trapping frequency $\omega_{B,z} = 30$ Hz, corresponding to $T_S = 460$ nK; it can be seen that the lower is the temperature, the greater is the "evaporative cooling" effect for three body losses. In the opposite limit, instead, as T exceeds T_S, the relative energy is positive- therefore three body processes heat up the sample-, and saturates at the value $2/3$ of the homonuclear case for $T/T_S \gg 1$. Even if in the experiments involving thermal samples we have never investigated this phenomenon, the behavior of the mixture with respect to three body losses seems to be somehow intriguing even in the thermal regime, once $T < T_S$ condition is reached, and could be the object of future investigations.

Note that when the interaction between the atoms is large three body losses can deeply modify in a short time the initial configuration of the two clouds: however, in thermal samples neither the relative center of mass position, nor the expansion after

release from the trap are influenced by the interspecies interaction.

Finally, despite three body recombination can strongly affect the system, at least at large scattering length values and low temperatures, the behavior of the sample is somehow *symmetric* with respect to attractive or repulsive interaction, since as in homonuclear case the K_3 coefficient scales as[3] $C \times a_{BF}^4$.

3.1.5 Quantum degenerate Bose-Fermi mixtures

I have shown above that the mean-field interaction plays an important role in the stability of a BEC, and many of the features of the condensate are strictly related to this interaction between the atoms. On the contrary, due to the suppression of any collisional process, the properties of a Fermi gas, composed by identical fermions, are simply determined by the quantum statistics (Fermi pressure) rather than an effective interaction between the atoms. I have also described the properties of a thermal mixture of bosons and fermions of different masses, and I remarked how the two gases displace one with respect to the other within a standard harmonic potential: the trap geometry, the sample temperature, the masses of the two species determine the shape and relative position of the gases in the confining potential.

The situation is quite different when we consider a quantum degenerate mixture composed by bosons and fermions mutually interacting. Indeed, in this case both the Gross-Pitaevskii and the Thomas-Fermi equations, describing respectively the Bose and the Fermi trapped gases, must contain an additional term describing the interaction between the two species. This additional term is proportional to the interspecies scattering length a_{BF} and its magnitude and sign determine the behavior of the mixture, modifying - sometimes very deeply - both the in trap behavior and the expansion of the mixture. The ground state properties of a degenerate system composed by a Fermi gas interacting with a Bose-Einstein condensate, trapped in a harmonic potential, is obtained solving the following coupled equations [109]:

$$n_F(\mathbf{r}) = \frac{\sqrt{2M_F^3}}{3\pi^2}[\mu_F - U_F(\mathbf{r}) - \frac{4\pi a_{BF}}{M_{BF}} n_B(\mathbf{r})]^{3/2} \tag{3.52}$$

$$[-\frac{1}{2M_B}\nabla^2 + U_B(\mathbf{r}) + \frac{4\pi a_{BF}}{M_{BF}} n_F(\mathbf{r}) + \frac{4\pi a_B}{M_B}\phi^2(\mathbf{r})]\phi(\mathbf{r}) = \mu_B \phi(\mathbf{r}) \tag{3.53}$$

where $\phi_B(\mathbf{r}) = \sqrt{n_B(\mathbf{r})}$, $M_{BF} = 2M_F M_B/(M_B + M_F)$ is twice the reduced mass of the pair, and the coupling between bosons is as usual given by the s-wave scattering

[3] This is not completely true, since a different constant C is expected for positive or negative values of a_{BF} [81, 112]. However, we have never observed such asymmetry in our experiments, and also a recent measurement of the K_3 coefficient for the mixture [116] didn't evaluate any significant asymmetry in the three body processes.

length a_B, that in the following I consider positive, since we are dealing with ^{87}Rb atoms. Solving simultaneously the coupled Eq. (3.52) and Eq. (3.53), one can obtain the density profiles of the two species. The solution of the system must be performed numerically, and no analytical expressions exist to my knowledge for describing the ground state of the interacting Fermi-Bose mixture, besides in the homogeneous case [106]. Our theoretical investigation of the system relies on a mean field model at zero temperature [107] that computes the local interaction energy and uses it as an additional effective potential for both species to evaluate the distribution of the mixture in the trap. This procedure is done recursively until the true ground state of the system in presence of interaction is found.

The term $4\pi a_{BF}/M_{BF}$, describing the interspecies interaction, is the key parameter for determining the stability or the instability of this system: in fact, similarly to what happens in the case of a BEC and the Gross Pitaevskij equation, also in Bose Fermi mixtures the solution of (3.52) and (3.53) not always exists. If the strength of the boson-fermion attraction becomes too large, then the mixture *collapses* towards high densities. In this case the attractive mean field is not stabilized by the positive kinetic-energy contribution or the repulsive boson-boson interaction any more, i.e., the gas can lower its energy by contracting and increasing the density in the central region, see [108, 109, 110]. Consequently, three body processes destroy the degenerate sample within few time, set by the trapping frequencies, and a thermal sample is left.

In the other limiting case, where the interaction between the mixture components is large and repulsive, the bosons and fermions tend to minimize their energy reducing the overlap region between the two clouds: also in this case, not only the shape of the samples is modified, but also the equilibrium positions of BEC and Fermi gas are shifted, due to the presence of the additional mean field effective potential. In the limit of large interspecies positive interaction the BEC is pushed out of the Fermi sea, and a *phase separation* of the two components takes place.

I remark here that mean field interaction modifies also the evolution of the mixture after release from the trap: the two degenerate systems continue to feel each other and the mean field energy can influence the first part of the expansion: this has been theoretically investigated [111] using a hydrodynamic description of the system [113], and also experimentally observed [114].

Let's now consider the degenerate regime of the mixture from the point of view of three body processes, as a function of the strength of the interspecies interaction: clearly these are not taken into account from eq. (3.52) and (3.53). Nevertheless, one

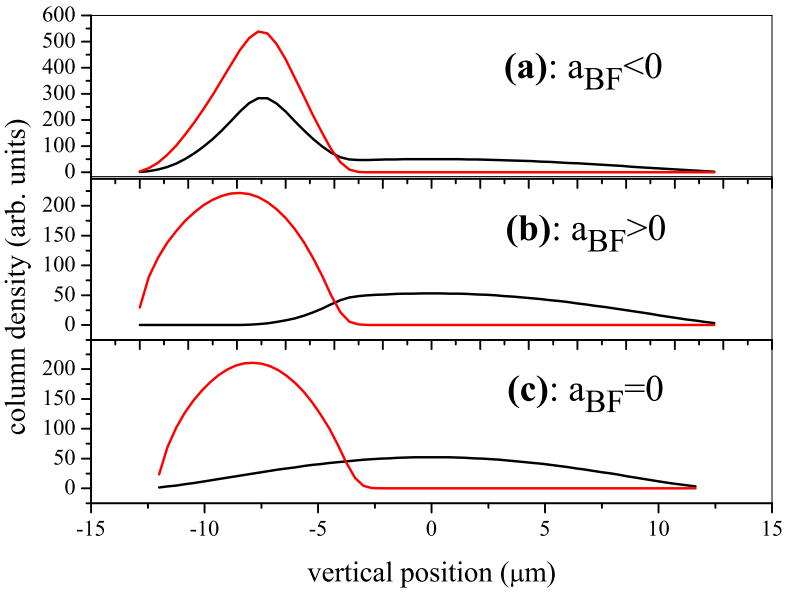

Figure 3.5: In-trap density profiles of a Fermi Bose degenerate mixture of $1 \cdot 10^5$ Rb (red line) and $7 \cdot 10^4$ K (black line) atoms loaded with different strength of the interspecies interaction. In Fig. (a) $a_{BF} = -350a_0$ and the two components strongly attract each other: the Fermi sea is enclosed within the BEC, and the overlap between the two components is large. Stronger attraction would cause the collapse of the system. Fig. (b) shows the opposite limit of strong repulsion ($a_{BF} = +250a_0$) of the two components: the BEC and the Fermi gas tend to reduce their spatial overlap and to phase separate. In Fig. (c) the two gases lay in the trap without interacting ($a_{BF} = 0$); the two clouds are separated by the relative sag, and no modification of the shape is induced by the mean field interaction.

can use the mean field model [107] for calculating the ground state of the system, and investigating its behavior with respect of three body collisions, evaluating some quantities of interest. In particular, remember what I already pointed out for the thermal case in the previous subsection: three body losses involve two bosonic atoms and a fermionic one, due to the statistics, and therefore the rate equations for the system are the (3.44). Consequently, the *event rate* (intended as the number of events

of three body processes per unit of time) is expected to depend on n_F and n_B as:

$$\Gamma_3 \sim K_3 \int n_B^2(\mathbf{r}) n_F(\mathbf{r}) dV \tag{3.54}$$

where $K_3 \propto a^4$ in the regime of large scattering lengths.

Let's consider now, within the degenerate regime, the effect of heating-cooling associated to three body collisions already treated for thermal mixtures in the previous subsection. Differently from the thermal case, in degenerate regime the dependence of the event rate on the scattering length is included also within the integral, and this makes the behavior of the system not trivial. In Fig. 3.6(a) the event rate (3.54) is plotted as a function of the scattering length, and in the inset this is compared to a bare a^4 dependence, that is expected for thermal samples. As one can see, the event rate is lower than in the thermal case, since phase separation occurs and lowers the overlap between the clouds, therefore reducing the value of the integral in (3.54). Note that the evaluation of this quantity is limited by the existence of the ground state for large attractive interaction. Furthermore, I have already shown that three body losses are expected to cause a heating of the sample, except for the case where the mixture has a temperature below the "critical value" T_S. As previously done in the thermal case, also in the degenerate regime we can evaluate the mean energy per lost particle (3.46):

$$\langle E_l \rangle = \frac{\int U(\mathbf{r}) n_B^2(\mathbf{r}) n_F(\mathbf{r}) dV}{\int n_B^2(\mathbf{r}) n_F(\mathbf{r}) dV} \tag{3.55}$$

where now I consider it with respect to the mean energy associated to a boson within the BEC. A reduced or increased overlap is expected to affect not only the three-body loss rate Γ_3, but also the ratio between the mean energy of particles in the overlap region and the mean energy of the whole system, which determines the heating rate. One can use the mean field model to calculate numerically the evolution of the overlap integral, the mean energy per lost particle and the mean energy per particle in the system, at T=0. In Fig. 3.6(b) is shown the energy released into the condensate per lost particle, normalized to the mean energy in the BEC:

$$\frac{\overline{E}_B - E_l}{\overline{E}_B}, \quad \text{where: } \overline{E}_B = \frac{\int U(\mathbf{r}) n_B(\mathbf{r}) d\mathbf{r}}{\int n_B(\mathbf{r}) d\mathbf{r}}. \tag{3.56}$$

For a_{FB}=0 the model predicts a relative energy gain of about 0.5, close tho the classical value discussed above of 2/3. The increase of heating on the $a_{FB} < 0$ side and the corresponding reduction on the $a_{FB} > 0$ side are apparent. Actually, this model indicates that three-body losses should eventually *cool down* the system as a_{FB} gets larger than $500a_0$, where the relative energy gain becomes negative.

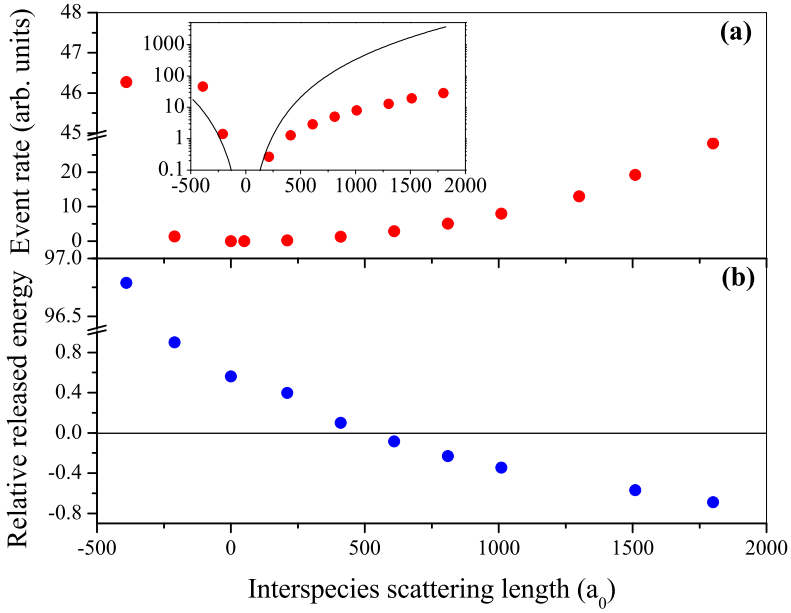

Figure 3.6: Losses and heating in a quantum degenerate mixture. Panel (a) In the graph the quantity $a_{BF}^4 \int n_B^2 n_F dV$ is plotted; this is proportional to the loss rate (3.54) as a function of interaction strength in degenerate regime. As the repulsion between the bosons and fermions become large, phase separation occurs, and this lowers the event rate, since it reduces the value of the overlap integral. In the inset is shown a comparison between the loss rate behavior in the degenerate regime and a bare a^4 dependence, typical of thermal samples where the overlap integral is expected to not vary. Panel (b) shows the energy released in the BEC by atoms undergoing a three body collision, normalized to the mean energy of a boson in the BEC. As the repulsion exceeds a certain value, the effect of the three body collision is to remove the most energetic atoms from the outer shells of the atomic clouds.

This clearly shows how in the degenerate case, in addition to the phenomena already mentioned for thermal mixtures, mean field interaction profoundly affects the three body processes physics. In the thermal case, for a fixed trap geometry, the cooling effect is connected to the shapes of the clouds, that for $T < T_S$ overlap only in a region where most energetic particles lay, and it would vanish if the sag would be reduced. In degenerate samples, instead, this still would be observable, since it

originates from mean field energy, that does not depend on the relative sag.

3.2 Experiments with a quantum Fermi Bose mixture

3.2.1 The route towards degenerate regime

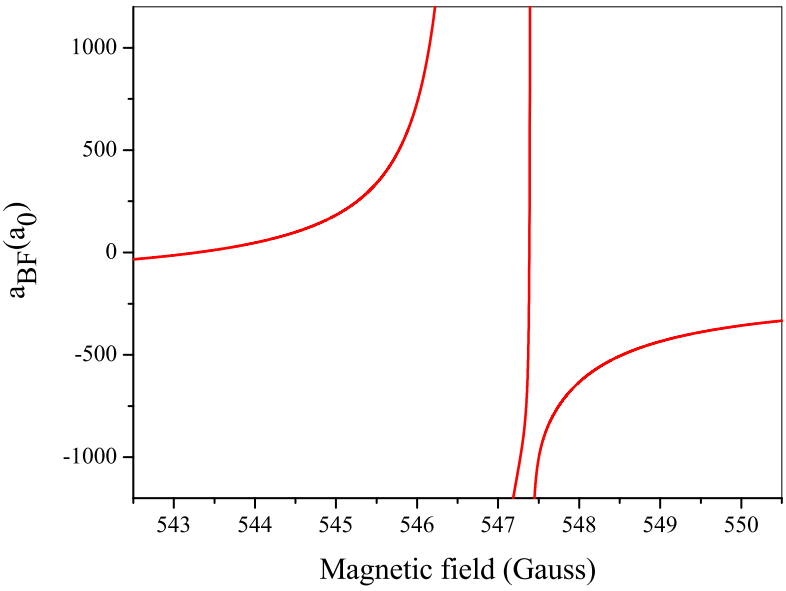

Figure 3.7: Magnetic field dependence of the interspecies scattering length close to the broadest resonance of the absolute ground state of the Fermi Bose mixture. Note that the dispersive behavior of the bare s-wave resonance is slightly modified by the presence of a narrow ($\Delta = 0.08$ Gauss) $s \rightarrow d$ spin resonance located at 547.4 Gauss.

We have investigated the behavior of the Bose Fermi mixture of ^{40}K-^{87}Rb employing the broadest resonance in the absolute ground state of the system ($|9/2, -9/2\rangle$ and $|1, 1\rangle$ respectively), located around 547 Gauss. In order to achieve quantum degeneracy, we start from a sample of typically 2 10^5 K fermions and 5 10^5 Rb bosons in their absolute ground state at about 1 μK held in the optical trap, as already described in previous chapters. The trap depth for both species is about 5 μK, and the trap frequencies $\omega/2\pi$ are (120,92,126) Hz for Rb and a factor about $\sqrt{(87/40)}$

larger for K. A homogeneous magnetic field is raised up, with the timescales already described, to B$\sim$550 G, in the vicinity of the broadest K-Rb Feshbach resonance for these states shown in Fig. 3.7; the mixture is further cooled by reducing the depth of the optical trap in 2.4 s and then re-compressed to the full depth in 150 ms: as already mentioned, selective evaporation of bosons is achieved by exploiting the lower trap depth for bosons, due to the larger contribution of gravity in shallow traps. This allows us to produce samples composed of up to 10^5 atoms per species, at $T < 0.2T_C$ for Rb and $T \sim 0.3T_F$ for K, where T_C=230 nK and T_F=630 nK. The Bose gas has a radius of the order of $5-7$ μm, and it is completely enclosed in the Fermi gas, whose dimensions are approximately as twice as large.

3.2.2 Thermal vs degenerate

We have at first performed a fine tuning of the interspecies interaction employing a cold sample, at temperatures of the order of 200 nK. For the atom numbers we had in the experiment, the critical temperature for rubidium is $\sim$ 180 nK, and the Fermi temperature for potassium is $\sim$ 490 nK: therefore, the ^{40}K is already degenerate, while the bosons are still not condensed. This condition is achieved by stopping the evaporation in the dipole trap just before reaching the fully degenerate regime, and re-compressing the trap up to the initial depth. During evaporation, the magnetic field is fixed at a value around 540 Gauss, sufficiently far from the resonance center to not affect the evaporation in the dipole trap. Once the sample is at the desired temperature, the magnetic field value is changed within few ms to values around the resonance, and the sample is held in the trap for 100 ms. Successively, the trapping potential and the magnetic field are switched off, and we let freely expand the fermionic and bosonic clouds for 8.5 ms and 12.5 ms respectively, after which an absorbtion image is taken. In Fig. 3.8 I plot the results of the experiment, showing the temperature of the two clouds[4], and the atom numbers of bosons and fermions as functions of the magnetic field.

As already mentioned in subsection 3.1.4, one expects that three body losses deeply affect the mixture population and temperature, once the interspecies interaction is tuned towards large values: note that for the trap parameters we have chosen ($\omega_z/2\pi$ equal to 126 Hz for Rb, see above) the parameter $T_S \sim 30$ nK, well

[4]Concerning bosons, the real temperature is plotted. For fermions, since the mixture is already below the Fermi temperature, I report the rescaled width of the potassium cloud, fitted as a gaussian function. However, the mixture components are quite always in thermal equilibrium, except when they are very close to the resonance center.

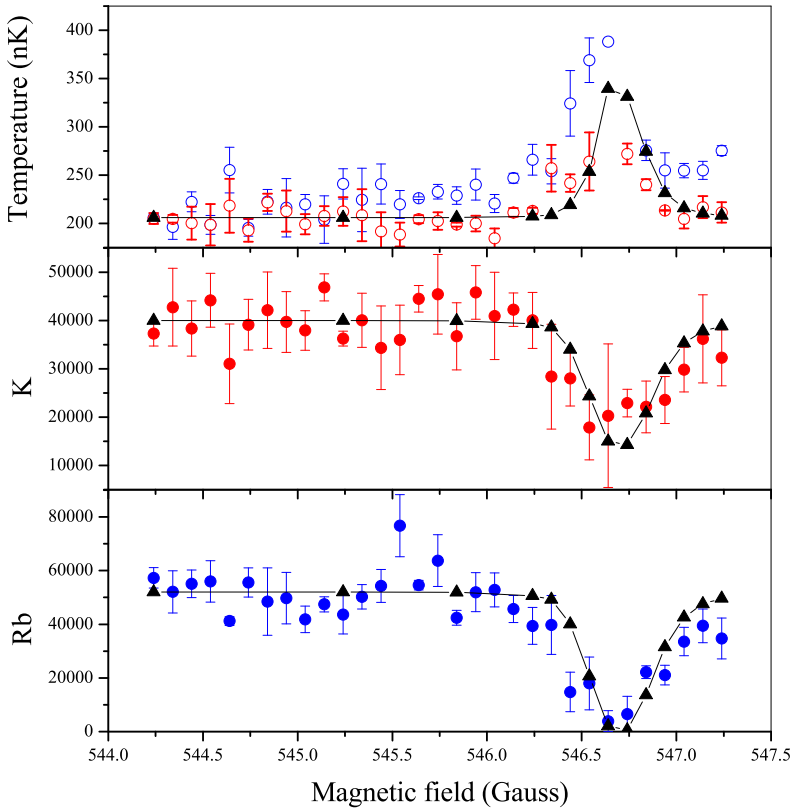

Figure 3.8: Atom numbers and temperatures of the Fermi (red points) Bose (blue points) mixture as a function of the magnetic field close to the broad interspecies resonance. The sample is prepared at 540 Gauss, brought to the final value of the magnetic field, and left there for 100 ms. Three body recombination rate is enhanced close to the resonance center since the scattering length diverges, and losses and heating are observed. A simulation based on Eq. (3.48) is also shown.

below both BEC critical temperature of rubidium and Fermi temperature of potassium; therefore, with this measurement, we cannot observe the peculiar behavior of "evaporative cooling" via three body processes described above. We can see that the number of three body processes increases as we move towards the resonance, and a strong heating accompanies the atom losses. The behavior is symmetric with respect

to the sign of the scattering length (at least, no significative asymmetry is detectable), both in the losses and the heating. I also show a simulation of the system, obtained by solving eq. (3.48) for $T_h = 0$, initializing the atom numbers and temperature to their experimental background values, and assuming a dependence $K_3 \propto a_{BF}^4$. The agreement with the experimental data is quite good, except in the strongly interacting region very close to resonance, where potassium and rubidium clouds seem not to be in thermal equilibrium. This can be explained considering an extra heating of the bosonic cloud due to the near resonant Feshbach molecule state ($T_h \neq 0$ close to resonance): in fact the magnetic moment of the Feshbach state relative to this resonance is -3.25 MHz/Gauss and the trap depth is of the order of 1 MHz. Furthermore, also a weak mean field interaction can start to play a role, slightly modifying the sample behavior, despite the degenerate regime for bosons is never reached.

Let us now consider a strongly interacting Fermi Bose quantum mixture: for investigating the BEC and Fermi gas mixture behavior versus the interspecies scattering length a_{BF}, we further evaporate the gas, as explained in the subsection 3.2.1, leaving the magnetic field few Gauss far from the resonance center. The physical property of the system that is directly related to a_{FB} is the total interspecies interaction energy $U_{FB} = 2\pi\hbar^2 a_{FB}/\mu \int n_B n_F d^3x$, where μ is the reduced mass of the system. As I already mentioned, each component is felt by the other one as an attractive (repulsive) potential for negative (positive) a_{FB}. At a Feshbach resonance U_{FB} is large, and it can substantially modify the distributions n_B, n_F: this can give rise to an instability towards the collapse for $a_{FB} < 0$ or bring the mixture towards phase separation for $a_{FB} > 0$, also affecting the behavior of three-body losses. We expect the resonance center to be a sharp interface between these two opposite scenarios. In a first experiment the field is increased in 50 ms from $B_i = 543.4$ Gauss to a final field B_f that is varied from 543.4 Gauss to 548 Gauss, in order to investigate the region of positive and large scattering length: the BEC and Fermi gas are held at the final value B_f for 10 ms and then released from the trap end let expand for 18 and 14 ms respectively. In order to characterize the behavior of the system in this regime, where the two components appear to be out of equilibrium, we find convenient to fit the bosonic and fermionic clouds with a single component gaussian function; the resulting widths are accurate - even if only qualitative -, markers of the excitations of the system. In particular, I focus the attention on the bosonic component of the mixture, since it has a lower chemical potential, and it is therefore more strongly affected by variations in U_{FB}. In Fig. 3.9 the vertical width behavior of the bosonic component as a function of the magnetic field is reported. When B_f approaches the

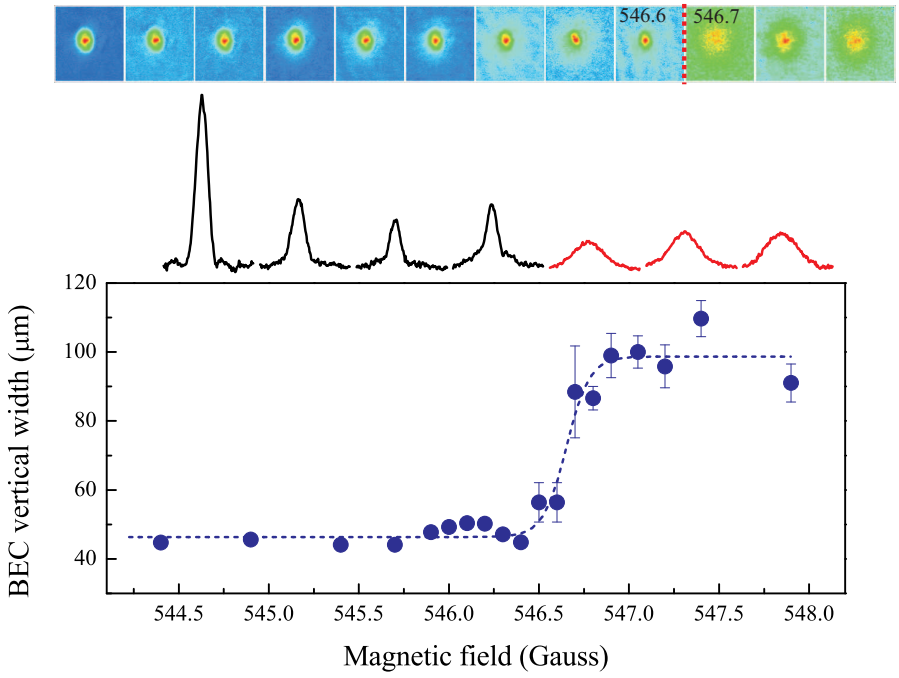

Figure 3.9: Vertical width of the BEC of rubidium interacting with the Fermi gas: the magnetic field is tuned towards the region of very large repulsive interspecies interaction, where phase separation is expected. In fact, we observe a strong loss of atoms from the condensate as we approach the resonance center, but no heating is observed until the resonance is crossed. Once this happens, the mixture collapses and a thermal sample is left. In the upper panel absorption images and density profiles of bosons are shown for some different magnetic field values.

resonance center, we can observe a decrease of the atom number as large as 80%, but the condensate surprisingly survives. This observation is in contrast with the expected heating associated to three body atom losses registered in thermal samples, and agrees with the results coming from mean field model described in subsection 3.1.5: for the large positive a_{FB} expected for $B_0 - B < 1.5$ Gauss, the two components tend to phase separate. The separation takes place preferentially in the z-direction due to the anisotropy originated by gravity. In this regime the two clouds overlap only at their boundaries (see for example Fig. 3.5(b)), where the most energetic atoms reside. Therefore three-body losses remove preferentially the warmest atoms in the

system and do not give rise to heating.

Once the field is tuned above B_0, the U_{FB} suddenly changes sign, and the two components tend to collapse at the center of the trap because such energy is larger than the local intraspecies repulsive energy. The sudden increase of the density overlap of the two components now promotes the loss of the coldest atoms at the trap center, with a resulting rapid heating of the system. We observe this collapse as B_f is tuned above 546.6 Gauss, where the condensate disappears, and one is left with a thermal gas at $T \sim 600nK$. This study therefore indicates that the scattering length changes sign between 546.6 and 546.7 Gauss. This value of B_0 is in good agreement with the value extracted from the loss feature in a thermal mixture and the from the fit of all resonances (see Tab. 2.2). A similar behavior, even if less evident, is observed for the Fermi component of the mixture: no appreciable heating is detectable below 546.6 Gauss, while a thermal cloud is left, suddenly after crossing the resonance center.

The intriguing fact that two samples, individually stable and with an intraspecies repulsive interaction, when come close to each other can become unstable due to a too large interspecies attraction, has been a fascinating topic for the cold atomic physics community. In the year 2002, the LENS group reported the collapse of a Fermi gas of potassium interacting with a BEC of rubidium [28]. The observation was performed in zero field conditions, therefore in "background" interaction strength, and could be explained only with a large and negative background interspecies scattering length of $-410a_0$: the result was based on the comparison between the experimental critical point for collapse and the mean field theory predictions. A similar observation was done few years after in the University of Hamburg in the same experimental conditions, but for much larger atom numbers [115]: this successive measurement could be explained in terms of an interspecies scattering length of $-280a_0$. Both the values of the a_{BF} derived from such experiments, strongly disagree with the one coming from Feshbach spectroscopy [41]: the possibility that now we have to control the interspecies interaction might shed new light on this phenomenon, since our quantum collision model now allow us to know precisely the magnetic field dependence of a_{BF}.

Let's see now the measurements on the negative side of resonance: we prepare the degenerate sample at a magnetic field of 551 Gauss, well above the resonance position, and then tune it adiabatically (50 ms linear sweep) towards values B_f closer to resonance, corresponding to a growing attraction between the mixture components. If we hold the sample at the final B_f for 20 ms, we observe a behavior totally

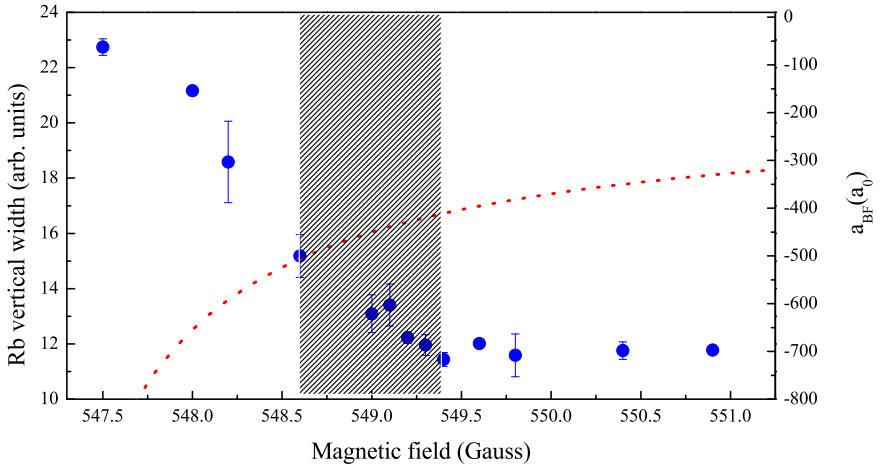

Figure 3.10: Vertical width of the BEC of rubidium interacting with the Fermi gas: the magnetic field is tuned towards the region of very large attractive interspecies interaction, until collapse of the system takes place. The vertical width of the bosonic cloud is fitted with a single gaussian function. The highlighted area indicates the magnetic field region where transition from stable to unstable system is expected.

different from the one shown in Fig. 3.9: the result is summarized in Fig. 3.10. In fact, for given trap strength and atom numbers, the collapse is expected to take place if a_{FB} is negative and larger in magnitude than a critical scattering length a_c. In this case, the width of the bosonic component stays constant until $B_f > 549.4$ Gauss, and then starts to increase, indicating the presence of a rapid heating of the system as a consequence of collapse. The field $B_f = 549.4(2)$ Gauss corresponds to $a_c = -390^{-365}_{-430} a_0$, which is in good accordance with the prediction of the static mean field model of a critical scattering length $a_c = -397 a_0$ for the nominal atom numbers $N_B = N_F = 4 \cdot 10^4$ in this specific experiment [5]. Our measurements are also in good agreement with the one made contemporaneously by the Hamburg group and described in [78]. However, a quantitative analysis of the collapse is difficult:

[5]Note that, since the measurement is performed in conditions of atom numbers and trapping frequencies that are comparable with the ones of [28], the mean field analysis gives a comparable critical value for the scattering length.

in particular the determination of the critical scattering length for which collapse occurs is not so straightforward. In fact, for every observation time there is a region of magnetic field in which the system is clearly excited, but not completely collapsed (highlighted area in Fig. 3.10): the impossibility to have a sharp signal between collapsed and non collapsed samples makes hard any precise measurement of the critical parameters (compare for example the extremely sharp interface between the regions $a_{BF} \gg 0$ and $a_{BF} \ll 0$ of Fig. 3.9, with the smooth raise of the boson cloud in Fig. 3.10).

An alternative way to see the asymmetric behavior of the degenerate mixture on the two sides of the resonance, is to observe the time evolution of the system for two fixed values of large interaction strength, $+\tilde{a}_{BF}$ and $-\tilde{a}_{BF}$ respectively. In Fig. 3.11 I report the evolution of the total bosonic atom number and of the condensed fraction for two values of strong attractive-repulsive interaction: $\tilde{a}_{BF} = -820^{+40}_{-40} a_0$ and $\tilde{a}_{BF} = +740^{+80}_{-70} a_0$ respectively. The first set is taken preparing the system at 551 Gauss and then bringing it to 547.6 Gauss; the second set is acquired by preparing the sample at 539 Gauss and then bringing it to 546.0 Gauss. At the negative interaction strength of $a_{FB} \sim -800 a_0$, the system is not stable against collapse: the sample presumably starts a compression phase just after the interaction energy is switched to a large and negative value. After a quarter of the trap period, i.e. 2.5 ms, a maximum of three-body loss rate is observed, accompanied by a large heating of the sample. The condensate is therefore rapidly heated into a thermal cloud, and the loss rate decreases because of the decreased density of the samples.

In the opposite case, $a_{FB} \sim +800 a_0$, the system is in the phase-separation regime, and the condensate remains stable for a much longer time interval. At a longer time in both cases the Bose gas is heated up into a pure thermal cloud. This however happens already at about 20 ms for negative a_{FB}, and only at about 100 ms for positive a_{FB}. During the whole time span, the total atom number in the bosonic sample decreases by about 50% in the case of negative a_{FB} and about 30% for positive a_{FB}. For the Fermi gas we similarly observe both atom loss and heating, which are larger for negative a_{FB}.

In conclusion of this section, some comments can be made:

- We have investigated for the first time a quantum degenerate Fermi Bose mixture in which the strength of the interspecies interaction can be tuned over a wide range of values. We have clear evidence of the effects of the mean field interaction, both for large repulsion and attraction of the two atomic samples, and we find a good agreement with the predictions of mean field theory. A

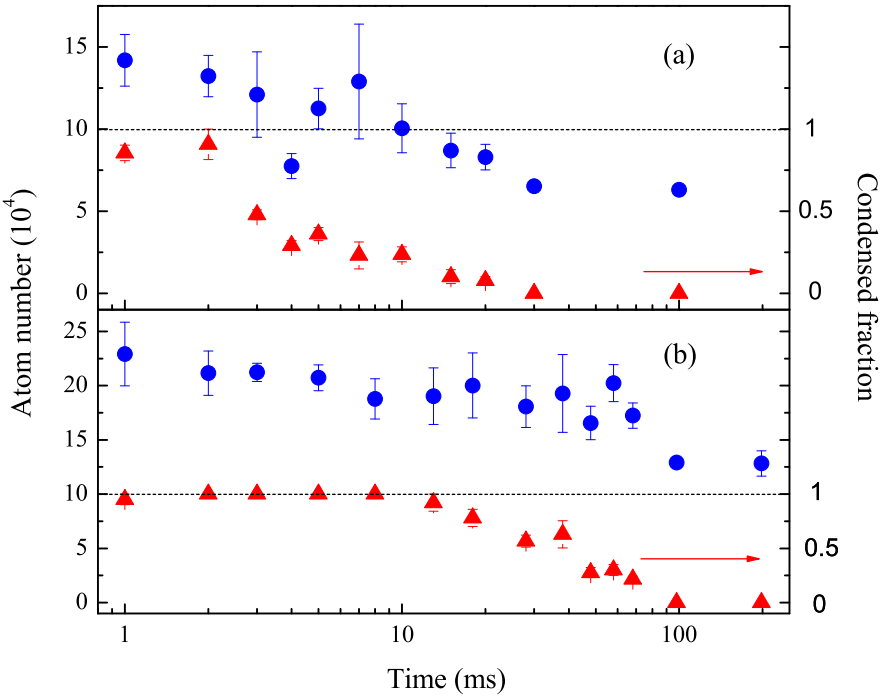

Figure 3.11: Asymmetric behavior of the mixture in degenerate regime vs sign of the interaction. (a) Evolution of bosonic component of the mixture for $a_{BF} = -820^{+40}_{-40} a_0$: total Rb atom number and condensed fraction are plotted vs time. The collapse depletes the condensate on a timescale shorter than the trap period, and within 20 ms the sample is completely thermal. (b) Same as in (a) but for $a_{BF} = +740^{+80}_{-70} a_0$. The condensate remains stable for longer time and after 80 ms a small condensed fraction is still observable.

clear asymmetry is observed in the three body processes on the two sides of the resonance.

- A more quantitative investigation of the phenomenon of the collapse is in principle possible, even if this would require more efforts, both experimental and theoretical. From the experimental point of view, one should be able to distinguish the mean field effects from the bare three body losses at large scattering lengths; furthermore, in the very first few ms of the evolution of the system

one should have the ability to distinguish the effects due to the sweep in the magnetic field needed to bring the system within the collapse region, from the one deriving from the evolution of the system at the final B_f.

In order to analyze the problem from the theoretical point of view, one should take into account finite temperature effects, including in the model not just mean field interaction, but also the dynamics connected to three body processes. Moreover, the role of the sweep in the interaction strength should also be taken into account.

- From our measurements it appears evident that any effect of collapse takes place on timescales of the order of a quarter of the trap period, therefore typically on the few ms scale. This is important in order to perform future experiments of molecule association via adiabatic sweeps in the magnetic field.

3.3 Molecule formation

An interspecies Feshbach resonance can also be exploited to associate pairs of atoms into KRb dimers, using the same techniques that has proven successful in the case of homonuclear systems. The idea is simple: since the resonance takes place in coincidence with a crossing of an atomic and a molecular state, one can adiabatically convert pairs of atoms into molecules with a magnetic-field sweep. This is the mechanism at the basis of the experimental detection of Feshbach resonances already shown in Fig. 2.6.

The magnetic-field dependence of the atomic and molecular state involved in the broad resonance relative to the absolute ground state are plotted in Fig. 3.12. The sweep needs to originate in the region $B > B_0$, where $E_a < E_m$, and end on the other side. A maximum ramp speed can be evaluated with a simple Landau-Zener model developed for homonuclear gases, which describes the number of molecules as

$$N_{mol} = N_{max}(1 - e^{-\delta_{LZ}}) \,, \quad \text{where} \quad \delta_{LZ} = \alpha n \Delta / \dot{B}, \tag{3.57}$$

and α=4.5(4)$\times 10^4$ m^{2}s^{-1} is an experimentally determined coupling constant [80]. The maximum conversion is reached when δ_{LZ} gets larger than one, which in this case corresponds to ramp speeds smaller than 50 Gauss/ms. We find that already sweep speed of the order of 10 Gauss/ms are sufficiently slow to reach the maximum conversion of atoms: slower ramps cause only an increase of three body losses, without giving a better conversion signal, that seems to be already saturated. Note that

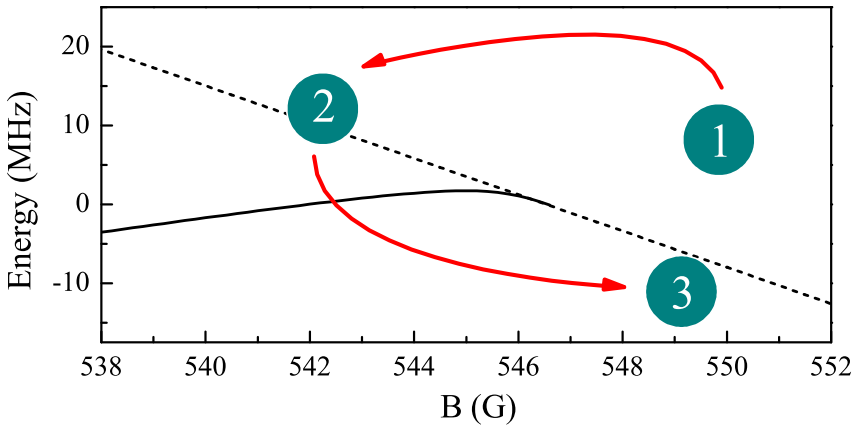

Figure 3.12: Magnetic-field dependence of the atomic (dashed line) and molecular (continuous line) states involved in the ground-state K-Rb Feshbach resonance, calculated with our quantum collisional model. The atomic state is $|9/2, -9/2\rangle \otimes |1, 1\rangle$, while the molecular state is labeled as F^{Rb}=2, ℓ=0, and has mixed singlet-triplet nature. In order to associate molecules one can perform a sweep in the magnetic field from above (1) to below (2) resonance. A backward sweep $(3) \rightarrow (1)$ re-dissociates the dimers.

our larger achievable speed is actually 10-20 Gauss/ms, since we exploit for generating them the Feshbach coils: smaller additional fast coils system can allow us generate faster sweeps, actually experimentally unreachable.

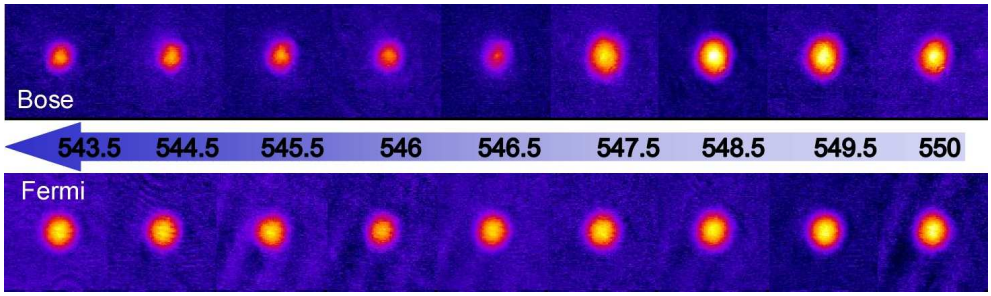

Figure 3.13: Evolution of the atom numbers in the mixture during a downward magnetic-field sweep at the ground-state Feshbach resonance. The sudden decrease in atom number for both components when the field crossed the resonance center at 546.6 indicates that atom pairs are associated into KRb dimers.

Fig. 3.13 shows a series of absorption images of the mixture taken at various intermediate magnetic fields during a sweep over the Feshbach resonances. The sweep is originating 4 G above the resonance, and ends after about 5 ms at a variable magnetic field across the resonance. The clouds are released from the optical trap right at the end of the sweep, and the images are taken at zero magnetic field, after ballistic expansion. Note how the number of atoms in both components drops as the field is brought below 547 G, that we interpret as the result of molecule formation. The transition energy of the molecules is indeed no longer resonant with the light used to image the atoms, and molecules are therefore not detected. It is important to note that the atoms are not lost because of three-body recombination while sweeping over the resonance center, where $a_{FB} \rightarrow \pm\infty$. Indeed, in that case one would detect also a strong heating of the system, which is not apparent in Fig. 3.13. Moreover, repeating the same sweep from below to above resonance, no effect on the population of the two species is detectable.

We can obtain some qualitative information on the process of molecule formation in this system through simple measurements. The maximum conversion efficiency we are able to observe is about 30-40%, that is not obtained at the lowest temperatures achievable in the experiment, but at temperatures around the condensation temperature of bosons T_c. This can be qualitatively understood in terms of the simple model and of the experiments on homonuclear systems presented in [80]. One

expects to reach the maximum conversion efficiency when the phase space overlap of the two components is maximum. This is reached for T=0 in the homonuclear Fermi or Bose cases, but not for a Fermi-Bose system, where the spatial overlap of the two samples starts to decrease rapidly as soon as T gets smaller than T_c. Instead, we find convenient to work at temperatures below T_f: below this, and until $T \geq T_c$ the efficiency recorded is almost temperature independent.

A crucial information about such molecules is obviously the stability of the molecular sample. In particular, if the sample is not purified by non transferred remnant atoms, one expects that the main mechanism of loss is due to atom-dimer collision with respect to dimer-dimer collisions, due to the fact that the molecules are fermionic particles. Moreover, one can also infer that the more probable events are boson (B)- dimer (BF) collisions: in fact, very close to resonance, the Feshbach molecules are weakly bound pairs of atoms ($\sim$ B+F), and the quantum statistic suppresses F+F+B collisions [81]. We have investigated this by reconverting the molecules into atoms via a backward sweep across the resonance. At the very first stage of our experiment, we performed backward sweeps with speeds of the order of few ms/gauss, after $\sim$ 1 ms the molecules had been created: these tests never gave a good signal of back conversion. This clearly showed us that the timescales on which the dimers are lost and atom-dimer collisions take place is of the order of hundreds of μs, or even less.

Therefore we have tried to reach an experimental condition where the samples are at $T \in [T_c, T_F]$, in order to have a good conversion efficiency, and with many more fermions than bosons, in order to convert most of the bosons into molecules and therefore limiting the events of boson-dimer collisions.

In Fig. 3.14 I report our clearest signal of molecule formation, obtained exploiting the Feshbach resonance located around 598 Gauss between the $|9/2, -7/2\rangle$ and $|1, 1\rangle$ states of the mixture. At the beginning, the number of fermions is approximatively twice that of bosons, at a temperature well below T_f, with rubidium only partially degenerate. The forward sweep is performed from $B_i = 604$ Gauss down to $B_f = 596$ Gauss, within $\sim 500\mu s$ (sweep speed ~ 14 Gauss/ms). The signal of molecule association is taken by switching off the magnetic field immediately after the field has reached B_f. The signal of molecule re-dissociation is instead taken after (a forward and) backward sweep, from B_f to B_i, with the same speed, started after $\sim 200\mu$ s that B_f has been reached. As one can see, after the first sweep most of rubidium atoms disappear, passing from 30000 to 5000. The potassium population passes from 75000 to 55000. The temperature of the sample remains almost constant

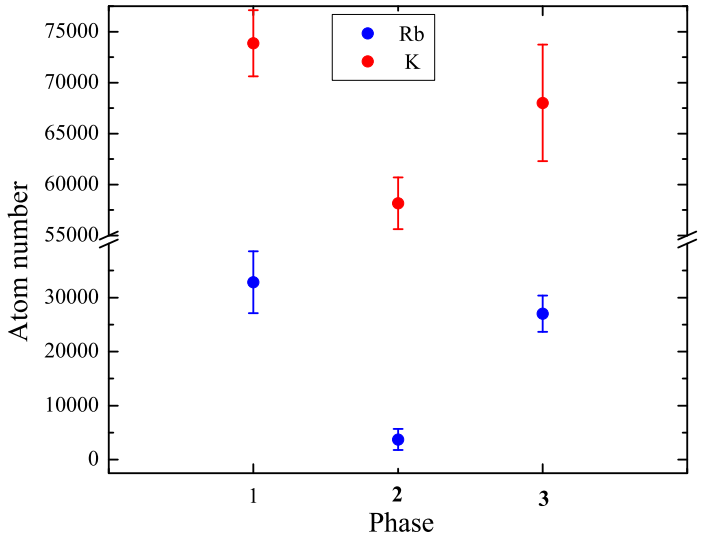

Figure 3.14: Association and re-dissociation of Feshbach molecules in the Fermi Bose mixture. I report the behavior of the atom number of the two species for: the initial condition (1); after the forward sweep where the molecules are associated (2); after both the forward and backward sweeps, where the molecules are re-dissociated into atoms (3). The imbalance between (large) fermionic and (small) bosonic population allows us to observe a good re-conversion signal, indicating a small loss of dimers via atom-dimer collisions.

after the first phase: around 20000 are associated. After the second sweep, molecules are back converted into atoms and we see that the final atom numbers approximatively recover the background initial value, indicating that only few dimers were lost between the association and the re-dissociation. Repeating the experiment with the population of bosons comparable with or larger than the one of fermions, the signal of associated molecules remains clear, but the one of re-converted atoms decreases rapidly. Since our capability of performing magnetic field sweeps is limited to few hundreds μ s, a timescale of the same order of the lifetime of the molecules in presence of remnant atoms, we can't investigate in a more quantitative way the lifetime of the Feshbach dimers. However, this preliminary investigation indicates that the main decay channel of the molecular sample is inelastic collisions with free bosonic atoms. Our qualitative observations have been confirmed by a recent experiment performed at JILA in the group of D. S. Jin, where an accurate study of atom-dimer

rate coefficient has been performed [116]: in fact, it results that for large and positive scattering lengths, of the order of 10^3 and more, the loss coefficient for BF+B collisions increases and is almost a factor 100 larger than the one relative to BF+F collisions. We have also investigated the possibility of revealing the molecular sam-

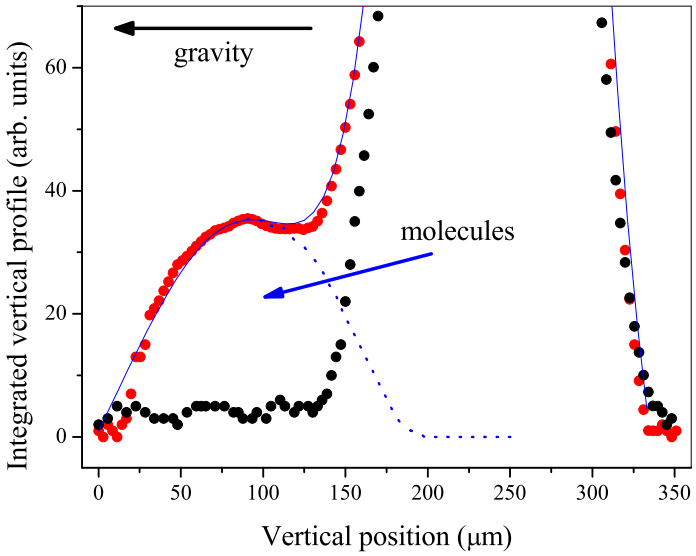

Figure 3.15: Density profiles integrated along the vertical direction both of a background image and of an image taken after the association of molecules, the application of a Stern Gerlach field that separates the dimers from the non transferred atoms, and the re-dissociation of the molecules via backward sweep.

ple by means of a Stern-Gerlach field gradient, that spatially separates the molecules from the remaining atoms [117]: the molecular and the atomic clouds are split in the momentum space, and therefore also in real space after time of flight. We associate the molecules by means of the forward magnetic field sweep, that starts at 607 Gauss and it reaches the final value 598.2 Gauss within $\sim$500 μs: note that this is just 200 mGauss far from the resonance center. Once the final field value is reached, we switch off the optical potential and contemporary we turn on the QUIC field. The rise of the gradient along the vertical direction causes two consequences: the first one is that the atoms and the weakly bound dimers are separated, since they have different magnetic moments. The second one is that during the fall the molecules

are automatically re-dissociated, since they are brought towards higher field values: therefore they cross the resonance center and are back converted into atom pairs; we let expand the two separated clouds and take an absorption image. In Fig. 3.15 I plot the density profiles integrated along the vertical direction for both a background image and an image taken after the molecules have been created and the Stern Gerlach field has been applied. As one can see, in the second case an additional small cloud, laying below the non transferred atoms is present. Note that due to the limited speed of the coils system actually available on the apparatus, we cannot clearly separate them, before the molecules are lost via atom-dimer collisions.

In conclusion, the investigation we have performed so far about molecule formation, even if only qualitative, demonstrated our capability of creating KRb dimers via magnetic field sweeps across an interspecies Feshbach resonance. We have discovered that atom dimer collisions take place on the timescale of a hundred μs, but already with sweep speeds of the order of ~ 15 Gauss/ms, the conversion efficiency is relatively high. Furthermore, by repeating the experiment of molecule formation with imbalanced population of bosons and fermions, we have indication of the fact that the main channel of inelastic decay of dimers is molecule-boson collision.

Chapter 4

^{39}K Bose Einstein condensate with tunable interaction

I have shown in previous chapter how the interactions play a major role in the properties of Bose-Einstein condensates (BECs) made of ultracold atoms: in particular they determine the stability of the system and modify its shape and dynamical behavior, moving it away from the ideal non interacting case, see 3.1.3. Atomic species with naturally large repulsive interactions, such as ^{87}Rb or ^{23}Na, have collision properties favorable for the preparation process: their large and positive scattering length assures the efficiency of the cooling process towards the degenerate regime, and stabilizes the sample against collapse. Moreover, the fact that atoms within the BEC interact and therefore that the system is not trivial, makes the Bose Eistein condensate a unique and peculiar subject of study. The possibility to control actively the interaction strength between the atoms enriches further the system: in fact, there is growing interest in studying Bose-Einstein condensates where the interactions can be precisely tuned, magnetic Feshbach resonances being the key tool in this respect.

One of the main motivations in this direction is the formation of an almost ideal condensate: despite interactions make the BEC system so interesting, the availability of a weakly interacting Bose gas is essential for studying phenomena where even a weak interaction can hide the underlying physics of interest. A noticeable example is in the field of disordered systems, where experiments performed with ideal quantum gases can shed new light on the interdisciplinary phenomenon of Anderson localization [18, 118]. An ideal BEC is also the most appropriate source for matter-wave interferometry, combining maximal brightness with the absence of collisional

decoherence [119]. The possibility of dynamically tuning the interactions in a BEC could also open new directions towards Heisenberg-limited interferometry [120].

Feshbach resonances have been already observed in several bosonic gases that is possible to bring to degeneracy, but only few of them allow a fine tuning of the interactions to small values around zero. This can be performed for example in lithium, a possibility already exploited to realize bright solitons in a weakly attractive BEC [13]. Cesium also presents an experimentally accessible region of nearly vanishing scattering lengths at which the small internal energy of a weakly interacting cesium BEC has been investigated [16]. In general, the zero crossing region is characterized by the fact that magnetic tuning allows one to lower down to vanishing values the phase shift associated to the s-wave component of the scattering amplitude during the collision process: the larger is the magnetic field region where this phase shift is small, the better is the experimental control available within the weakly interacting regime. The reason for which not all the atomic species offer the possibility of a fine tuning of the interaction strength, can be easily understood if we consider the dispersive behavior of the scattering length close to a Feshbach resonance (2.34):

$$a(B) = a_{bg}(1 - \frac{\Delta}{B - B_0}) \tag{4.1}$$

that within the region close to the zero crossing point can be approximated as:

$$a(B) \sim \frac{a_{bg}}{\Delta}(B - B_{ZC}) \tag{4.2}$$

For a fine tuning of the interaction within the region of vanishing interaction, the most appropriate systems will be those exhibiting broad resonances and small background scattering lengths: the smaller is the slope a_{bg}/Δ, the better can be the experimental control of the scattering length achievable by means of the magnetic tuning.

In this chapter I report the realization of Bose-Einstein condensation of ^{39}K. Combination of broad Feshbach resonances and a small background scattering length $a_K = -33a_0$ (see section 2.3) makes this system very promising for the study of weakly interacting condensates. I have mentioned in Chapter 1 that sympathetic cooling with ^{87}Rb works for ^{39}K as efficiently as for the other potassium isotopes, but condensation is prevented by the negative value of a_K. ^{39}K can be brought to quantum degeneracy by a combination of sympathetic cooling with ^{87}Rb and direct evaporative cooling, exploiting the resonant tuning of both inter- and intra-species interactions at Feshbach resonances.

Presence of one broad homonuclear Feshbach resonance allows us to tune a_K in the condensate from large positive values to small negative values. The possibility

of precisely adjusting a_K around zero is demonstrated by studying the condensate expansion and its stability.

4.1 Achievement of a ^{39}K BEC

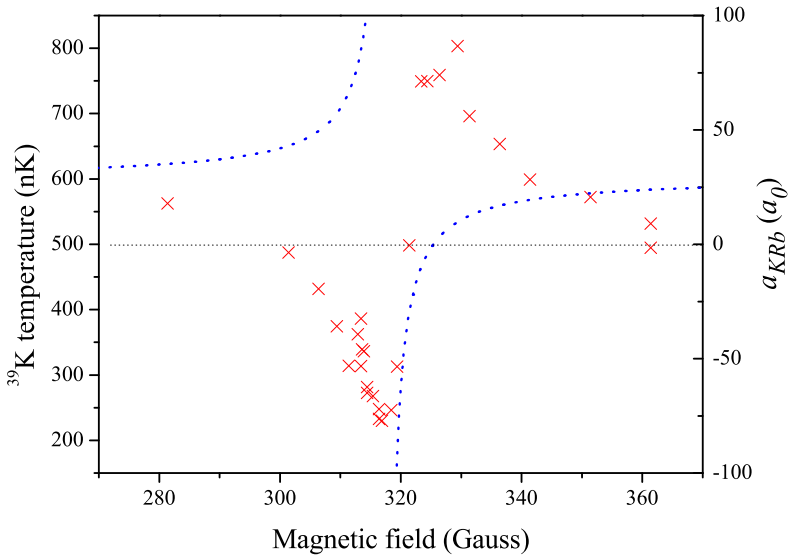

Figure 4.1: Sympathetic cooling efficiency versus the applied bias magnetic field, after the first stage of evaporation into the optical trap. As the interspecies scattering length is increased going close to the interspecies Feshbach resonance, the increased elastic cross section makes the cooling process more efficient. The large temperature values reported around 325 Gauss correspond to the presence of the resonance zero crossing.

The starting point is a mixture of typically 10^6 rubidium and 6×10^5 potassium atoms at 800-1000 μK in their absolute ground state, held in an optical potential. Remember that the interspecies scattering length is $a_{KRb} = 28a_0$, and this makes the efficiency of sympathetic cooling relatively low, considering also that as the trapping beam intensity is lowered the overlap between the mixture components is reduced (see Fig. 3.2). To overcome this problem, we exploit the possibility of tuning the interspecies scattering length, by means of a Feshbach resonance located at $\sim$ 318

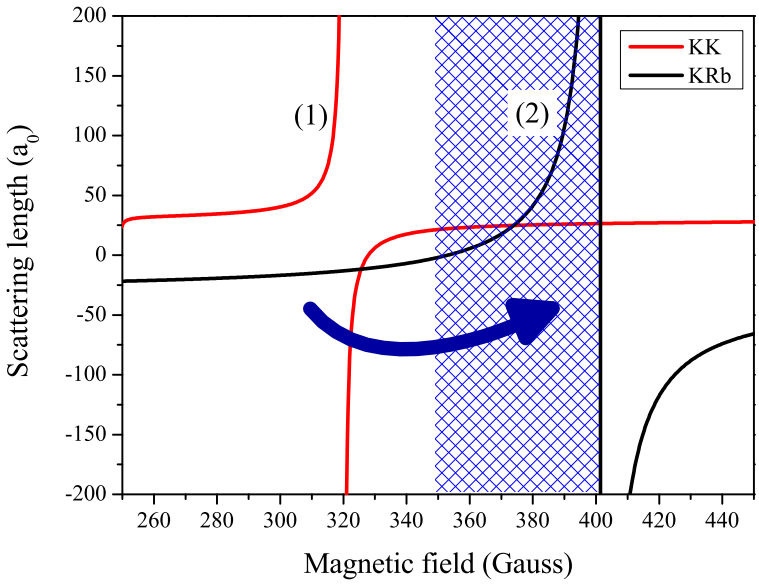

Figure 4.2: Scheme of both inter- and intra-species resonance features within the 300-400 Gauss region. The first part of evaporation is performed close to the heteronuclear resonance (red line), in order to increase the efficiency of sympathetic cooling. Once a temperature of $\sim$ 200 nK is approached, we move close to the homonuclear resonance (black line), where we stabilize the potassium against collapse by tuning the scattering length to positive values, and perform the last 1 s evaporation ramp. The hatched area shows the magnetic field stability region of the BEC of ^{39}K.

Gauss: before starting lowering the trap depth, we switch on the magnetic field and fix it in the vicinity of the heteronuclear feature. A larger scattering length causes an increase of the sympathetic cooling efficiency, since the elastic cross section scales as a_{KRb}^2. We then lower the trap beams intensity with exponential ramps of 2.4 seconds and with time constant of 450 ms, at the end of which we record the temperature of the rubidium and potassium clouds by taking an absorption image. We have performed a previous characterization of this first stage of the evaporation, plotting the temperature of the gases versus the magnetic field, i.e. versus the interspecies interaction strength, see Fig. 4.1. As one can see, the sample temperature strongly decreases as a_{KRb} is increased towards values of the order of $\geq 100a_0$. Obviously,

the interaction strength cannot exceed too large values, otherwise three body recombination can start to affect the sample: a competition between a better efficiency and a detrimental increase of three body losses sets the best strength at which it's convenient to perform the evaporation. Experimentally we find that sympathetic cooling is optimized at a field of 316 Gauss, where $a_{KRb} \sim 150a_0$. At this magnetic field the homonuclear ^{39}K cross-section is still small, $a_K \sim -33a_0$. Note that also the zero crossing position relative to the interspecies resonance is clearly visible around 325 Gauss, evidenced by a large increase of the temperature, similarly to what I showed in Fig. 2.9.

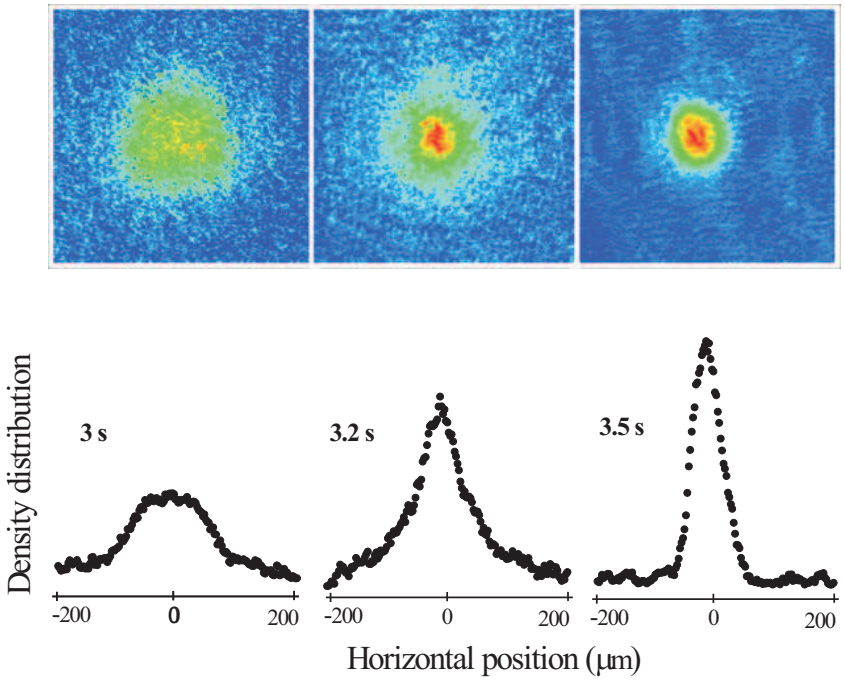

Figure 4.3: Phase transition to a ^{39}K BEC. The three images are taken at different times during the final stage of forced evaporation in the optical potential, after release from the trap and 15 ms of ballistic expansion. The profiles are obtained by vertically integrating the column density.

When both gases are close to quantum degeneracy ($T \sim 150$ nK) potassium is not stabilized against collapse, unless a_K is turned to positive values. We do this by shifting the magnetic field in proximity of the 52 Gauss-wide ^{39}K resonance, centered

at 402.4 Gauss, and we continue the evaporation for 1 s, see Fig. 4.2.

Due to the different trap depths for the two species, Rb is soon completely evaporated and further cooling of K relies just on intra-species collisions. Since the last part of the cooling process cannot rely on sympathetic cooling, it is convenient to have a scattering length not only positive, but also large. We find for this phase an optimal scattering length $a_K \sim 180a_0$ obtained for B=395.2 Gauss. At this field the two species are only weakly coupled, since $a_{KRb} \sim 28a_0$. Fig. 4.3 shows the phase transition of the K cloud to a Bose-Einstein condensate, detected via absorption imaging after a ballistic expansion. The critical temperature we measure is around 150 nK, and the condensates we can produce contain up to 10^5 atoms. The frequencies of the optical trap at the end of the evaporation are $\omega/2\pi = (65, 74, 92)$ Hz in the (x,y,z) directions respectively.

4.2 The expansion of the BEC

Once the condensate is produced, a_K can be further tuned, in order to explore the magnetic-field region below the homonuclear Feshbach resonance in which the condensate is stable. The starting point is a pure BEC created at B_0=395.2 Gauss. We then adiabatically bring the field to a final field B_f in 30 ms. After 5 ms, the optical trap is switched off and the cloud expands for 31.5 ms before absorption imaging is performed with a resonant beam propagating along the y direction. The magnetic field is switched off just 5 ms before imaging, to ensure that a_K does not change during the relevant phases of the expansion, modifying the mean field energy during the time of flight. Examples of absorption images are shown in Fig. 4.4. In Fig. 4.5 I plot the measured atom number and the mean width $\sigma = (\langle x^2 \rangle + \langle z^2 \rangle)^{1/2}$, together with the magnetic-field dependence of a_K as calculated using our quantum collision model (see section 2.3). The stability region of the BEC of ^{39}K is evident: on the left, between 350.2 Gauss and 350.0 Gauss, the sudden drop of the atom number can be attributed to a collapse of the BEC for too large negative a_K. In this regime the sample is no more in equilibrium and the presence of strong excitations is evident, see the leftmost images in Fig. 4.4. On the other extreme, instead, the field can be brought in proximity of the resonance center: here the BEC is depleted by three-body recombination, whose rate is enhanced as we get close to resonance (see section 2.1.5 and [74]). For example, the lifetime of the BEC in the optical trap, which is typically around 3 s, is shortened to about 200 ms when the field is set to 399.2 Gauss, where a_K=440(40) a_0.

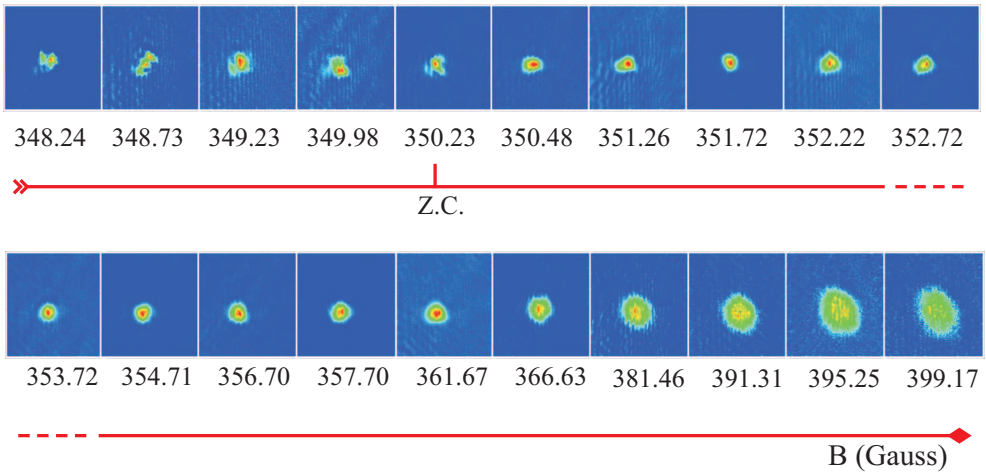

Figure 4.4: Tuning of the interaction strength in a ^{39}K BEC. Once the condensate is prepared at B_0=395.2 Gauss we adiabatically bring the field to a final field B_f in 30 ms. After 5 ms, the optical trap is switched off, the cloud expands for 31.5 ms in the magnetic field that is switched off just 5 ms before imaging. The theoretical position of the zero crossing, at 350.2(3) Gauss, is also schematically reported.

As the magnetic field is brought from values close to the resonance center down to the zero-crossing region, the width of the condensate after the expansion features a decrease by almost a factor three (see Fig. 4.5 b) and 4.4): this is due to the variation of the interaction strength in the condensate, since at the long expansion time of this experiment $\sigma \propto \sqrt{E_{rel}}$, where E_{rel} is the release energy of the condensate. The latter quantity is expected to decrease as $a_K^{2/5}$ in the Thomas-Fermi limit, i.e. for large positive a_K. Its value equals the kinetic energy of the harmonic oscillator ground state for a_K=0, and becomes even smaller for $a_K < 0$. As the system is no more stable against collapse, we observe also the presence of excitations into the atomic sample.

We have now the experimental points as a function of the external applied field, and the quantum collision model that allows us to "translate" magnetic fields into scattering length values: combining these with a numerical solution of the Gross Pitaevskii equation for variable strengths of the interaction, we can compare theoretical and experimental data, see Fig. 4.6. Here I plot σ as a function of a_K calculating the abscissa values for the experimental data using the theoretical a_K(B). Note that the horizontal error bar is dominated by the uncertainty in the model for a_K(B),

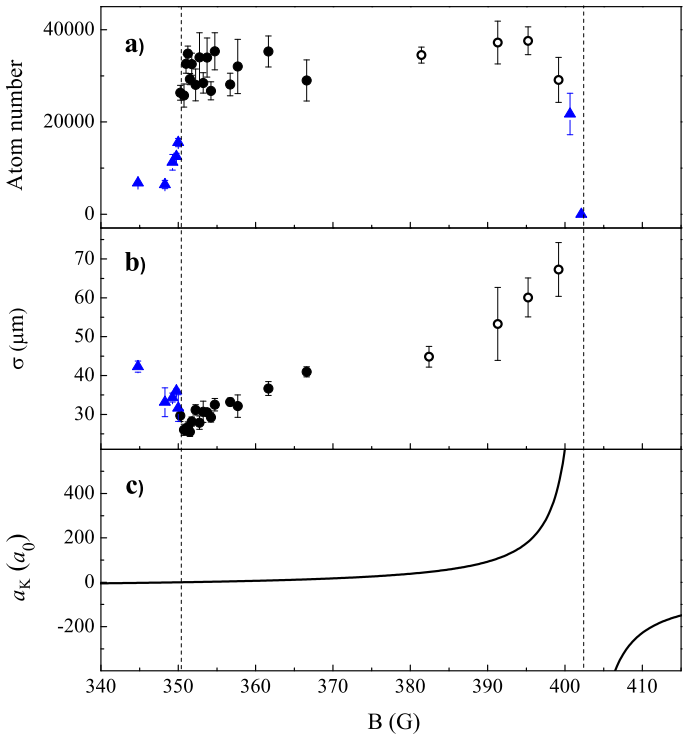

Figure 4.5: Tuning the interaction in a ^{39}K condensate. a) atom number; b) width of the cloud after 31.5 ms of ballistic expansion; c) theory prediction for the scattering length. The two dashed lines indicate the expected position of the zero-crossing and resonance center. Condensates are either fitted with a Thomas-Fermi profile (circles) in the region of large interactions or a gaussian profile (dots) in the region of weak interactions. Atom number and width of uncondensed clouds are directly extracted from the raw images (triangles).

which amounts to about 0.27 a_0 in the zero-crossing region.

The decrease in σ with decreasing a_K is the result of two general effects: i) a reduction of the condensate width in the trap, due to the reduced effect of the total mean field energy; ii) a reduction of the interaction energy released during the first phases of the expansion. Note in Fig. 4.6 a) the good agreement between theory and experiment in the broad range of values of a_K in which the condensate is stable. The slow decrease of σ for moderately large and positive a_K is followed by a faster

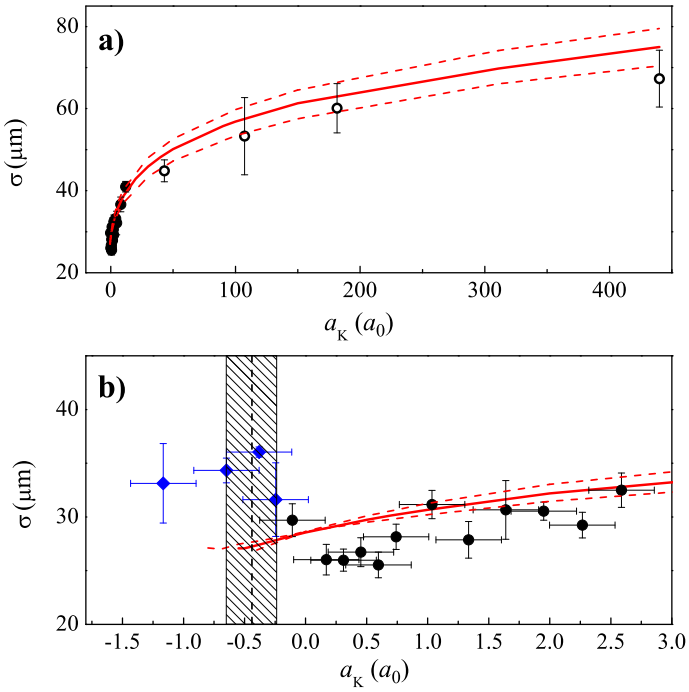

Figure 4.6: a) Scattering-length dependence of measured (dots) and calculated (lines) mean width σ. The two dashed lines indicate the range of variation of σ due to a 30% systematic uncertainty on atom numbers. b) Zoom into the zero-crossing region. Both condensed samples (dots) and collapsed samples (triangles) are shown. The horizontal error bars are determined by the uncertainty on a_K(B). The hatched region indicates the critical a_K for collapse as predicted by the numerical calculation, including its variation due to the uncertainty in the atom number.

decrease in the region of the zero-crossing. Note also that the data points, both in the ideal Bose gas and Thomas Fermi regimes, are excellently fitted by means of the analytic descriptions that in these limiting cases are available. In Fig. 4.6 b) theory and experiment are compared on a much smaller region around the zero-crossing, including also the experimental data points corresponding to a collapsed cloud. The hatched region indicates the critical scattering length for collapse a_c=-0.57(20) a_0 predicted by the theory for the nominal atom number we had in this experiment, N=3.5

10^4. The width of the cloud keeps on decreasing as a_K gets negative and increases again at collapse. In this experiment, collapse is apparently happening at a slightly subcritical scattering length a_K=-0.2(3) a_0. We speculate that this is due to the fact that the magnetic field ramp is not more adiabatic in this region of negative a_K. In fact, although the ramp duration is much longer than the trap period, it might still excite the monopole collective mode of the condensate which has a vanishing frequency as a_K approaches a_c [113].

4.3 Detection of zero crossing via interferometric measurements

I have shown in the previous section that the scattering length in ^{39}K can be precisely tuned over a large range, and adjusted around zero. As I already mentioned, this atomic species is particularly advantageous in producing a weakly interacting condensate, since it combines a broad Feshbach resonance with a small back ground scattering length. For the resonance we have been exploiting the theoretical model predicts a sensitivity $da_K/dB \sim 0.6a_0$/Gauss around 350 Gauss. Therefore, in principle, a magnetic field stability of the order of 0.1 Gauss can allow us to tune the scattering length to zero to better than 0.1 a_0. This degree of control is superior to that achievable in every other species which feature either narrower resonances and/or larger background scattering lengths, the only exception being ^{7}Li [13]. However, the measurements presented above are not appropriate to verify the effective sensitivity in the tuning of the scattering length experimentally available with this system. The most precise determination of the zero crossing position, and of our current resolution in tuning the scattering length within the weakly interacting regime, has been performed in a recent experiment in which we exploited atom interferometry techniques [121].

The experiment employs a tunable Bose Einstein condensate of ^{39}K that is adiabatically loaded from the optical trap into a vertical optical lattice $V(z) = V_0 \sin^2(2\pi z/\lambda)$. The atomic system, if gravity is not counterbalanced by an external force (in our case generated by a magnetic field gradient added to the optical potential of the crossed trap), undergoes the well known phenomenon of Bloch oscillations [122]. I will not enter here into the details of the experiment, and I'll only recall the essential features of a BEC undergoing Bloch oscillations, necessary to understand the interferometric determination of the zero crossing position. The macroscopic wave function of the condensate into the lattice and in presence of the gravity can be written as a coherent

superposition of the eigenfunctions of the system, i.e. of the Wannier Stark states φ_j (see leftmost part in upper panel of Fig. 4.7), parameterized with the lattice site index j [123]:

$$\psi = \sum_j \varphi_j \sqrt{\varrho_j} \exp(i\vartheta_j t) \tag{4.3}$$

In the absence of interaction the phase of each state evolves according to the energy shift induced by the external potential, i.e. $\vartheta_j = Mg\lambda j/(2h)$. By releasing the condensate from the lattice, a periodic pattern with period $T_{Bloch} = h/(Mg\lambda/2)$ is obtained, resulting from a macroscopic interference between different Wannier Stark states, see rightmost part of the lower panel of Fig. 4.7. I just remark here that a measurement of the frequency of such (Bloch) oscillations allows a direct measurement of the external force. However, in real situation atoms interact, and this affects sig-

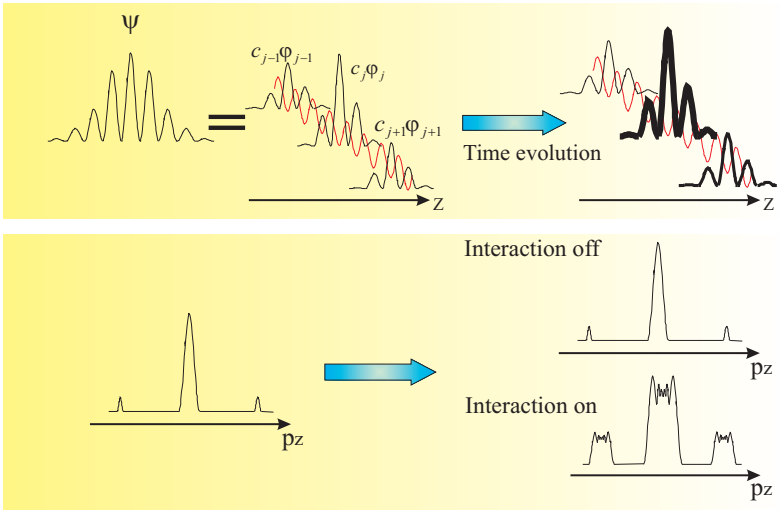

Figure 4.7: Upper panel: scheme of the decomposition of the BEC wavefunction in terms of Wannier Stark states. The evolution in presence of gravity induces an oscillatory behavior of the system. This is measurable in time of flight images, i.e. in momentum space. Lower panel: if the BEC does not interact, the interference pattern visible in momentum space does not change after some oscillation periods. If atom atom interaction are present, this interference pattern is destroyed after some time, due to phase diffusion. The interference peaks in momentum space are broadened during the time evolution, moving away from the initial distribution.

nificantly the time evolution of the system. In fact, since the occupation number associated to different sites is not the same ($N_j \neq N_k$), also the mean field energy as-

sociated to them is in general different ($E_{MF,j} \propto a_K N_j \neq E_{MF,k} \propto a_K N_k$), and this must be taken into account. Since the relative occupation number is incoherently distributed, interaction causes a dephasing between the different Wannier Stark components. Consequently, phase diffusion [124] takes place, destroying the interference pattern, see lower panel in Fig. 4.7: the larger is a_K, the faster is the decoherence of Bloch oscillations. Generally atom atom interactions can be taken into account introducing a complex system of non linear equations for ϱ_j and ϑ_j. However, in the weakly interacting limit, ϱ_j don't change significantly, and the extra phase terms have a linear dependence on time, so that interaction modify only ϑ_j that becomes $\vartheta_j = Mg\lambda j/(2h) + (4\pi\hbar^2 a_K/hM)\varrho_j\gamma_j$; the coefficient γ_j is a term that takes into account for the site-to-site interaction. As an example, I report in Fig. 4.8 the first two cycles of oscillations in two limiting regimes of interaction strength: a_K= 100 a_0 and 1 a_0, respectively. As it is clearly visible, the interatomic interaction causes a significant modification of the interference pattern in the case of strong interacting system after just two cycles of the oscillation, while it does not have such detrimental effect in the limit of vanishing scattering lengths. A study of the temporal evolution of the

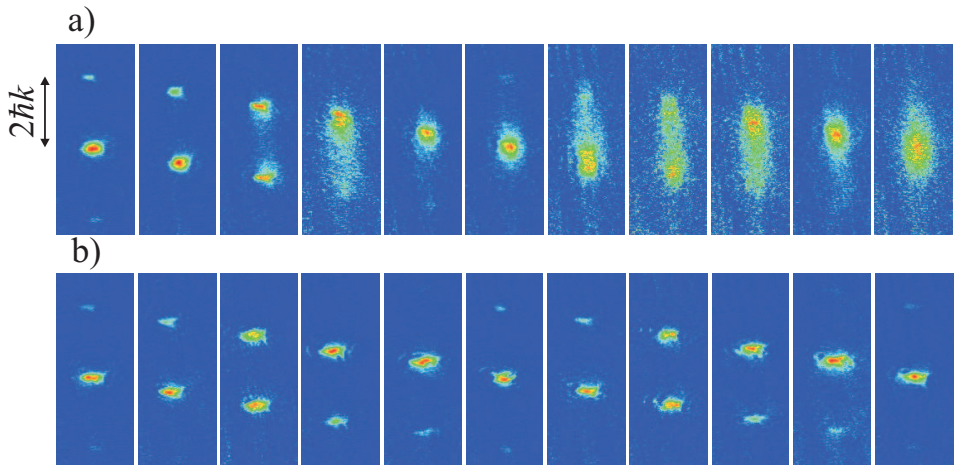

Figure 4.8: Bloch oscillations from 0 to 4 ms, in steps of 0.4 ms, for a condensate with a) 100 a_0 and b) 1 a_0 scattering length. The picture shows absorption images of the cloud after release from the lattice. The expansion lasts 12.5 ms and the scattering length is changed to the background value of -33 a_0 only 3 ms before the images acquisition. The arrow shows the momentum separation 2$\hbar$k between the interference peaks, where k = $2\pi/\lambda$, λ being the lattice wavelength.

central peak width of the interference pattern can give an estimate of the effect of the interaction strength on the oscillating system. In particular, after sufficiently long observation times, if an interaction is still present, the central peak width will saturate at the value corresponding to the first Brillouin zone: the initial narrow wavepacket associated to the BEC will be spread over the whole first band of the system. We con-

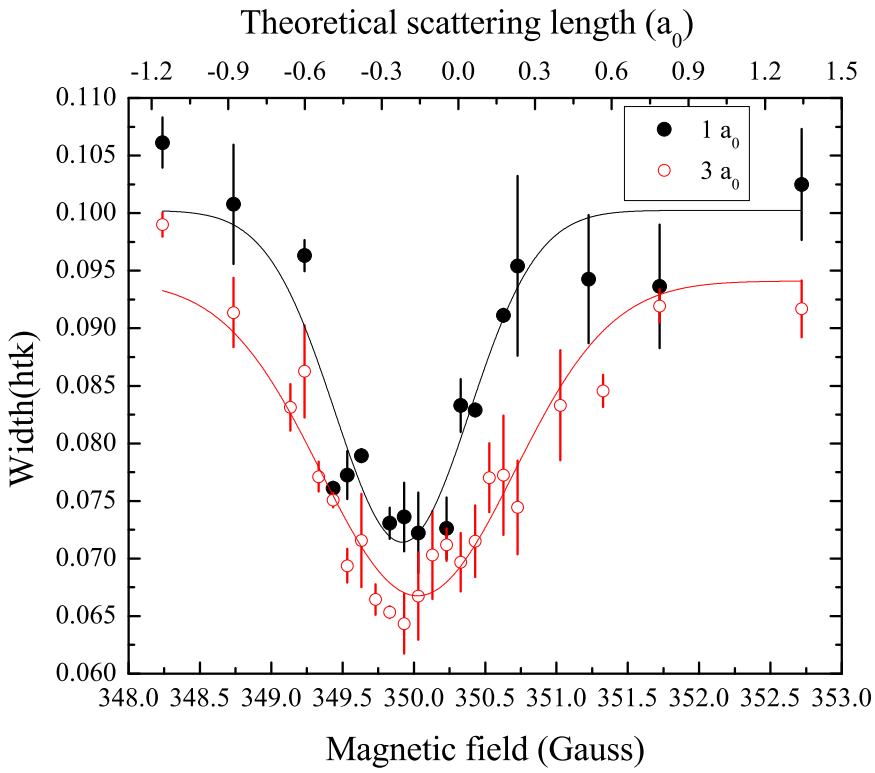

Figure 4.9: Interferometric detection of the zero crossing. Interference peak width as a function of the magnetic field after 180 ms of Bloch oscillations. The condensate is prepared for two different values of the scattering length, 3 a_0 (red circles) and 1 a_0 (black circles), and within the first 2 ms of oscillation the magnetic field is brought to the final value. The abscissa values on the top represent the theoretical scattering length corresponding to the applied magnetic field, calculated using our quantum collisional model. The theoretical uncertainty on the zero crossing position is ± 0.4 Gauss. The lines represent a gaussian fit to the data.

centrate the attention on the weakly interacting regime, and perform a measurement of the width of the peak as a function of the applied magnetic field strength. This is done by adiabatically loading the condensate from the optical trap (characterized by frequencies (ν_x, ν_y, ν_z)= (43,44,76)(Hz)) at an initial scattering length $a_k = 3a_0$ into the lattice; this has a height of s $\sim 6E_R$ and $E_R = h^2/2M\lambda^2$ is the recoil energy from absorption of a lattice photon (λ = 1032nm). The the dipole trap is switched off and contemporarily the magnetic field is brought within 2 ms at a final value in the region around the theoretical zero crossing position. This procedure allows to load the cloud in the lattice with always the same initial density, that is sufficiently low to completely exclude the effect of three body losses (see below) and to prevent the condensate from immediately collapsing on the negative side of the zero crossing. The system starts oscillating with a certain interatomic interaction, and after 180 ms we switch off the lattice, and let expand the cloud that is revealed after 12 ms via absorption imaging. The expansion is performed at a magnetic field value of 350.3 Gauss, that is reasonably close to the zero crossing position, in order to cancel the effect due to a residual interaction during the time of flight.

In Fig. 4.9 the interference peak width as a function of the magnetic field is shown (black dots). This reveals a minimum of the decoherence at 350.0 Gauss, that coincides with the position of the zero crossing (350.4 $\pm$0.4) Gauss predicted by our model for ^{39}K. The parabolic trend of the data confirms that the decoherence depends on the magnitude and not on the sign of the scattering length. Note that a gaussian fit of the data points would determine the position of the minimum to be (350.027$\pm$0.038) Gauss, i.e. with a relative uncertainty of $\sim 10^{-4}$. This indicates also the ability we have to appreciate a difference in the interaction strength of $\sim$0.06 a_0, corresponding to the experimental step of 100 mGauss. Moreover, note that the system at such low interaction is influenced by a detrimental laser noise that is an additional source of decoherence for the system: a better optical lattice (and eventually a greater stability of the magnetic field) can allow us to perform the experiment at longer interrogation times (and smaller field steps), further increasing the precision of the measurement [125].

If we repeat the same investigation at higher densities, by following the same procedure but preparing the condensate at an initial $a_i = 1a_0$, we observe a slightly different behavior (black). In particular, a larger width of the peak on the minimum confirms that tuning of the scattering length at the 0.06 a_0 level is not enough to completely cancel the decoherence effects induced by the residual interaction.

The slight disagreement between the experimental minimum of decoherence and

the theoretical position of the zero crossing could also be due to the presence of a residual dipole dipole interaction, responsible for a non vanishing *d*-wave contribution to the total cross section. In fact, this interaction cannot be zeroed by exploiting the Feshbach resonance and therefore the total cross section cannot vanish completely. Furthermore, the presence of dipolar interaction (that for the geometry of this experiment has a repulsive character) could affect the effective minimum of the interaction, moving it towards values of the magnetic field where the bare *s*-wave scattering length is already negative.

4.4 Three body losses in a non interacting BEC

I have shown in previous section that ^{39}K system, with our current magnetic field stability of 100 mGauss, allows us to appreciate differences in the interaction strength of $\sim$0.06 a_0. This makes this atomic species an appealing candidate for the achievement of a nearly ideal Bose gas, that can find interesting applications in the field of atom interferometry with trapped degenerate gases. One of the main advantages of such a system, is that the high degree of tunability allows us to achieve extremely low decoherence rates, that can result in extremely long observation times; furthermore, since the tuning of the scattering length leads also to the possibility of controlling the size of the condensate, down to 1 μm size, one can employ the ^{39}K BEC for precise measurements of weak forces at the micron scale [126].

In fact, once the BEC reaches the dimensions of the harmonic oscillator for a trap of frequencies of the order of 100 Hz ($a_{ho} \sim 1.5,\ \mu$m), the peak density exceeds 10^{15} atoms/cm^3, and in principle three body processes can seriously limit the lifetime of the system.

We have investigated this problem, evaluating the K_3 coefficient for the ^{39}K BEC within the region of the zero crossing. In order to do this, we have taken a measurement of the atom number and temperature versus time for the condensate loaded into three different trapping geometries. The mean frequency of the harmonic trap in the three cases is $\bar{\nu} = (48(2),\ 73.5(2),\ 96.0(2))$ (Hz), respectively. Once the BEC is produced within the way previously described, we adiabatically change the power of one of the beams of the dipole trap, and after some tens of ms we lower the magnetic field from the initial value down to the zero crossing point; we then take absorption images after 31.5 ms of expansion, and record the atom number and the dimensions of the atomic cloud. A condensate with vanishing interaction occupies the ground state of the harmonic trap, and therefore it has a gaussian profile; we

analyze the atomic cloud by fitting it with a double gaussian function, in order to distinguish the condensed fraction from the thermal component.

In fact, we have found for all the three cases that the three body losses take place, but no distinguishable heating is associated to them: the cloud is always well fitted with a single component whose width remains constant in time. The reason for this can be understood if we consider that the atoms of the ideal Bose gas are occupying the ground state of the harmonic trap: while the dimensions of an interacting BEC depend on the atom number composing the system, in the limiting case of vanishing interactions this doesn't happen. Furthermore, all the condensed atoms occupy the ground state of the system, and every particle has the same energy, independently from the atomic density: therefore, every particle expelled from the trap will not cause any heating to the remnant sample.

This is already a very positive fact: eventually the interferometer will lose atoms, and therefore the contrast will be lowered, but three body collisions do not introduce any detrimental heating of the system, and the remnant particles are still condensed[1].

Since the width of the cloud of remnant atoms doesn't change as a function of time, an extremely simple treatment can be built up for evaluating the K_3 coefficient relative to a non interacting Bose Einstein condensate: following what suggested in [74], we integrate the rate equation (2.35), considering that the profile of the condensate along every direction is always the ground state of the trap, whose dimensions are fixed by the trapping frequencies, and constant in time. We obtain the following rate equation:

$$\frac{\partial N}{\partial t} = -AN^3 - \alpha N \tag{4.4}$$

where $A \equiv K_3/(\sqrt{27}\pi^3\bar{\omega}^6)$ and α takes into account for background losses. The solution of this equation is trivial, and defining N_0 the initial atom number, we have the following evolution of the BEC population:

$$N(t) = \frac{N_0\sqrt{\alpha}}{\sqrt{(\alpha + AN_0^2)\exp(2\alpha t) - AN_0^2}} \tag{4.5}$$

If the effects of the background losses are negligible, the (4.5) reduces to:

$$N(t) = \frac{N_0}{\sqrt{1 + 2AN_0^2 t}} \tag{4.6}$$

We have analyzed the experimental data with both fitting functions, living A and α as only free parameters; we can conclude that the effects of background collisions are

[1]Note that this is another exception, as well as the thermal heteronuclear mixture below T_S (see section3.1.4) to the standard behavior associated to three body recombination.

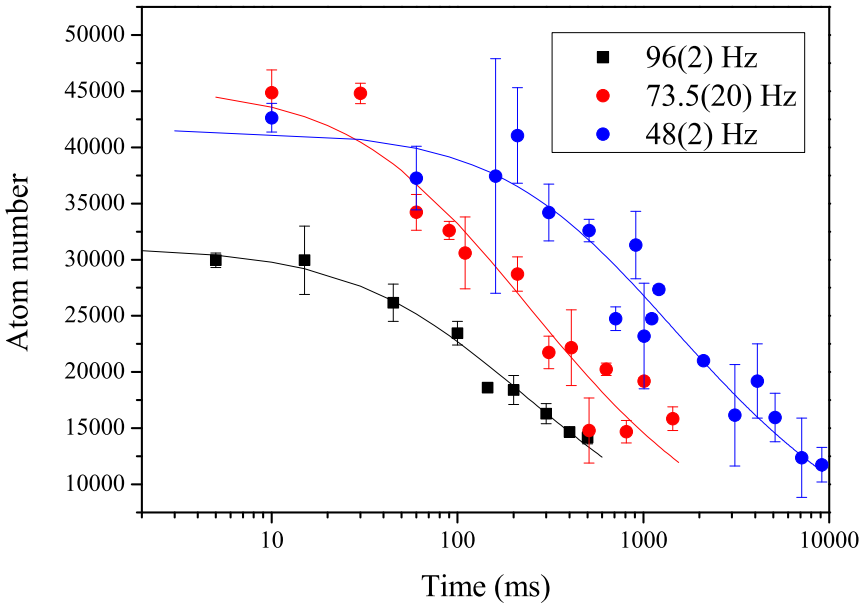

Figure 4.10: Number of atoms of the non interacting BEC versus time spent in trap for three different confinement conditions. Three body losses take place and lower the population of the sample, but no heating is associated to them, so that the condensate is not destroyed. The lines are a fit according to the model described in the text, where the only free parameter is A, from which we derive the K_3 coefficient.

negligible compared to the one of three body recombination, as it can be expected from the extremely high densities of the sample.

The results of the measurement and the best fit functions are reported in Fig. 4.10: as one can see, the model well describes the temporal evolution of the condensate, and from this analysis we can derive the K_3 coefficient, given the fit values of the A parameter. The measurements performed at different densities produce values for K_3 that all coincide within a standard deviation: we assume the mean of these three measurement to be our most accurate determination of K_3. This results to be:

$$K_3 = 1.30(25) \cdot 10^{-29}\,\mathrm{cm}^6/\mathrm{s} \tag{4.7}$$

This result is a very good new, since it is comparable with the K_3 of a ^{87}Rb condensate in its background condition [127]. Note that the above result is not in principle obvious for every system: in fact, even if the resonance is broad, and we are within the region of the zero crossing, the molecular state below threshold could however influence the three body recombination coefficient. Fortunately, in our case the binding energy associated to the molecular level in correspondence of the zero crossing is already of $\sim 100\,\mathrm{MHz} \times \mathrm{h}$.

Outlook

In conclusion of this report, I would like to spend some words about the possible future available directions. As I have shown in the previous chapters, during the three year I spent in the laboratory of Prof. Giovanni Modugno and Prof. Massimo Inguscio at LENS of Florence, several experiments we did allowed us to gain a detailed knowledge of the ultracold atomic systems we have been working with from the collisional point of view. In particular, the capability to control both homonuclear an heteronuclear interactions of the potassium rubidium systems we have been working with, offers the possibility of several interesting future investigations. From the point of view of molecular physics, many words have been spent in this thesis and in literature concerning the interest in achieving a degenerate gas of polar molecules. From this point of view, our apparatus can be exploited to associate KRb heteronuclear molecules, as first measurements previously described clearly indicate. In order to bring them into the ground state, where they exhibit a large electric dipole moment, some further important steps must be done, also considering the recent promising results obtained on this mixture at Hamburg University [32] and at JILA [116].

A system of laser lights is necessary to purify the molecular sample from the untransferred atoms, once the dimers have been associated: this is already available for Rb atoms (the most crucial collision partners for Feshbach molecules), and it has already been successfully tested, allowing us to blast away the atoms close to the Feshbach resonance in the absolute ground state of the Fermi Bose mixture within few μs.

First attempts to associate the KRb molecules have revealed an extremely fast decay of the dimers by means of atom-molecule collisions: this requires that the

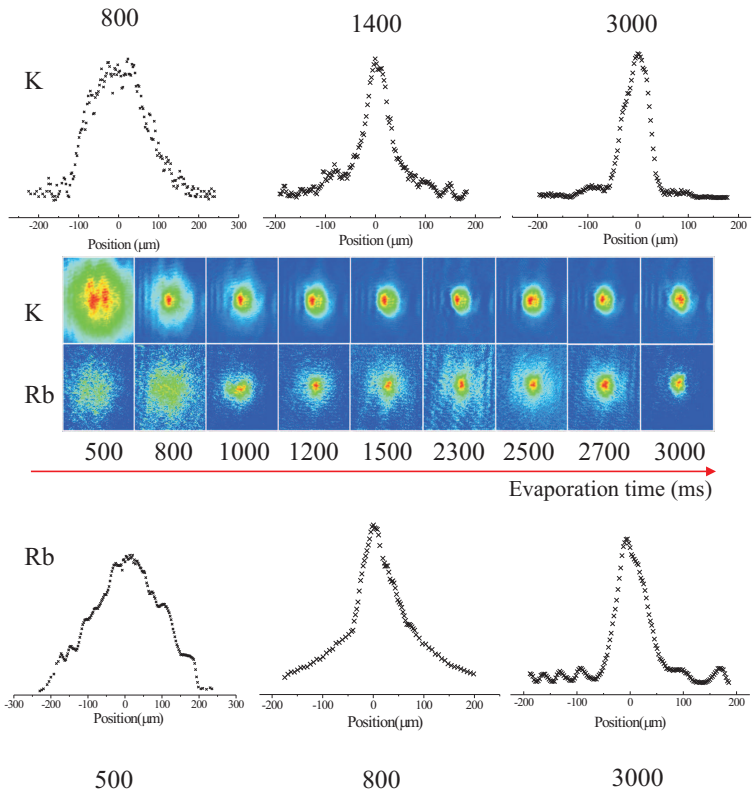

Figure 4.11: Absorption images of the Bose Bose mixture as a function of time during the evaporation in the optical trap: the trap depth is lowered within three seconds. The starting point is the same of the experiments previously discussed, while the final part of the evaporation ramp is modified in such a way that condensation of potassium can take place at a trap depth sufficiently high to trap also rubidium. The first second of evaporation is performed at 316.2 Gauss, where $a_{KRb} \sim 100a_0$, and sympathetic cooling is highly efficient. The last two seconds of evaporation take place at a magnetic field of 396.2 Gauss, where the interspecies scattering length is approximatively 26 a_0, while $a_K \sim 150a_0$, and the potassium BEC is stable against collapse. The density profiles of the two species are also shown, indicating the phase transition for both the samples. Note that rubidium exhibits the onset of condensation before potassium, and this is due to the larger Rb atom number.

stage of association must be performed extremely fast. In order to do this, if one purposes to associate the Feshbach molecules performing a magnetic field sweep across the resonance, a fast coils system is necessary.

Concerning the possibility of separating the atomic pairs into a deep three dimensional optical lattice in order to reduce the fast decay of the dimers, we are planning to upgrade the apparatus also in this direction, also in view of future experiments with polar molecules. It has been demonstrated that this system works fine [32], even if it reduces the association efficiency when one works with the degenerate Fermi Bose mixture, due to the only partial overlap between the mixture components.

This scheme can be extremely interesting if one works with a Bose Bose mixture of potassium and rubidium to produce bosonic dimers. The production of a double BEC of ^{41}K and ^{87}Rb has been already demonstrated [128], and we recently achieved a double BEC of ^{39}K and ^{87}Rb, see Fig. 4.4: both are interesting alternatives to the Fermi Bose mixture, in the field of Feshbach molecules, since both the mixtures present broad resonances. The bosonic character of the Feshbach molecules does not prevent vibrational quenching induced by dimer-dimer collisions, and therefore the lattice would be crucial in order to increase the lifetime of the molecular sample.

Let's consider here the case of ^{39}K and ^{87}Rb already available on our apparatus: if one takes into account the magnetic field dependence of a_K and a_{KRb} shown in Fig. 4.2, one could produce the degenerate Bose Bose mixture around 390 Gauss, where the potassium component is stable; at such magnetic field $a_{Rb} \sim a_K$, and therefore the two condensates have almost the same density distribution. At the same time, the interspecies scattering length is small: $a_{KRb} \sim 26a_0$. Therefore, reducing the relative sag, e.g. by means of a magnetic gradient or an appropriate optical beam, one can expect to have a very good overlap between the two components, not available in the case of Fermi Bose mixtures; playing with the trap parameters one can reach the most convenient densities in order to load the samples into a deep lattice, assuring a good number of sites occupied by only one potassium and one rubidium atom. Since the potassium atoms into the lattice are stabilized against collapse, one can decrease the magnetic field down to the heteronucear resonance and associate the dimers. Note that, until the optical potential is on, the dimers cannot collide, and therefore one can hopefully perform the transfer to the ground state. With respect to this, we have also been working to prepare the light sources and the phase lock system needed to perform a STIRAP pulse (stimulated Raman adiabatic passage) [129], in order to transfer the molecules from the weakly bound Feshbach level onto the ground state.

The possibility of exploiting the Bose Einstein condensate of ^{39}K for interferometric measurements has been recently successfully investigated [121], and we have been working now to employ a weakly interacting BEC in the field of disordered systems and Anderson localization.

Very appealing seems to be also the direction of studying this new system with respect of dipolar interaction: in fact, even if exploiting the Feshbach resonance we are able to tune to almost zero the s-wave scattering length, still a weak residual dipolar interaction [130] is expected to be present. This could allow us to study a system with anisotropic interaction and to observe in an alkali atom similar behavior to that recently investigated in Chromium [131].

Finally, the presence of broad resonances can make both the mixtures and the bosonic potassium interesting candidates for studies in the field of Efimov physics [14, 15]. Concerning the Fermi Bose mixture, we have already made preliminary studies in this direction, investigating the behavior of three body losses in the system close to some of the broadest resonances available. This research allowed us to discover extremely weak spin resonances located few hundreds mGauss far from the center of some of the main features, but didn't give us any evidence of Efimov states. Also the recent study presented in [116] concerning the broadest resonance in the absolute ground state of the Fermi Bose mixture reports a negative response. Consequently, if the possibility of having Efimov states within a heteronuclear system makes this research extremely appealing, at least the Fermi Bose mixture does not seem to be promising for the observation of such kind of features. Moreover, recent theoretical studies show that the K Rb Fermi Bose mixture should exhibit Efimov states for values of the scattering length periodically separated by a factor e^{π/s_0} >100 [81], therefore limiting the observation to one Efimov feature at the most.

From this point of view, the ^{39}K system seems to be more promising (homonuclear systems have all the periodicity factor e^{π/s_0} equal to 22.7). In particular, the presence of resonances broader than 50 Gauss, combined with a small background scattering length, can in principle allow to precisely scan both the left and right sides of a resonance, and the observation of more than one Efimov feature could be achievable [98].

Bibliography

[1] M. H. Anderson, J. R. Ensher, M. R. Matthews, C. E. Wieman, and E. A. Cornell, Science **269**, 198 (1995).

[2] K. B. Davis, M. O. Mewes, M. R. Andrews, N. J. van Druten, D. S. Durfee, D. M. Kurn and W. Ketterle, Phys. Rev. Lett. **75** 3969, (1995).

[3] C. C. Bradley, C. A. Sackett, J. J. Tollett and R. G. Hulet, Phys. Rev. Lett. **75**, 1687 (1995).

[4] B. DeMarco and D. S. Jin, Science **285**, 1703 (1999);

[5] Grimm, R.,M.Weidemüller and Y. B. Ovchinnikov, Adv. At.Mol. Opt. Phys. **42**, 95 (2000).

[6] E. Tiesinga, B. J. Verhaar, H. T. C. Stoof, Phys. Rev. A **47**, 4114 (1993).

[7] J. Stenger, S. Inouye, M. R. Andrews, H. J. Miesner, D. M. Stamper-Kurn, and W. Ketterle, Phys. Rev. Lett. **82**, 2422 (1999)

[8] T. Loftus, C. A. Regal, C. Ticknor, J. L. Bohn, and D. S. Jin, Phys. Rev. Lett. **88**, 173201 (2002).

[9] S. Inoyue, M. R. Andrews, J. Stenger, H.-J. Miesner, D.M. Stamper-Kurn, and W. Ketterle, Nature **392**, 151 (1998).

[10] Herbig, J., T. Krämer, M.Mark, T.Weber, C. Chin, H.-C. Nägerl and R. Grimm, Science **301**, 1510 (2003).

[11] Xu, K., T.Mukaiyama, J. R. Abo-Shaeer, J. K. Chin, D. E.Miller and W. Ketterle, Phys. Rev. Lett. **91**, 210402 (2003).

[12] Dürr, S., T. Volz, A.Marte and G. Rempe, Phys. Rev. Lett. **92**, 020406 (2004).

[13] L. Khaykovich, F. Schreck, G. Ferrari, T. Bourdel, J. Cubizolles, L. D. Carr, Y. Castin, C. Salomon, Science **296**, 1290 (2002); Strecker K E, Partridge G B, Truscott A G and Hulet R G Nature **417**, 150 (2002).

[14] V. Efimov, Phys. Lett. B. **33**, 563 (1970); V. Efimov, Sov. J. Nucl. Phys. **12**, 589 (1971).

[15] T. Kraemer, M. Mark, P. Waldburger, J. G. Danzl, C. Chin, B. Engeser, A. D. Lange, K. Pilch , A. Jaakkola, H.-C. Naegerl, R. Grimm, Nature **440**, 315 (2006).

[16] T. Weber, J. Herbig, M. Mark, H.-C. Nägerl, and R. Grimm, Science **299**, 232 (2003).

[17] A. Peters, K. Y. Chung and S. Chu, Nature **400**, 849 (1999); J. M. McGuirk, G. T. Foster, J. B. Fixler, M. J. Snadden, and M. A. Kasevich, Phys. Rev. A **65**, 033608 (2002); S. Gupta, K. Dieckmann, Z. Hadzibabic, and D. E. Pritchard , Phys. Rev. Lett. **89**, 140401 (2002).

[18] P. W. Anderson, Phys. Rev. **109**, 1492 (1958).

[19] Y. Castin and J. Dalibard, Phys. Rev. A **55**, 4330 (1997); G.-B. Jo, J.-H. Choi, C. A. Christensen, Y.-R. Lee, T. A. Pasquini, W. Ketterle, and D. E. Pritchard, Phys. Rev. Lett. **99**, 240406 (2007).

[20] J. E. Lye, L. Fallani, M. Modugno, D. S. Wiersma, C. Fort, and M. Inguscio Phys. Rev. Lett. **95**, 070401 (2005)

[21] D. Clément, A. F. Varón, M. Hugbart, J. A. Retter, P. Bouyer, L. Sanchez-Palencia, D. M. Gangardt, G. V. Shlyapnikov, and A. Aspect, Phys. Rev. Lett. **95**, 170409 (2005)

[22] A. G. Truscott, K.E. Strecker, W.I. McAlexander, G.B. Patridge, and R.G. Hulet, Science **291**, 2570 (2001).

[23] F. Schreck, L. Khaykovich, K. L. Corwin, G. Ferrari, T. Bourdel, J. Cubizolles, and C. Salomon ,Phys. Rev. Lett. **87**, 080403 (2001).

[24] Z. Hadzibabic, C. A. Stan, K. Dieckmann, S. Gupta, M. W. Zwierlein, A. Görlitz, and W. Ketterle, Phys. Rev. Lett. **88**, 160401 (2002).

[25] G. Roati, F. Riboli, G. Modugno, and M. Inguscio, Phys. Rev. Lett. **89**, 150403 (2002).

[26] G. Modugno, M. Modugno, F. Riboli, G. Roati, M. Inguscio, Phys. Rev. Lett. **89**, 190404 (2002).

[27] C. Silber, S. Günther, C. Marzok, B. Deh, Ph.W. Courteille, and C. Zimmermann, cond-mat/0506217.

[28] G. Modugno, G. Ferrari, G. Roati, R. J. Brecha, A. Simoni, and M. Inguscio, Science **294**, 1320 (2001).

[29] Chin, C., M. Bartenstein, A. Altmeyer, S. Riedl, S. Jochim, J. H. Denschlag and R. Grimm, Science **305**, 1128 (2004).

[30] Regal, C. A.,M. Greiner and D. S. Jin, Phys. Rev. Lett. **92**, 040403 (2004).

[31] Zwierlein, M.W., C. A. Stan, C. H. Schunck, S.M. F. Raupach, A. J. Kerman andW. Ketterle, Phys. Rev. Lett. **92**, 120403 (2004).

[32] C. Ospelkaus, S. Ospelkaus, L. Humbert, P. Ernst, K. Sengstock, and K. Bongs, Phys. Rev. Lett. **97**, 120402 (2006).

[33] S. B. Papp and C. E. Wieman, Phys. Rev. Lett. **97**, 180404 (2006).

[34] H. Heiselberg, C. J. Pethick, H. Smith, and L. Viverit, Phys. Rev. Lett. **85**, 2418 (2000); M. J. Bijlsma, A. Heringa, and H.T. C. Stoof, Phys. Rev. A **61**, 052601 (2000); L. Viverit, Phys. Rev. A **66**, 023605 (2002).

[35] M. Lewenstein, L. Santos, M. A. Baranov, and H. Fehrmann, Phys. Rev. Lett. **92**, 050401 (2004).

[36] A. Sanpera, A. Kantian, L. Sanchez-Palencia, J. Zakrzewski, and M. Lewenstein, Phys. Rev. Lett. **93**, 040401 (2004).

[37] M. A. Baranov, M. S. Marenko, V. S. Rychkov, and G.V. Shlyapnikov, Phys. Rev. A **66**, 013606 (2002); B. Damski, L. Santos, E. Tiemann, M. Lewenstein, S. Kotochigova, P. Julienne, and P. Zoller, Phys. Rev. Lett. **90**, 110401 (2003); M. Wouters, J. Tempere, and J.T. Devreese, Phys. Rev. A **67**, 063609 (2003).

[38] G. Roati, F. Riboli, G. Modugno, and M. Inguscio, Phys. Rev. Lett. **89**, 150403 (2002).

[39] G. Roati, M. Zaccanti, C. D'Errico, J. Catani, M. Modugno, A. Simoni, M. Inguscio, and G. Modugno Phys. Rev. Lett. **99**, 010403 (2007).

[40] L. De Sarlo, P. Maioli, G. Barontini, J. Catani, F. Minardi, and M. Inguscio, Phys. Rev. A **75**, 022715 (2007).

[41] F. Ferlaino, C. D'Errico, G. Roati, M. Zaccanti, M. Inguscio, G. Modugno, A. Simoni, Phys. Rev. A **73**, 040702 (2006).

[42] S. Inouye, J. Goldwin, M. L. Olsen, C. Ticknor, J. L. Bohn, and D. S. Jin, Phys. Rev. Lett. **93**, 183201 (2004).

[43] C. Klempt, T. Henninger, O. Topic, J. Will, W. Ertmer, E. Tiemann, and J. Arlt, Phys. Rev. A **76**, 020701(R) (2007).

[44] S. Kotochigova, P. S. Julienne, and E. Tiesinga Phys. Rev. A **68**, 022501 (2003).

[45] C. D'Errico, M. Zaccanti, M. Fattori, G. Roati, M. Inguscio, G. Modugno, and A. Simoni, New J. Phys **9**, 223 (2007).

[46] S. L. Cornish, N. R. Claussen, J. L. Roberts, E. A. Cornell, and C. E. Wieman, Phys. Rev. Lett. **85**, 1795 (2000).

[47] J. L. Roberts Phys. Rev. Lett. **86**, 4211 (2001).

[48] E.G.M. van Kempen, et al., Phys. Rev. Lett. 88, 093201 (2002).

[49] G. Roati, PhD Thesis, University of Trento (2003).

[50] W. Petrich, M. H. Anderson, J. R. Ensher, and E. A. Cornell, J. Opt. Soc. Am. B **11**, 1332 (1994).

[51] Esslinger, T., I. Bloch and T.W. Hänsch Phys. Rev. A **58**, R2664 (1998).

[52] F. Ferlaino, PhD Thesis, University of Florence (2004).

[53] E. de Mirandes, PhD thesis, University of Florence (2005).

[54] C. D'Errico, Master Thesis, University of Florence (2005).

[55] D. Wang, J. Qi, M. F. Stone, O. Nikolayeva, H. Wang, B. Hattaway, S. D. Gensemer, P. L. Gould, E. E. Eyler, and W. C. Stwalley, Phys. Rev. Lett. **93**, 243005 (2004).

[56] A. Pashov, O. Docenko, M. Tamanis, R. Ferber, H. Knoeckel, and E. Tiemann, Phys. Rev. A **76**, 022511 (2007).

[57] Burke J. P. Jr., Greene C. H., Bohn J. L.,Wang H., Gould P. L. and Stwalley W. C., Phys. Rev. A **60**, 4417 (1999).

[58] Williams C. J., Tiesinga E., Julienne P. S.,Wang H., Stwalley W. C. and Gould P. L., Phys. Rev. A **60**, 4427 (1999).

[59] De Marco B., Bohn J. L., Burke J. P. Jr., Holland M. and Jin D. S., Phys. Rev. Lett. **82**, 4208 (1999).

[60] Regal C. A., Ticknor C., Bohn J. L. and Jin D. S., Phys. Rev. Lett. **90**, 053201 (2003).

[61] Wang H., Nikolov A. N., Ensher J. R., Gould P. L., Eyler E. E., Stwalley W. C., Burke J. P. Jr., Bohn J. L., Greene C. H., Tiesinga E.,Williams C. J. and Julienne P. S., Phys. Rev. A **62**, 052704 (2000).

[62] A.Simoni, F. Ferlaino, G. Roati, G. Modugno, and M. Inguscio, Phys. Rev. Lett. **90**, 163202 (2003).

[63] S. Inouye, J. Goldwin, M. L. Olsen, C. Ticknor, J. L. Bohn, and D. S. Jin, Phys. Rev. Lett. **93**, 183201 (2004).

[64] J. M. Goldwin, PhD thesis, University of Colorado (2005).

[65] E. Tiesinga, A. J. Moerdijc, B. J. Verhaar, and H. T. C. Stoof, Phys. Rev. A **46**, R1167 (1992).

[66] J. Brown and A. Carrington, *Rotational Spectrocopy of diatomic molecules*, Cambridge University Press, Cambridge (2003).

[67] L. D. Landau and E. M. Lifshitz, *Quantum Mechanics* (Pergamon Press, Oxford) 1977, sect. 131.

[68] M. Inguscio, S. Stringari, C. E. Wieman Eds., *Bose-Einstein Condensation in Atomic Gases*, Proceedings of the International School of Physics "Enrico Fermi" Course CXL (IOS Press Amsterdam 1999).

[69] B. M. Smirnov and M. S. Chibisov, Zh. Eksp. Teor. Fiz. **48**, 939 (1965).

[70] C. Eckart, Rev. Mod. Phys. **2**, 305 (1930); E. P. Wigner, Z. Phys. **43**, 624 (1927).

[71] T. Köhler, K. Goral, P. Julienne, Rev. Mod. Phys. **78**, 1311 (2006).

[72] A. J. Moerdijk, B. J. Verhaar, and A. Axelsson, Phys. Rev. A **51**, 4852 (1995).

[73] H. M. J. M. Boesten, A. J. Moerdijk, and B. J. Verhaar, Phys. Rev. A **54**, R29 (1996).

[74] T. Weber, J. Herbig, M. Mark, H.-C. Nägerl, and R. Grimm, Phys. Rev. Lett. **91**, 123201 (2003).

[75] P. O. Fedichev, M. W. Reynolds, and G. V. Shlyapnikov, Phys. Rev. Lett. **77**, 2921 (1996).

[76] C. Ticknor, C. A. Regal, D. S. Jin, and J. L. Bohn, Phys. Rev. A **69**, 042712 (2004).

[77] S. Jochim, M. Bartenstein, A. Altmeyer, G. Hendl, S. Riedl, C. Chin, J. Hecker Denschlag and R. Grimm, Science **302**, 2101 (2003).

[78] S. Ospelkaus, C. Ospelkaus, L. Humbert, K. Sengstock, and K. Bongs, Phys. Rev. Lett. **97**, 120403 (2006).

[79] M. Zaccanti, C. D'Errico, F. Ferlaino, G. Roati, M. Inguscio, and G. Modugno, Phys. Rev. A **74**, 041605(R) (2006).

[80] E. Hodby, S. T. Thompson, C. A. Regal, M. Greiner, A. C. Wilson, D. S. Jin, E. A. Cornell, and C. E. Wieman, Phys. Rev. Lett. **94**, 120402 (2005).

[81] J. P. D'Incao, , B. D. Esry, Phys. Rev. A, **73**, 030703 (2006).

[82] A. Derevianko, J. F. Babb, and A. Dalgarno, Phys. Rev. A **63**, 052704 (2001).

[83] S. G. Porsev and A. Derevianko, J. Chem. Phys. **119**, 884 (2003).

[84] W. T. Zemke, R. Côté, and W. C. Stwalley, Phys. Rev. A **71**, 062706 (2005).

[85] S. Rousseau, A. R. Allouche, and M. Aubert-Frécon, J. Mol. Spectrosc. **203**, 235 (2000).

[86] C. Amiot and J. Vergès, J. Chem. Phys. **112**, 7068 (2000).

[87] R. J. Le Roy, **RKR1 2.0**: *A Computer Program Implementing the First-Order RKR Method for Determining Diatomic Molecule Potential Energy Curves*, University of Waterloo Chemical Physics Research Report CP-657R (2004).

[88] F. H. Mies, C. J. Williams, and P. S. Julienne, J. Res. Natl. Inst. Stand. Technol. **101**, 521 (1996).

[89] S. Falke, E. Tiemann, and C. Lisdat, arXiv:0.706.2290v1.

[90] J. Bohn, J. P. Burke Jr., C. H. Greene, H. Wang, P. L. Gould and W. C. Stwalley, Phys. Rev. A **59**, 3660 (1999).

[91] C. J. Williams, E. Tiesinga, P. S. Julienne,H. Wang, W. C. Stwalley and P. L. Gould, Phys. Rev. A **60**, 4427 (1999).

[92] H. Wang, A. N. Nikolov, J. R. Ensher, P. L. Gould, E. E. Eyler, and W. C. Stwalley, J. P. Burke, Jr., J. L. Bohn, and Chris. H. Greene, E. Tiesinga, C. J. Williams, and P. S. Julienne, Phys. Rev. A **62**, 052704 (2000).

[93] E. Tiesinga, private communication.

[94] G. Zhao, W. T. Zemke, J. T. Kim, H. Wang, J. T. Bahns, W. C. Stwalley, Li Li, A. M. Lyyra and C. Amiot, J. Chem. Phys. **105**, 7976 (1996).

[95] M. Marinescu, H. R. Sadeghpour and A. Dalgarno, Phys. Rev. A **49**, 982 (1994).

[96] G. Thalhammer, K. Winkler, F. Lang, S. Schmid, R. Grimm and J. Hecker Denschlag, Phys. Rev. Lett. **96**, 050402 (2006).

[97] K. Goral, T. Köhler, S. A. Gardiner, E. Tiesinga and P. S. Julienne, J. Phys. B ,**37** 3457 (2004).

[98] P. Massignan and H. T. C. Stoof, arXiv:cond-mat/0702462v2.

[99] B. DeMarco, PhD thesis, University of Colorado (2001).

[100] K. Huang "Statistical Mechanics" (John Wiley and Sons, New York).

[101] L. Vichi, M. Inguscio, S. Stringari, G. M. Tino, J. Phys. B: At. Mol. Opt. Phys. **31**, L899 (1998).

[102] C. J. Pethick and H. Smith "Bose-Einstein Condensation in Dilute Gases" Cambridge University Press (2002).

[103] F. Dalfovo, S. Giorgini, L. P. Pitaevskii, and S. Stringari, Rev. Mod. Phys. **71**, 463 (1999).

[104] E. A. Donley, N. R. Claussen, S. L. Cornish, J. L. Roberts, E. A. Cornell and C. E. Wieman, Nature **412**, 295 (2001).

[105] Y. Castin, and R. Dum, Phys. Rev. Lett. **77**, 5315 (1996).

[106] L. Viverit and S. Giorgini, Phys. Rev. A **66**, 063604 (2002)

[107] M. Modugno, F. Ferlaino, G. Roati, G. Modugno, and M. Inguscio, Phys. Rev. A **68**, 043626 (2003).

[108] K. Mølmer, Phys. Rev. Lett. **80**, 1804 (1998).

[109] R. Roth, and H. Feldmeier Phys. Rev. A **65**, R021603 (2002).

[110] M. Modugno, F. Ferlaino, F. Riboli, G. Roati, G. Modugno, and M. Inguscio, Phys. Rev. A **68**, 043626 (2003).

[111] H. Hu, X. J. Liu, and M. Modugno, Phys. Rev. A **67**, 063614 (2003).

[112] J. P. D'Incao, and B. D. Esry, Phys. Rev. Lett. **94**, 213201 (2005).

[113] S. Stringari, Phys. Rev. Lett. **77**, 2360 (1996).

[114] F. Ferlaino, E. de Mirandes, G. Roati, G. Modugno, and M. Inguscio, Phys. Rev. Lett. **92**, 140405 (2004).

[115] C. Ospelkaus, S. Ospelkaus, K. Sengstock and K. Bongs, Phys. Rev. Lett. **96**, 020401 (2004).

[116] J. J. Zirbel, K.-K. Ni, S. Ospelkaus, J. P. D'Incao, C. E. Wieman, J. Ye, D. S. Jin, arXiv:0710.2479.

[117] S. Dürr, T. Volz, A. Marte, and G. Rempe, Phys. Rev. Lett.**92**, 020406 (2004).

[118] See for example J. E. Lye, L. Fallani, C. Fort, V. Guarrera, M. Modugno, D. S. Wiersma, M. Inguscio, cond-mat/0611146, and references therein.

[119] B. P. Anderson and M. A. Kasevich, Science **282**, 1686 (1998); Y. Shin, M. Saba, T. A. Pasquini, W. Ketterle, D. E. Pritchard, and A. E. Leanhardt, Phys. Rev. Lett. **92**, 050405 (2004); G. Roati, E. de Mirandes, F. Ferlaino, H. Ott, G. Modugno, and M. Inguscio, Phys. Rev. Lett. **92**, 230402 (2004).

[120] P. Bouyer and M. A. Kasevich, Phys. Rev. A **56**, R1083 (1997); L. Pezz'e, L. A. Collins, A. Smerzi, G. P. Berman, and A. R. Bishop, Phys. Rev. A **72**, 043612 (2005); G.-B. Jo, Y. Shin, S. Will, T. A. Pasquini, M. Saba, W. Ketterle, D. E. Pritchard, M. Vengalattore, and M. Prentiss, Phys. Rev. Lett. **98**, 030407 (2007).

[121] M. Fattori, C. D'Errico, G. Roati, M. Zaccanti, M. Jona-Lasinio, M. Modugno, M. Inguscio, G. Modugno, arXiv:0710.5131.

[122] F. Bloch, Z. Phys. **52**, 555 (1928); C. Zener, Proc. R. Soc. Lond. Ser. A **145**, 523 (1932).

[123] D. Witthaut, M.Werder, S. Mossmann and H. J. Korsch, Phys. Rev. E **71**, 036625 (2005).

[124] Y. Castin and J. Dalibard, Phys. Rev. A **55**, 4330 (1997).

[125] M. Gustavsson, E. Haller, M. J. Mark, J. G. Danzl, G. Rojas-Kopeinig, H.-C. Nägerl, arXiv:0710.5083.

[126] I. Carusotto, L. Pitaevskii, S. Stringari, G. Modugno, and M. Inguscio, Phys. Rev. Lett. **95**, 093202 (2005).

[127] E. A. Burt, R. W. Ghrist, C. J. Myatt, M. J. Holland, E. A. Cornell, and C. E. Wieman, Phys. Rev. Lett. **79**, 337 (1997).

[128] G. Modugno, M. Modugno, F. Riboli, G. Roati, and M. Inguscio, Phys. Rev. Lett. **89**, 190404 (2002).

[129] K. Winkler, F. Lang, G. Thalhammer, P. v. d. Straten, R. Grimm, and J. Hecker Denschlag, Phys. Rev. Lett. **98**, 043201 (2007).

[130] M. Baranov, Ł. Dobrek, K. Góral, L. Santos, M. Lewenstein, Phys. Scr. **T102**, 74 (2002).

[131] T. Lahaye, T. Koch, B. Fröhlich, M. Fattori, J. Metz, A. Griesmaier, S. Giovanazzi and T. Pfau, Nature **448**, 672 (2007).